WORKSHOP 2 ON FISH DISTRIBUTION (WKFISHDISH2; outputs from 2022 meeting)

Errata (08/02/2023): Correction to volume and issue number

VOLUME 5 | ISSUE 7

ICES SCIENTIFIC REPORTS

RAPPORTS
SCIENTIFIQUES DU CIEM

ICES INTERNATIONAL COUNCIL FOR THE EXPLORATION OF THE SEA
CIEM COUNSEIL INTERNATIONAL POUR L'EXPLORATION DE LA MER

International Council for the Exploration of the Sea
Conseil International pour l'Exploration de la Mer

H.C. Andersens Boulevard 44-46
DK-1553 Copenhagen V
Denmark
Telephone (+45) 33 38 67 00
Telefax (+45) 33 93 42 15
www.ices.dk
info@ices.dk

ISSN number: 2618-1371

ICES Scientific Reports

Volume 5 | Issue 7

WORKSHOP 2 ON FISH DISTRIBUTION (WKFISHDISH2; outputs from 2022 meeting)

Recommended format for purpose of citation:

ICES. 2023. Workshop 2 on Fish Distribution (WKFISHDISH2; outputs from 2022 meeting). ICES Scientific Reports. 5:7. 127 pp. https://doi.org/10.17895/ices.pub.21692246

Editors

Alan Baudron • Anna Rindorf • Maria Teresa Spedicato

Authors

François Bastardie • Alan Baudron • Casper Berg • Aaron Berger • Logan Binch • Isabella Bitetto • Clyde Blanco • Joanna Bluemel • Derek Bolser • Julia Calderwood • Natacha Carvalho • Liesa Celie • Chun Chen • Guillem Chust • Elena Couce • Dimitrios Damalas • Jochen Depestele • Niall Fallon • Paul Fernandes • Manuel Hidalgo • Georgina Hunt • Leire Ibaibarriaga • Romaric Jac • Nis Sand Jacobsen Claudia Junge • Stefanos Kavadas • Alexander Kempf • Bernhard Kuehn • Alessandro Ligas • Max Lindmark • Irida Maina • Federico Maioli • Porzia Maiorano • Paco Melià • Tobias Mildenberger Claudia Musumeci • Osman Neto • Bríd O'Connor • Iosu Paradinas • Jan Jaap Poos • Nikolaus Probst Eros Quesada • David Reid • Joseph Ribeiro • Anna Rindorf • Guldborg Søvik • Maria Teresa Spedicato Klaas Sys • Dorota Szalaj • Anna Nora Tassetti • Marc Taylor • Sebastian Uhlmann • Berthe Maria Vastenhoud • Louise Vaughan • Youen Vermard • Damian Villagra Villanueva • Ching Villanueva Morten Vinther • Mathieu Wolliez • Fabian Zimmermann • Walter Zupa

ICES International Council for the Exploration of the Sea
CIEM Conseil International pour l'Exploration de la Mer

Contents

i Executive summary

The objective of WKFISHDISH2 was to develop a standardized and open-source way of routinely using trawl survey data to produce distribution maps which can be easily updated. To do so, workshop participants (i) reviewed models that can produce distribution maps from survey data in DATRAS and MEDITS formats, (ii) considered best practice guidance for data, and models, (iii) implemented best practice to produce distribution maps in a transparent manner, and (iv) populated an ICES repository with distribution maps and associated scripts. Nine models were reviewed, seven of which were considered appropriate to produce distribution maps using survey data. The two models excluded failed to estimate gear standardization factors. Best practice for data should consider the following: correct/remove erroneous observations, account for changes in haul duration/timing affecting catchability, use species-specific modelled areas, remove gears/surveys with no observations to reduce model converging time, and include appropriate explanatory variables. A step-by-step list to preprocess survey data was provided. Best practice for models should consider the following: account for skewed distribution of survey data by exploring different statistical error distributions, use open-source models able to reproduce distributions from simulated data, consider the complexity of the model required vs. the run-time (e.g. number of knots), avoid extrapolating the model to areas/depths where the species is not observed, and perform relevant model diagnostics/model selection. To compare distribution estimated by different models, the SPAtial EFficiency metric (SPAEF) was used together with centres of gravity, biomass hot spots (90^{th} percentile), and effective occupied areas. All seven models were able to produce satisfactory distribution maps for at least one species within the workshop time constraints, both with DATRAS data in the Atlantic and the MEDITS data in the Mediterranean. Comparisons between model estimates showed reasonable consistency overall, although discrepancies were noted owing to different model structures. Distribution maps produced during the workshop and the associated script are available at the ICES SharePoint. Participants identified priorities for future research to be tackled during a subsequent workshop: combine outputs of different models in a single distribution map, include fish length in models, investigate environmental covariates and their use for predictions, investigate models' abilities to reproduce known distributions and further consider the impact of vessel/gear effects.

ii Expert group information

Expert group name	Workshop 2 on Fish Distribution (WKFISHDISH2)
Expert group cycle	Annual
Year cycle started	2021
Reporting year in cycle	1/1
Chairs	Anna Rindorf, Denmark
	Alan Baudron, UK (Scotland)
	Maria-Teresa Spedicato, Italy
Meeting venue and dates	27–30 June 2022, Copenhagen, Denmark (63 participants)

1 Introduction

Workshop 2 on Fish Distribution – Terms of Reference (ToRs)

2021/WK/FRSG36

Workshop 2 on Fish Distribution (WKFISHDISH2), chaired by Maria Teresa Spedicato*, Italy, Alan Baudron*, UK, and Anna Rindorf*, Denmark, will be established, and meet at ICES HQ, Copenhagen, Denmark (with online option) 27–30 June 2022 to:

a) Review models to derive spatial distribution of fish and cephalopods from survey data in DATRAS and MEDITS formats, with the aim of producing temporally resolved distribution maps for individual species based on data from surveys with varying in spatio-temporal coverage (Science Plan codes: 5.2, 5.4, and 6.3);
   → See section 2 of this report.
b) Consider best practice guidance for model structure to derive distribution maps including but not limited to the choice of response variable, error distribution, selection of area/data based on available non-zero observations, inclusion of landmasses, survey effort and gear standardizations and the use of correlates (Science Plan codes: 4.2);
   → See section 3 of this report.
c) Implement best practice approaches to produce distribution maps and define and establish an efficient and transparent approach to producing updates of these maps (Science Plan codes: 4.2);
   → See section 4 of this report.
d) Populate an ICES hosted repository with scripts (models) and resulting distribution maps for several species (Science Plan codes: 4.2).
   → See section 5 of this report.

In April 2022, formats for data and model reviews will be defined by correspondence. WKFISHDISH2 will report by 15 August 2022 for the attention of ACOM.

2 ToR a: Review of models with species distribution mapping potential

Review models to derive spatial distribution of fish and cephalopods from survey data in DATRAS and MEDITS formats, with the aim of producing temporally resolved distribution maps for individual species based on data from surveys with varying in spatio-temporal coverage (Science Plan codes: 5.2, 5.4, and 6.3);

2.1 Approach to model reviews

Prior to the workshop, workshop participants were asked to contribute with reviews of models they felt could be useful in the mapping of species distribution from trawl survey catch rates. The reviews followed a prespecified format:

1. Model name and reference
2. Summary of approach
3. Response variable error assumption(s) including treatment of 0-observations
4. Spatial functions and possibility to account for landmasses
5. Sensitivity to unbalanced survey effort in space and time
6. Standardization between gears
7. Potential use of correlates
8. Possible use of the model for forecasting
9. Possibility to include more than one life stage
10. Is the model able to reproduce known operating model distributions when fitted to simulated data?
11. Is the model implemented in a software package (e.g. R or other)?
12. Which species has the model been applied to?

After presentation, the degree to which the models fulfilled specified criteria was evaluated in subgroups by the workshop participants.

2.1.1 Model 1: Approximate Bayesian inference using integrated nested Laplace approximation (INLA)

Presented by: Joanna Bluemel

2.1.1.1 Model name and reference

Approximate Bayesian inference using integrated nested Laplace approximation (INLA; Rue *et al.*, 2009; Martins *et al.*, 2013).

2.1.1.2 Summary of approach

INLA is used to make Bayesian Inference for Latent Gaussian Models, which includes many statistical models used today, e.g. Generalized Additive Models (GAMs) and Generalized Linear Mixed Models (GLMM). This approach has had a large affect because of the accuracy and speed of the approximations possible with INLA, which can also be used for spatial modelling with Stochastic Partial Differential Equations. The Stochastic Partial Differential Equations (SPDE)

approach applies a differential operator to a stochastic process in order to describe a desired covariance function, e.g. the Matérn function. The INLA method and its implementation in the R-INLA library provide a rich toolbox for statistical space-time modelling while sidestepping typical convergence problems arising with simulation-based techniques using Markov Chain Monte-Carlo codes for large and complex hierarchical models. Uncertainties arising in model parameters and in pointwise spatio-temporal predictions are naturally captured in the posterior distributions computed through INLA using appropriate approximation techniques that can be visualized through maps of various properties. INLA also allows for direct simulation from the estimated posterior model, such that we can conduct statistical inferences on more complex functionals of the multivariate predictive distributions by analogy with MCMC frameworks.

2.1.1.3 Response variable error assumption(s) including treatment of 0-observations

Can model with many different model structures (GLM, GLMM, GAM, zero-inflated) and error distributions including those that deal with zero-inflation (Poisson, NB, ZIP/ZAP etc).

2.1.1.4 Spatial functions and possibility to account for landmasses

Can include spatial correlation (using Matérn correlation and Stochastic Partial Differential Equations (SPDE)) and include 'barrier' areas (landmasses) into the mesh (required as part of finite element approach to obtain hyperparameters required for the GMRF) to ensure that resulting spatial correlation estimation cannot cross land. Spatial correlation can be modelled as one spatial random field or as separate spatial random fields by time-step (e.g. year) or other grouping variables, with the possibility of linking them through autocorrelation or random walk processes.

2.1.1.5 Sensitivity to unbalanced survey effort in space and time

Can incorporate both spatio-temporal correlation into model structure but do need relatively even spread of samples in space and number per period or will need to exclude some years/areas from the model.

2.1.1.6 Standardization between gears

Can include random gear effect into the model structure.

2.1.1.7 Potential use of correlates

Can include correlates into the model structure.

2.1.1.8 Possible use of the model for forecasting

Possible, see Engel, M., Mette, T. and Falk, W., 2022. Spatial species distribution models: Using Bayes inference with INLA and SPDE to improve the tree species choice for important European tree species. Forest Ecology and Management, 507, p.119983.

2.1.1.9 Possibility to include more than one life stage

Can include life stage as a covariate, but only one response variable at a time (not a multispecies model).

2.1.1.10 Is the model able to reproduce known operating model distributions when fitted to simulated data?

INLA allows for direct simulation from the estimated posterior model, such that we can conduct statistical inferences on more complex functionals of the multivariate predictive distributions by analogy with MCMC frameworks.

2.1.1.11 Is the model implemented in a software package (e.g. R or other)?

R package 'INLA'.

2.1.1.12 Which species has the model been applied to?

Wide application for species distribution modelling and spatial analysis in ecology (e.g. Beguin *et al.,* 2012; Leach *et al.,* 2016; Engel *et al.,* 2022), including for fish stocks (e.g. Berg *et al.,* 2021) and index standardization (e.g. Zhou *et al.,* 2019).

2.1.2 Model 2: Bayesian Additive Regression Trees (BART)

Presented by: Elena Couce

2.1.2.1 Model name and reference

Bayesian Additive Regression Trees (BART) (Chipman *et al.,* 2010).

2.1.2.2 Summary of approach

BART is a technique based on an ensemble of classification tree models, each built by sequentially splitting the data in two groups based on the value of the explanatory variables, with the aim to separate data into groups as homogenous as possible with respect to the response variable (which can be species presence/absence, or any measure of abundance). BART differs from other frequently used tree ensemble models --such as Random Forest or Boosted Trees-- in that the sequence of trees is built relying on a Bayesian probability model, with the tree structure dictated by priors and a likelihood for the data in the terminal nodes of the trees. An iterative Bayesian back-fitting Markov Chain Monte Carlo algorithm is used to fit the individual trees, with the contribution of each tree to the final prediction constrained by a prior to be small. The probability approach makes it possible to calculate confidence intervals for the predictions (i.e. prediction error).

2.1.2.3 Response variable error assumption(s) including treatment of 0-observations

Errors should be normally distributed and homoscedastic.

2.1.2.4 Spatial functions and possibility to account for landmasses

Landmasses are normally excluded from marine species distribution models.

2.1.2.5 Sensitivity to unbalanced survey effort in space and time

Model assumes data has been standardized and does not consider spatio-temporal correlations, although this could be build-in if desired (i.e. by including terms explicitly for time and for the distance of each cell in the grid to all the others. Such approaches have been developed for Random Forest models and could be included in a similar way for BART, although it might not be computationally feasible). However BART models, like other tree-based techniques, tend to have good performance even if ignoring spatio-temporal correlations, compared to other techniques that do explicitly consider it.

2.1.2.6 Standardization between gears

Model is not suitable for multiple gears (unless modelling only presence/absence). However, it assumes all entries are similar and treats it the same, so data should be standardized before using it for models.

2.1.2.7 Potential use of correlates

Similar to other tree-based techniques

2.1.2.8 Possible use of the model for forecasting

Predictions and confidence intervals can be generated for novel data.

2.1.2.9 Possibility to include more than one life stage

Individual models can be fitted for different life stages.

2.1.2.10 Is the model able to reproduce known operating model distributions when fitted to simulated data?

Yes. Performance is comparable and often superior to that of Random Forests.

2.1.2.11 Is the model implemented in a software package (e.g. R or other)?

In R, for example packages "bartMachine" or "embarcadero" (though the later only does presence/absence models).

2.1.2.12 Which species has the model been applied to?

At Cefas the models have been applied to presence/absence of more than 700 fish species and fish-species size classes, and beyond species, also to other concepts such as benthic production.

2.1.3 Model 3: GAM model with random effects and train/test approach

Presented by: Isabella Bitetto

2.1.3.1 Model name and reference

GAM model with random effects and train/test approach (Wood 2017).

2.1.3.2 Summary of approach

GAM models are used in SDM with different approaches, from the simpler, based only on presence/absence data and few basic covariates (coordinates and depth), as in Carbonara *et al.* (2020) to more complex, in which different modelling approaches are combined including environmental variables, as in Panzeri *et al.* (2021a).

The candidate SDM here proposed for the south Adriatic and western Ionian Sea can test three different GAM models (Gaussian, Tweedie and Delta), validated by training and testing them on randomly split datasets, to provide more robust estimations. Geo-referred observations available from MEDITS trawl survey and fisheries dependent data from observers onboard (Data Collection Framework and EUMAP) will be analysed to allow the predictions of multi-annual and seasonal spatial variations in abundance (Gonzalez *et al.*, 2021). The spatio-temporal distribution of species abundance can be explained through different types of not redundant covariates (VIF analysis; Zuur *et al*., 2010): i) spatio-temporal variables; ii) sampling effort and coverage (number of hauls by year, haul duration, etc.); iii) environmental variables according to the species. The covariates will be further selected to provide forecasting projections under selected climate changes scenarios (possible grid resolution 1/16°). Fixed and random effects, as well as different types of smoothers and tensors will be considered. The selection of the best model will be based on explained deviance and AIC (Akaike, 1974), estimated on training data, as well as MAE (Willmott and Matsuura, 2005) and correlation coefficient (R^2), estimated on the testing dataset. A similar approach was used in Panzeri *et al*. (2021a,b). The approach here proposed can be tuned after a first phase of testing on selected target species.

2.1.3.3 Response variable error assumption(s) including treatment of 0-observations

Current implementations of GAMs contain a wide range of distribution families, including compound (hurdle) models to deal with the combination of zeroes and continuous observations data or zero-inflation. In the Delta approach for continuous data (e.g. weight) containing zeroes, the response variable error can be assumed to be distributed as a Gaussian, Gamma or lognormal for the positive observations, while as binomial for presence/absence submodel, the latter accounting for 0-observations. 0-observations can also be treated assuming the Tweedie error distribution of the response variable. Solutions for count data include Poisson, negative binomial, ZIP, ZAP, etc.

2.1.3.4 Spatial functions and possibility to account for landmasses

The canonical thin plate smoothers on latitude, longitude and depth, as well their interactions will be included in the model (e.g. bi-dimensional smoothers, tensors). Furthermore, the possibility to account for landmasses will be explored through the use of Markov random field smoother and soap film smoothers (Rue and Held, 2005; Wood *et al.*; 2008; Baudron *et al.*; 2020).

2.1.3.5 Sensitivity to unbalanced survey effort in space and time

The inclusion of explanatory variables representing the factors affecting the unbalance of the sampling effort in space and time (e.g. shift of survey season, number of sampling stations, vessels) can be included in the model in order to evaluate the impact of their variations on SDM prediction over a standardized spatio-temporal grid.

2.1.3.6 Standardization between gears

A calibration of catch rates values across multiple gears characterizing the different sources of geo-refereed abundance information will be carried out (Gonzalez *et al.*, 2021[3]). Gear effects can be also accounted for through random effects.

2.1.3.7 Potential use of correlates

Specific environmental variables will be selected as potential correlates, according to the biology of the studied species. For example, the use of sea surface water temperature is expected to be more informative for coastal species rather than for deep water ones.

2.1.3.8 Possible use of the model for forecasting

GAM approach can be effectively used for forecasting species distribution including environmental variables in the models (Chen *et al.*, 2021) derived, for the study area, from the FAIRSEA project and Copernicus Climate Service.

2.1.3.9 Possibility to include more than one life stage

This approach can be applied to the entire population as well as to specific life stages corresponding to two main groups, i.e. juveniles (e.g. below Lm25 or MCRS) and adults (e.g. above Lm25 or MCRS). In this case the more suitable approach among the ones previously presented will account for the spatio-temporal distribution of the available data. For example, in case of juveniles 0-inflated models could be more suitable than other approaches.

2.1.3.10 Is the model able to reproduce known operating model distributions when fitted to simulated data?

The proposed approach is not tested with simulated data but trained and tested with 50 random datasets composed respectively of 70% (train) and 30% (test) of the original dataset.

2.1.3.11 Is the model implemented in a software package (e.g. R or other)?

A set of R script/functions, based on *mgcv* R package, for implementing the train/test of the models have been developed and are available.

2.1.3.12 Which species has the model been applied to?

A similar approach was applied to the one here for (Panzeri *et al.*, 2021b):

- European hake (*Merluccius merluccius*)
- red mullet (*Mullus barbatus*)
- common sole (*Solea solea*)
- mantis shrimp (*Squilla mantis*)
- common cuttlefish (*Sepia officinalis*)

2.1.4 Model 4: Spatio-temporal generalized additive models (GAMs)

Presented by: Irida Maina

2.1.4.1 Model name and reference

Spatio-temporal generalized additive models (GAMs; Augustin *et al.*, 2013; Wood. 2017).

2.1.4.2 Summary of approach

The model was applied to estimate the spatio-temporal distribution (seasonal, annual) of certain commercial species. Catch data can be included based on information collected by onboard observers within the framework of EU-MAP (former DCF) and survey data derived from MEDITS. After an exploratory analysis of the dataset including an investigation of possible time-trends, generalized additive mixed effects models were used to explore the relationships between the catch rates and a series of environmental and time related variables. In order to avoid model misspecifications, random effects (e.g. vessels and haul characteristics) as well as dedicated smoothers considering for spatial or/and temporal variability were included in the model selection (e.g. soap-film smoothers Wood, 2017). Model configuration selection was based on the Root Mean Squared Prediction Error and AIC. In order to examine whether the final selected model has eliminated spatio-temporal autocorrelation in residuals, semivariograms and Partial Auto-Correlation Function plots were considered. The data were also randomly divided in a training and test dataset.

2.1.4.3 Response variable error assumption(s) including treatment of 0-observations

The analysis for each species and size group was based on: (a) estimating the presence of each species (using binomial error distribution), (b) estimating the catch rates (using dedicated error distributions e.g. Tweedie), (c) combine the steps (a) and (b) to remove from the final layers the values that each species was found to be absent.

2.1.4.4 Spatial functions and possibility to account for landmasses

A GAM, incorporating interaction of space -time through smoothers, was included in the model selection aiming to obtain a model flexible enough to adequately represent the spatio-temporal variability of each species. In particular, a soap film smoother for space and a penalized regression spline for time was implemented to avoid model misspecifications, which can result in over smoothing. Additionally, a simple Markov random field and other spatial smoothers, were also tested.

2.1.4.5 Sensitivity to unbalanced survey effort in space and time

Dedicated smoothers were included in the model selection for space. In addition, time related parameters e.g. season and year were also included. Furthermore, spatio-temporal outcomes were explored along with 95% Bayesian credible intervals.

2.1.4.6 Standardization between gears

Catchability differences were considered in the model using variables related to vessels characteristics, duration and swept-area of bottom trawls (no other gears used).

2.1.4.7 Potential use of correlates

Environmental and oceanographic parameters were included in the model selection. Collinearity issues were explored between the explanatory variables to drop collinear covariates from the final model selection (VIF analysis).

2.1.4.8 Possible use of the model for forecasting

Environmental variables can be used as predictors in the model. In addition, based on our previous experience with models applied on these certain species and on similar datasets some environmental variables (mainly related to primary productivity) are significantly correlated with the response variable (fish catch rate).

2.1.4.9 Possibility to include more than one life stage

Given that the spatial distribution of each species is expected to vary during their biological life cycle, two different size groups were analysed (small and large individuals). For now, two spatial models were applied for each species: 1) on individuals belonging to the "small" size group, i.e. in most cases approaching individuals lower than the Minimum Conservation Reference Size and 2) large individuals (over MCRS).

2.1.4.10 Is the model able to reproduce known operating model distributions when fitted to simulated data?

Theoretically yes, but not tested.

2.1.4.11 Is the model implemented in a software package (e.g. R or other)?

The core model was implemented in R mgcv r-package.

2.1.4.12 Which species has the model been applied to?

For the Eastern Ionian CS, similar models (but not taking into account space-time interactions) have been previously applied by Maina *et al.* (2016), Maina *et al.* (2021) including the same species. Part of the approach described here has been previously applied to explore spatio-temporal dynamics of bottom trawl in Aegean Sea (Maina *et al.*, 2018) and for some species in Eastern Ionian Sea (unpublished data). The model was applied in WKFISHDIS2 for the species *Merluccius merluccius*, *Mullus barbatus* and *Parapenaeus longirostris*.

2.1.5 Model 5: GAM model with random effects

Presented by Tobias Mildenberger and Casper Berg

2.1.5.1 Model name and reference

Spatio-temporal generalized additive models (GAMs) following the approach of Berg *et al.* (2014).

2.1.5.2 Summary of approach

Generalized additive models (GAMs) are powerful statistical tools that can be used to estimate abundances of fish populations while correcting for confounding factors such as spatial position of the haul, depth, time of day, or swept-area. GAMs allow the definition of non-linear smooth relations between the response (e.g. abundance) and explanatory variables (e.g. year, season and position of haul). The inclusion of spatial and spatio-temporal smooth functions allows to predict fish abundances in space and time. This approach builds upon the methodology and R package described in Berg *et al*. (2014).

2.1.5.3 Response variable error assumption(s) including treatment of 0-observations

Dependent on response variable, it is straightforward to switch between a lognormal, negative binomial or Tweedie distribution for the response variable errors. In this case zeros would be included, but delta distributions are implemented in the R package and straightforward to apply.

2.1.5.4 Spatial functions and possibility to account for landmasses

By default the model includes a smooth function of a fine spatial grid and more coarse time-varying spatial grids as explanatory variables.

2.1.5.5 Sensitivity to unbalanced survey effort in space and time

Arguably sensitive, but this remains to be investigated.

2.1.5.6 Standardization between gears

By default gear or gear category included as a fixed effect in model. Can also be included as a random effect.

2.1.5.7 Potential use of correlates

Any number of correlates or smooth functions thereof can easily be incorporated into the model.

2.1.5.8 Possible use of the model for forecasting

Model can be used for forecasting.

2.1.5.9 Possibility to include more than one life stage

Straight-forward to run models for different life stages or by age class.

2.1.5.10 Is the model able to reproduce known operating model distributions when fitted to simulated data?

Yes.

2.1.5.11 Is the model implemented in a software package (e.g. R or other)?

Yes, the model is implemented in the R package "surveyIndex" by Casper W. Berg. Spin-up version in the R package *fishdist*.

2.1.5.12 Which species has the model been applied to?

The model has been applied to multiple species in the North Sea, such as cod and sprat to estimate an age-based abundance index. Further, it has been applied to several elasmobranchs and cephalopods in the Northeast Atlantic.

2.1.6 Model 6: VAST

Presented by: Klaas Sys

2.1.6.1 Model name and reference

VAST (Vector Autoregressive Spatio-temporal model) (Thorson and Barnett, 2017)

2.1.6.2 Summary of approach

VAST is a species distribution model (SDM) that allows to model catch per unit effort data. It is a state space model and consequently accounts for both process error caused by e.g. spatio-temporal and grouping effects, and observation error. Depending on the statistical nature of the data, the model consists of both a presence-absence model that fits to occurrence data, and a model to fit the positive catch rates. Covariates that affect both catchability and abundance can be included as well. Since VAST is a vector autoregressive model, it allows to model different species / life stages simultaneous. A spatial factor analysis can be applied to reduce the dimensions of the spatio-temporal models (Thorson *et al.*, 2015).

VAST is written in C++ and implemented in TMB, as such it takes advantage in terms of computation efficiency through use of (i) the Laplace approximation to fit the process models, automatic differentiation, and Eigen, a C++ library for linear algebra.

2.1.6.3 Response variable error assumption(s) including treatment of 0-observations

VAST comprises a variety of statistical models that allow to deal with count and continuous data. Depending on the rate of zero observations, the model can be extended to include a model that deals with occurrence data only (a binomial model).

2.1.6.4 Spatial functions and possibility to account for landmasses

The spatial modelling approach in VAST relies on the routines developed in the INLA software. The Stochastic Partial Differential Equations (SPDE) model is used to efficiently approximate a Gaussian Markov Random Field (GMRF) which is an approximation to the Gaussian Field that represents the underlying spatial process. The SPDE model estimates the nodes of a triangulated mesh that includes the entire spatial field, and that links the observations to the nodes of the mesh. Spatial correlation in the GMRF is governed through a Matérn correlation function.

In case of land masses, or physical boundaries that break down the correlation structure, a Barrier model can be used that permits to model non-stationary spatial processes.

2.1.6.5 Sensitivity to unbalanced survey effort in space and time

VAST allows to model spatio-temporal processes and can deal with unbalanced survey data in space and time (see https://github.com/James-Thorson-NOAA/VAST/wiki/Unbalanced-data).

2.1.6.6 Standardization between gears

VAST can deal with different surveys. A random intercept model deals with differences in catchability between surveys.

2.1.6.7 Potential use of correlates

VAST allows to include different types of correlates affecting both species density as well as catchability.

2.1.6.8 Possible use of the model for forecasting

The model can be used for forecasting future changes in distribution or abundance (Thorson, 2019).

2.1.6.9 Possibility to include more than one life stage

VAST is a multispecies model and can include multiple life stages or species in the model. It can also include species interactions.

2.1.6.10 Is the model able to reproduce known operating model distributions when fitted to simulated data?

Grüss *et al.* (2019) and Brodie *et al.* (2020) fitted VAST to simulated data. Both studies showed that VAST is able to reproduce the operating model in some conditions. However, in Brodie *et al.* (2020), VAST was not able to capture non-linear relationships between fish abundance and environmental covariates in contrast to GAM (Generalized Additive Model) and BRT (Boosted Regression Trees) models.

2.1.6.11 Is the model implemented in a software package (e.g. R or other)?

The model is available through an R package called VAST that can be installed from the authors GitHub page (https://github.com/James-Thorson-NOAA/VAST). The core of the model is written in C++ making use of the R package TMB. The VAST package offers some functionalities to prepare the data, and the spatial interpolation grid, as well as routines for model fitting, assessment, simulation and prediction, and visualization.

2.1.6.12 Which species has the model been applied to?

The model is applied to a wide range of, mainly teleost, fish species, mainly situated in the Northwest Pacific. It has also been tested for gadoid species in the Celtic Sea (ICES 2020), and scallops around the Isle of Man.

2.1.7 Model 7: Conditional Geostatistical Simulations

2.1.7.1 Model name and reference

Conditional Geostatistical Simulations (CGS) (Petitgas *et al*., 2017; Fernandes and Fallon, 2020).

2.1.7.2 Summary of approach

Geostatistical simulation is an approach to modelling that attempts to reproduce the range of values (fish densities) present in the data, as well as the spatial variability described by the variogram. Instead of producing a single, average case estimate, a geostatistical simulation produces several alternative and equiprobable joint realizations of the local values of a variable of interest. This contrasts with the more common geostatistical estimation procedure, kriging, which does not reproduce local spatial detail (it is unrealistically smooth, despite honouring the sample values). Furthermore, and more importantly, a simulation produces many realizations, which form a statistical distribution of abundance estimates from which, for example, confidence intervals can be determined. They also preserve the variance of the fitted random function model, reproducing the histogram and variogram. Geostatistical simulations can either be conditional, which honour the data values at the datapoints, or non-conditional, which will not. In this case conditional simulations are applied (Petitgas *et al.*, 2017).

2.1.7.3 Response variable error assumption(s) including treatment of 0-observations

The approach transforms the observed density data Z to a normal distribution Y before simulations are realized, by applying a Gaussian anamorphosis and using a Gibbs sampler to simulate values of the Y where Z = 0.

2.1.7.4 Spatial functions and possibility to account for landmasses

The spatial structure is determined through the variogram, which is calculated at various stages to deal with zero inflation. Landmasses may be accounted for, but there are edge effect issues.

2.1.7.5 Sensitivity to unbalanced survey effort in space and time

Not very sensitive, but this remains to be investigated.

2.1.7.6 Standardization between gears

Data from different gears should be standardized, e.g. by expressing density (numbers or weight per unit of sampled [swept] area) before use in the model.

2.1.7.7 Potential use of correlates

Potentially using PluriGaussian simulations.

2.1.7.8 Possible use of the model for forecasting

Has not been tested, but unlikely as there are no predictive variables.

2.1.7.9 Possibility to include more than one life stage

Yes, life stages are simulated separately in this approach.

2.1.7.10 Is the model able to reproduce known operating model distributions when fitted to simulated data?

Has not been tested, but very likely.

2.1.7.11 Is the model implemented in a software package (e.g. R or other)?

R using RGeostats package (Geostatistical R Package - Home (free.fr)).

2.1.7.12 Which species has the model been applied to?

North Sea: Anglerfish, Cod, Haddock, Hake, Plaice, Saithe, Whiting. Western Shelf: Anglerfish, Cod, Haddock, Hake, Rockall Haddock, Saithe, Whiting.

2.1.8 Model 8: LGNB-SDM

2.1.8.1 Model name and reference

LGNB-SDM (Log-Gaussian Negative Binomial Species Distribution Model; Rufener *et al.,* 2021)

2.1.8.2 Summary of approach

LGNB-SDM is a flexible species distribution model (SDM) that can estimate and predict a species' spatio-temporal abundance dynamics based on either survey or survey and commercial fisheries data combined. The model is a state-space model that can be applied to any count-related data (e.g. Nage, Nsize), where both process and observation error are modelled separately. LGNB-SDM is written in C++, implemented in TMB, and wrapped into user-friendly R scripts. The LGNB-SDM integrates observer and survey data addressing several data-related pitfalls in

a unifying framework. As such, it can provide a more detailed understanding of a species' spatio-temporal dynamics.

2.1.8.3 Response variable error assumption(s) including treatment of 0-observations

The LGNB-SDM can be applied to discrete data. The underlying model describing the observations is a Negative Binomial probability distribution, which allows 0-observations.

2.1.8.4 Spatial functions and possibility to account for landmasses

Given the state-space nature of the model, spatial and temporal dependence is accounted for in the process error through a Gaussian Random Field (GMRF) and auto-regressive process of order 1 (AR-1), respectively. A squared grid is used to conduct both abundance estimates and predictions, whereby the spatial and temporal resolution can be tailored according to the case study under concern. The spatial grid automatically avoids landmasses, although the spatial correlation does not account for a proper barrier structure, such as in Bakka *et al.* (2016).

2.1.8.5 Sensitivity to unbalanced survey effort in space and time

The model can address spatio-temporal dependencies simultaneously and can explicitly model the differences in fishing catchability and effort when commercial fisheries data are additionally used. Due to these aspects, unbalanced efforts in both space-time dimensions are intrinsically accounted for by the process error structure. Besides, the degree of preferential sampling (known to occur in the commercial fishery data) can be estimated when integrated into the model formulation.

2.1.8.6 Standardization between gears

The observation (catch) process of the input data source(s) can be affected by different factors, such as catchability and environment. The model can explicitly model differences in catchability and effort, reported as fixed and/or random effects in the model formulation.

2.1.8.7 Potential use of correlates

Besides the catchability and effort-related effects mentioned in the above section, the LGNB-SDM model also allows describing the species abundance dynamics as a function of environmental predictors (e.g. salinity, temperature, oxygen, bathymetry). Environmental effects can be integrated both at the level of species abundance (process error) and catchability (observations), thereby conferring greater flexibility to case-specific applications (details at https://github.com/mcruf/LGNB/wiki/model.R:-section-8).

2.1.8.8 Possible use of the model for forecasting

The LGNB-SDM can be applied to predict a species' abundance both in space and time due to the inclusion of spatial and temporal correlation structures. This means that the LGNB-SDM can be used to predict abundances at unsampled sites and time stamps and for forecasting purposes depending on the use of correlates.

2.1.8.9 Possibility to include more than one life stage

The LGNB-SDM can be applied to either different age groups or size groups and can be further applied to follow cohorts. However, correlation among age/size groups is not accounted for at this stage. Yet, with minimal adaptations, the present model can be extended to a similar structure as in Nielsen *et al.* (2014) to account for correlation among size/age groups.

2.1.8.10 Is the model able to reproduce known operating model distributions when fitted to simulated data?

This aspect has not yet been tested, but there is no practical reason why the model could not be tested on simulated data as long as they follow the model's basic assumptions (e.g. discrete data that are spatially and temporally correlated).

2.1.8.11 Is the model implemented in a software package (e.g. R or other)?

No. However, R scripts and extensive documentation are available at https://github.com/mcruf/LGNB

2.1.8.12 Which species has the model been applied to?

The model was initially applied to different age groups of the western Baltic cod. The LGNB-SDM model was also applied to different size groups of a suite of North Sea species within the NORDFO project, including North Sea cod, Saithe, Haddock, Plaice, Sole, Dab, Sprat, Herring, Whiting, and Mackerel. Additionally, in NORDFO, the model outcomes were then separated into two life stages (juveniles and adults) from the different length groups knowing the sex maturity-at-length specific to species and identified in the literature.

2.1.9 Model 9: sdmTMB

2.1.9.1 Model name and reference

sdmTMB (Anderson *et al*., 2022).

2.1.9.2 Summary of approach

sdmTMB implements geostatistical spatial and spatio-temporal GLMMs using TMB for model fitting and R-INLA to set up SPDE (stochastic partial differential equation) matrices. It provides a fast, flexible, and user-friendly formula interface similar to lme4 and glmmTMB. This, among other things, distinguishes it from the similar R package VAST, which is a popular and powerful tool to model spatial and spatio-temporal data with the SPDE approach.

2.1.9.3 Response variable error assumption(s) including treatment of 0-observations

It includes a wide range of families: all standard R families plus tweedie() (for modelling non-negative continuous data with zeroes), nbinom1(), nbinom2(), lognormal(), and student(), plus some truncated and censored families. The delta/hurdle approach is also implemented.

2.1.9.4 Spatial functions and possibility to account for landmasses

In sdmTMB, barriers and landmasses can be accounted for by adapting the mesh such that the spatial correlation decays faster when crossing the barrier. See this link for an example: https://haakonbakkagit.github.io/btopic128.html

2.1.9.5 Sensitivity to unbalanced survey effort in space and time

Spatio-temporal random fields can be set to follow a first-order auto regressive, AR(1) process or random walk. In the first case, the spatio-temporal random field reverts to the mean in the absence of data, and in the latter the field can change over time.

2.1.9.6 Standardization between gears

Different gear types can be modelled with fixed or random effects.

2.1.9.7 Potential use of correlates

Covariates might be included as:

- linear or polynomial terms
- smooth terms, using the familiar s() notation from mgcv
- breakpoint (hockey-stick) or logistic
- time-varying (coefficients modelled as random walks)
- spatially varying coefficients (typically a non-spatially varying index variable)

2.1.9.8 Possible use of the model for forecasting

Interpolation or forecasting over missing or future time slices can be done, results rely on the structure of the spatio-temporal random field (AR1 or random walk)

2.1.9.9 Possibility to include more than one life stage

Yes, though the models are for univariate response variables

2.1.9.10 Is the model able to reproduce known operating model distributions when fitted to simulated data?

Yes.

2.1.9.11 Is the model implemented in a software package (e.g. R or other)?

The model is implemented as an R package available at https://pbs-assess.github.io/sdmTMB/index.html.

2.1.9.12 Which species has the model been applied to?

- 38 demersal species in the Pacific Northeast [https://doi.org/10.1111/faf.12613]
- 113 groundfish species in British Columbia [https://www.dfo-mpo.gc.ca/csas-sccs/Publications/ResDocs-DocRech/2019/2019_041-eng.html]
- Arrowtooth flounder (*Atheresthes stomias*) [10.1111/ecog.05176]
- Sablefish (*Anoplopoma fimbria*)[10.7717/peerj.12783]
- Atlantic cod (*Gadus morhua*)[https://doi.org/10.1101/2022.04.19.488709]

2.1.10 Model 10: Kriging

This model was added after WKFISHDIS2 meeting and hence not included in model comparisons.

2.1.10.1 Model name and reference

Kriging (Rivoirard *et al.*, 2000).

2.1.10.2 Summary of approach

Kriging, also known as best linear unbiased prediction (BLUP) or best linear unbiased estimation (BLUE) is an interpolation technique that applies [kriging] weights to unsampled locations based on the spatial structure (derived from the variogram or spatial covariance). There are various types, depending on the assumptions of stationarity: ordinary kriging, used here, assumes a constant, unknown mean within the search neighbourhood. Other forms (simple, universal, IRFk, indicator, disjunctive) make other assumptions (e.g. accounting for trend) with different methods to calculate weights.

2.1.10.3 Response variable error assumption(s) including treatment of 0-observations

Presence of many zeros and extreme values can make variogram difficult to model, so log back-transform available (Rivoirard *et al.*, 2000)

2.1.10.4 Spatial functions and possibility to account for landmasses

The spatial structure is determined through the variogram, but rarely account for distances across landmasses.

2.1.10.5 Sensitivity to unbalanced survey effort in space and time

Not very sensitive, but this remains to be investigated.

2.1.10.6 Standardization between gears

Data from different gears should be standardized, e.g. by expressing density (numbers or weight per unit of sampled [swept] area) before use in the model.

2.1.10.7 Potential use of correlates

Extensions include external drift and co-kriging which allow for use of correlates.

2.1.10.8 Possible use of the model for forecasting

Has not been tested, but possible using above extensions.

2.1.10.9 Possibility to include more than one life stage

Yes.

2.1.10.10 Is the model able to reproduce known operating model distributions then fitted to simulated data?

No.

2.1.10.11 Is the model implemented in a software package (e.g. R or other)?

R using RGeostats package (Geostatistical R Package - Home (free.fr)).

2.1.10.12 Which species has the model been applied to?

Herring, blue whiting, cod, haddock, whiting (Rivoirard *et al.*, 2000)

2.1.11 Model 11: Inverse distance

This model was added after WKFISHDIS2 meeting and hence not included in model comparisons.

2.1.11.1 Model name and reference

Inverse distance weighting (Chen *et al.*,2016).

2.1.11.2 Summary of approach

Simple approach that applies weights to unsampled locations based on the distance to the nearest data point. Can have various exponents, the most common being inverse distance squared.

2.1.11.3 Response variable error assumption(s) including treatment of 0-observations

Many studies have compared ordinary kriging (OK) with inverse distance weighting (IDW). There are cases where one outperforms the other (e.g. Weber and Englund 1992), with the chief distinction being how well the spatial structure (i.e. the variogram) can be determined: the better the knowledge of spatial structure the better OK. Both techniques are very common in the environmental sciences, where data are less patchy (fewer zeros) than fisheries data, but there is little in the literature which tests the effect of zero inflation on either method.

2.1.11.4 Spatial functions and possibility to account for landmasses

None.

2.1.11.5 Sensitivity to unbalanced survey effort in space and time

Likely to be sensitive, but this remains to be investigated.

2.1.11.6 Standardization between gears

Data from different gears should be standardized, e.g. by expressing density (numbers or weight per unit of sampled [swept] area) before use in the model.

2.1.11.7 Potential use of correlates

No.

2.1.11.8 Possible use of the model for forecasting

No.

2.1.11.9 Possibility to include more than one life stage

Yes.

2.1.11.10 Is the model able to reproduce known operating model distributions then fitted to simulated data?

No.

2.1.11.11 Is the model implemented in a software package (e.g. R or other)?

R using RGeostats package (Geostatistical R Package - Home (free.fr)).

2.1.11.12 Which species has the model been applied to?

Unknown.

2.2 Expert evaluation of models in relation to the purpose of the group

The workshop participants were split in subgroups to discuss and evaluate candidate models 1 to 9. The outcomes are summed up in Table 2.2.1. All models except two lived up to all of the requirements, and the two models that failed a requirement both failed the need to estimate gear standardization factors. The models differed slightly in their run time and somewhat more in user friendliness. Among the models fulfilling all requirements, the models considered easiest to use were the GAM type models and sdmTMB. sdmTMB run time seemed to be somewhat less than the GAM model run times, but it is not clear if this was a general trait at all complexities.

Model name and reference	Appropriate treatment of skewed data with substantial proportion of zeros?	Appropriate use of explanatory variables?	Possible to standardize between gears in method?	Demonstrated ability to reproduce simulated data?	Implemented in an open source package?	Run time (one species)	User friendlness
1. Approximate Bayesian inference using integrated nested Laplace approximation (INLA)	Yes, the model can cope with it: INLA can use different error distributions	Yes, covariates can be included, although if the Spatial Random Field alone can explain distribution covariates may not add anything to the model	Yes, the model can include random gear effects	Yes, INLA allows for direct simulation from the estimated posterior model, such that we can conduct statistical inferences on more complex functionals of the multivariate predictive distributions	Yes: R-INLA	Medium	Medium
2. Bayesian Additive Regression Trees (BART)	Limited: errors need to be normally distributed and homoscedastic	Yes, covariates can be included. The impact of covariates can also be compared between life stages e.g. adults and juveniles	No, the model is not suitable for multiple gears (unless modelling only presence/absence) and assumes all entries are similar and treats them as such. If using different gear then the data should be standardized before using it in the model	Yes, the performance is comparable and often superior to that of Random Forests	Yes: bartMachine	Short	High
3. GAM model with random effects and train/test approach	Yes, the model can use different error distributions: Gaussian, Tweedie and Binomial	Yes, covariates can be included	Yes, catch rates can be calibrated across multiple gears	Yes	Yes: mgcv	Medium	High
4. GAM model with random effects	Yes, the model can use different error distributions	Yes, covariates can be included	Yes, gear effects can be included?	Yes	Yes: mgcv	Medium	High

Model name and reference	Appropriate treatment of skewed data with substantial proportion of zeros?	Appropriate use of explanatory variables?	Possible to standardize between gears in method?	Demonstrated ability to reproduce simulated data?	Implemented in an open source package?	Run time (one species)	User friendlness
5. Spatio-temporal generalized additive models (GAMs)	Yes, the model can use different error distributions: lognormal, Tweedie and negative binomial	Yes, covariates can be included	Yes, gear category is included as a fixed effect by default	Yes	Yes: surveyIndex and fishdist	Medium	High
6. VAST	Yes, the model can use different statistical distributions	Yes, covariates can be included	Yes, the model can deal with different surveys	Yes	Yes: VAST	Long	Low
7. Conditional Geostatistical Simulations	Yes, by transforming the data to a normal distribution before use in the model	Yes, some covariates can be included	No, the data needs standardized across gears before being used in the model	No	Yes: Rgeostats	Medium	Medium
8. LGNB-SDM	Yes, by using a negative binomial distribution	Yes, covariates can be included	Yes, the model can include gear as fixed and/or random effects	Yes	No, but R scripts and documentation are publicly available on github	Medium	Medium
9. sdmTMB	Yes, the model can use a wide range of different statistical distributions	Yes, covariates can be included	Yes, gears can be modelled as fixed effects	Yes	Yes: sdmTMB	Short	High

3 ToR b: Best practice guidance for model structure to derive distribution maps

Consider best practice guidance for model structure to derive distribution maps including but not limited to the choice of response variable, error distribution, selection of area/data based on available non-zero observations, inclusion of landmasses, survey effort and gear standardizations and the use of correlates (Science Plan codes: 4.2);

3.1 Best practice for data

A first requirement for producing reliable maps of species distribution is that the data used are correctly recorded and prepared. This includes cleaning the data for errors, considering major sources of changes to catchability, designation of land areas, decisions on whether to exclude parts of the dataset and attaining information on appropriate covariates to include in the model.

Correcting or removing erroneous observations continue to be a major task when using the DATRAS data. Changes in species codes over time or between areas must be checked for as these may greatly, and erroneously, affect the distribution. If discrepancies are found, the cause of these should be identified and corrected prior using the data in models. The estimation of swept-area is a major task, particularly in the Baltic where data are sparse, and estimates require filtering to remove unrealistically high swept-areas.

Large changes in haul times (e.g. halving haul time) within a survey time-series may affect catchability and if possible, should be considered. Likewise, the timing of the hauls (i.e. day/night, or dawn/dusk) is likely to have an effect on catchability and may need to be considered in a site-specific way or accounted through an explicit daytime or sun height effect in the modelling approach. Lastly, size is an important factor in both distribution (e.g. ontogenetic deepening) and catchability (e.g. larger individuals swimming faster with a higher chance of escaping). Preferably, this should be addressed directly unless the species is so rare that it leads to unacceptable proportion of zero catches. Using biomass rather than numbers can to some degree alleviate the influence of juveniles on the distribution maps. Modelling approaches that allow for a size-based approach (i.e. separate size classes) may be preferable if size information of sufficient quality and consistency is available.

Land should be excluded to avoid models fitting distributions across landmasses, an issue that is mainly relevant when using models that include spatial correlation. Also, the modelled area should be species-specific, as few species occur in all areas. However, zero values in the data (i.e. a species not observed in a haul in an area or time where it is observed at other times or by other vessels) should not be excluded within the modelled area, as these provide information on locations where a given species is absent, and therefore on a species overall density. Depending on the species modelled, depths where the species in question is never observed (i.e. outside normal habitat) can be excluded from the data to decrease model run time and avoid unrealistic distributions being estimated. Likewise, it may be wise to exclude poorly sampled areas or seasons, gears with very few positive observations and/or time slots in order to avoid spurious results.

"Grooming" the data prior to use in the model should be considered to improve model convergence. For example, gears or survey areas with no observations of a species should be excluded before fitting the model as these can hamper model convergence and increase run time without

improving the knowledge of a species' distribution. It is preferable to assume that the area does not contain the species or that the species catchability to a given gear is very low. Not removing combinations with no observations will still, in most cases, result in a converging model but the associated predicted densities will be very uncertain in areas and gears with few or no observations of the species. For rare species, the data will naturally include many zero values, but these do not really provide information on distribution and increase model run times.

Lastly, the data should include appropriate explanatory variables to explain the distributions observed. At the very least, the gear employed and trawling distance/time (or if available, swept-area) should be included in the data in order to have a gear effect in the model and allow the full use of all survey data as well as future data from fisheries observer programmes. Further, where more than one season is sampled, this effect should be explicitly considered together with differences between years unless this is not possible due to extreme sparsity of positive catches as can be the case for very rare species. Species distribution modelling can potentially benefit greatly from including relevant environmental variables, such as bottom depth, bottom substratum, temperature, etc. as they typically constrain the range of a species.

In accordance with these guidelines, the DATRAS data were preprocessed as described in section 3.1.1.

3.1.1 Data preprocessing

3.1.1.1 Species misidentification

A number of species are not reliably determined to species level or are identified only to family or genus level. Species sometimes registered only to family or genus level in DATRAS data include *Raja* sp/Rajidae, *Lophius* sp/Lophidae and Phycidae. In the DATRAS data from 1983 onwards, recordings of *Raja*/Rajidae larger than 5 cm occur in 55 hauls in the total of 88469 hauls (0.06%). The other two families/genera mentioned occur in 14 and 18 hauls, respectively. There are additional examples where only one species is recorded in the genus/family (e.g. *Conger* sp.). These can reliably be reassigned to species level. WKABSENS (2021) recommended not to reassign species from genus to species levels in cases where more than one species occurred in the data as the number of cases was small. WKABSENS also recommended using both misrepresentations and correct representations. WKSKATE (2021) suggested excluding individuals smaller than 5 cm and this procedure was also followed in WKABSENS and should preferably also be followed in WKFISHDIS2.

3.1.1.2 Estimation of number caught per haul

Analysing data from surveys requires knowledge of the data as well as decisions in cases of apparently conflicting information. To estimate the number caught per haul of each of the species from DATRAS data, the following steps should be conducted:

1. Download ICES DATRAS data (HH and HL) (WKABSENS notes that there was an error in the column names of the surveys SP-PORC year 2016 and SWC-IBTS year 1987 which should be corrected if still present)
2. Create a unique Haul-ID: Survey * Year * Quarter * Country * Ship * Gear * StNo * HaulNo
3. Remove hauls with duplicated ID's in HH (differences in WindSpeed)
4. Remove hauls if haul-ID is not in HL (no length or number data available for the haul)
5. Merge HH and HL and SweptArea index based on Haul-ID
6. Predict StatRec from latitude and longitude if NA
7. Use gear categories for gear (see section 1.4)
8. Only keep hauls that fulfil the criteria:
    a. HaulVal == ("V", "A")

   b. StdSpecRecCode == 1
   c. SpecVal ∈ (1,4,7,10)
   d. Lat != NA & Lon != NA
9. Combine Scottish surveys and Rockall surveys (corrections of catch rates are later estimated based of differences in gear code):
   a. SCOWCGFS → SWC-IBTS
   b. SCOROC → ROCKALL
10. Convert -9 to NA
11. Assign species to AphiaID
12. Combine AphiaIDs for species were several AphiIDs are observed (see section 1.4).
13. Remove hauls based if species are not recorded according to bycatch and standard species codes (e.g. in some NS IBTS hauls prior to 1991)
14. Remove hauls from BITS survey that use different gears than TVS or TVL and remove hauls from NIGFS survey that occurred before 2007 due to inconsistent sampling
15. Create dummy dataset with N = 0
16. Subset data based on AphiaID list in table 2.1
17. Estimate numbers (Count)
   a. If HLNoAgeLngt == NA, use TotalNo and set SubFactor = 1
   b. Multiplier = HaulDur/60 if DataType ∈ ("C")
   c. Multiplier = SubFactor if DataType ∈ ("S","R")
   d. Count = HLNoAtLngt * Multiplier
18. If desired, divide individuals into juveniles and adults based on length at 50% maturity (see section 1.4)
19. N = sum Count for Haul-ID and round

Data from the MEDITS survey in the Mediterranean were used merging the files TA (haul data), TB (number and weight by species) and TC (length, sex and maturity by species) (AA. VV., 2017; Spedicato *et al.*, 2019).

3.1.1.3 Criteria for excluding surveys

Surveys which have never caught a certain species should be excluded from all analyses of that species as they give estimation issues. Furthermore, WKABSENS recommended excluding surveys with less than five years of data from further analyses. For DATRAS, this means the exclusion of the Deep water survey (four years of data), Irminger Sea International Deep pelagic survey (one year of data) and the Norwegian Sea International Deep pelagic survey (four years of data). Further, the Canadian Maritimes Trawl Survey was excluded by WKBSENS as the spatial coverage is far from the other surveys. A list of the years and surveys included by WKABSENS using these criteria is given in Table 3.1.1.1. The coverage of the surveys can be seen in Figure 3.1.1.1.

Table 3.1.1.1. List of the years and surveys included by WKABSENS.

Survey	Quarter	Years
BITS	1	1996-2020
BITS	4	1999–2020
BTS	1	2006–2020
BTS	3	1985–2020
BTS	4	2006–2020

Survey	Quarter	Years
DYFS*	3	2002–2020
DYFS	4	2002–2020
EVHOE	4	1997–2020
FR-CGFS	4	1998–2020
IE-IGFS	4	2003–2020
NIGFS	1	2006–2020
NIGFS*	4	2006–2020
NS-IBTS	1	1967–2020
NS-IBTS	3	1991–2020
PT-IBTS*	4	2002–2018
ROCKALL*	3	1999–2020
SNS*	3	2002–2020
SNS*	4	2004–2019
SP-ARSA*	1	1996–2020
SP-ARSA*	4	2002–2020
SP-NORTH*	3	2001–2010
SP-NORTH*	4	1990–2020
SP-PORC*	3	2001–2020
SP-PORC	4	2003–2007
SWC-IBTS	1	1985–2020
SWC-IBTS	2	1995–1995
SWC-IBTS*	4	1990–2020

∗ Missing years

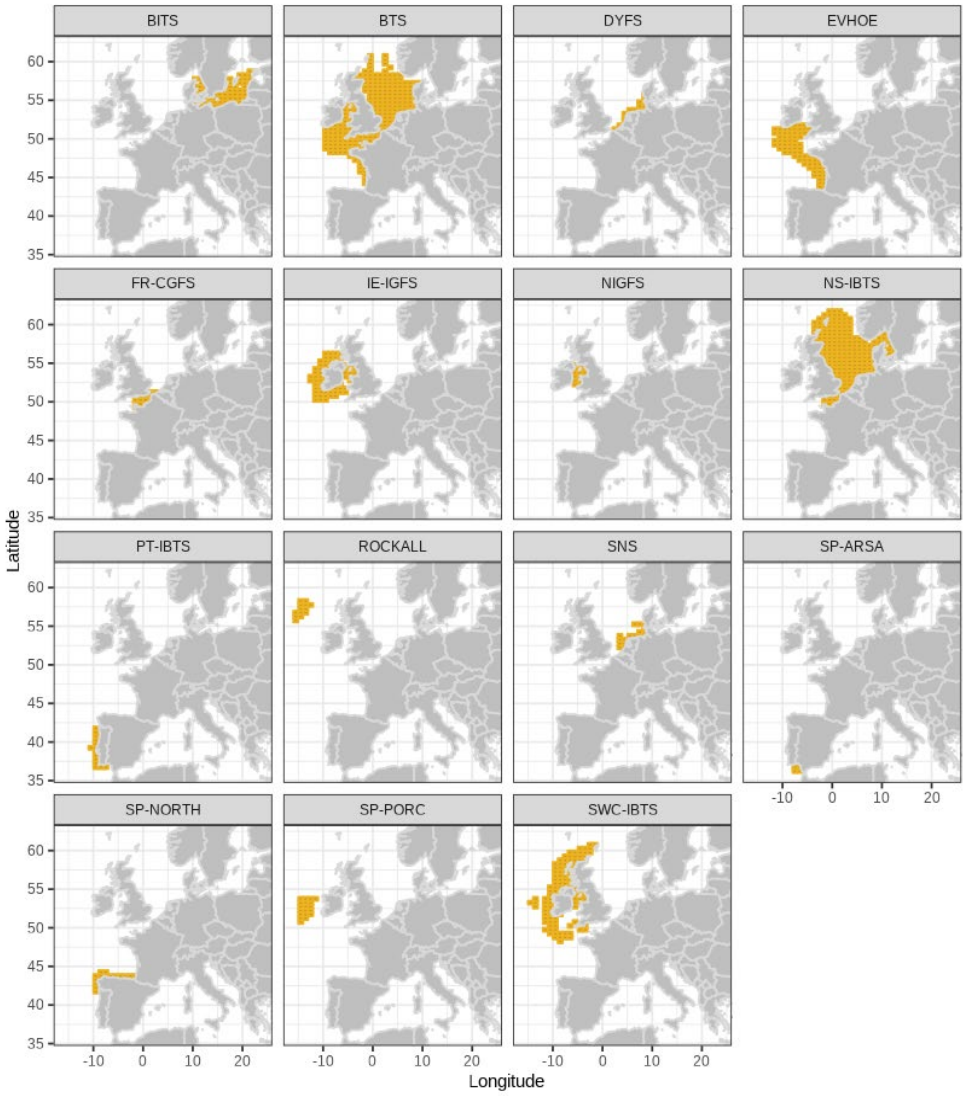

Figure 3.1.1.1. Spatial coverage of the surveys included.

3.1.1.4 AphiaID corrections

Some species are classified with more than one AphiaID. Examples of such species are given in table 3.1.1.2. Others can be added as discovered.

Table 3.1.1.2. Species registered with more than one AphiaID

Species	AphiaID	Comment
Alosa spp.	125715 416357 126413 126415	Uncertain species ID, combined into *Alosa* spp. by WKABSENS
Amblyraja radiata	105865 148824	Some reports of misidentification issue with *R. clavata*
Anarhichas lupus	125912 126758	

Species	AphiaID	Comment
Anguilla anguilla	125620 126281 125425	
Chelidonichthys lucerna	127262 274877	
Conger conger	125624 126285 125427	
Coregonus spp. (excluding *C. oxyrhinchus*)	127178 127180 126139	Combined by WKABSENS
Deania calcea	105903 105905	Not distinguished from *D. profundorum* (105905) prior to 2002 (Portuguese surveys)/2012 (Spanish surveys) so the two species are combined (WKABSENS)
Dipturus batis complex	105762 105869 148868 711847 711846	Uncertain ID, WKABSENS combined *Dipturus*, *D. batis*, *D. flossada* and *D. intermedia* in abundance indices.
Dipturus oxyrinchus	105872 293392	
Galeus melastomus	105812 105811	Uncertain species ID between *G. melastomus* and *G. atlanticus* (105811) hence the two species are joined by WKABSENS
Mustelus spp.	105732 105821 105822	Uncertain species ID, WKABSENS combined *M. mustelus* and *M. asterias*. Some reports of identification issues with *Galeorhinus galeus*
Petromyzon marinus	101169 101174 101163	
Phycis blennoides	125475 126501	
Raja brachyura	367297 105882 271509	Including misclassified *Bathyraja brachyurops*. Some reports of misidentification issues with *R. montagui*

Species	AphiaID	Comment
Rajella lintea	105870	
	1019591	
Salmo trutta	127187	
	223866	
Scophthalmus maximus	127149	
	154473	
Scyliorhinus canicula	105814	
	399562	
Sebastes marinus/mentella/norvegicus	127253	Uncertain species ID, WKABSENS combined with *S. marinus, S. mentella* and *S. norvegicus*
	127254	
	151324	
Squalus acanthias	105923	
	160604	
	160616	
Synaphobranchus kaupi	126328	
	125436	
Tetronarce nobiliana	321911	
	157868	
	321911	

3.1.1.5 Gear effects

There are both differences and similarities between the gears used and reported in survey databases. In some cases, the differences are related mainly to scaling of the gear (e.g. TVS and TVL in DATRAS) whereas in other cases, the differences are substantial (e.g. between beam trawl and demersal trawl). WKABSENS derived an approach that takes advantage of knowledge that some gear types are more similar than others. The group divided the DATRAS gear into categories with the assistance of Rob Kynoch and Finlay Burns (Table 3.1.1.3).

The DATRAS trawls were categorized based on the information on trawl height and ground contact under the assumption that wing spread swept-area is accounted for separately in the model:

a) Beam trawls can be grouped together. They are similarly rigged but will differ by swept-area, which is dictated by beam length. Beam trawl headline would be around 0.6m and the low headline trawls ~ 2.5–3 m and therefore are a separate category;
b) GOV gear can be split into two categories: clean gear and rock-hoppers/bobbins;
c) Herring bottom opening trawls can be grouped into the GOV type A gears. These were nets used in IBTS prior to standardizing in 1982. Given their similar properties to the GOV (i.e. high opening), it's likely there was agreement to move from herring trawls to GOV;
d) Norwegian Campell trawl is also a high headline height so can also be grouped into GOV type A gears;

e) Baka trawls are low headline nets, ~ 2.5m compared with the ~ 5.5m of GOVs. The exception is the Porcupine baka, which has a higher headline;
f) Foto midwater is a pelagic gear. 'Pelagic trawlnet Kabeljaubomber' is also classified as pelagic though there is no detailed information on this gear available;
g) Old gears are grouped together with unknown bottom trawls: Granton, Vinge, bottom trawl FGAV019 and Sov-Net.
h) This resulted in the groupings in Table 3.1.1.4.

In the MEDITS survey in the Mediterranean a gear designed following the same common scheme GOC 73 has been used since the start of the survey in 1994 (AA. VV., 2017; Bertrand *et al.*, 2002). The data on wing opening and haul duration for the computation of the swept-area in the investigated geographical subareas (GSA according to GFCM classification) is included in the TA file.

Table 3.1.1.3. Gear categories.

Gear category	Description
BT	Beam trawls
TV	TV-3 trawl used in BITS
GOV CL	Demersal trawl with clean gear and high headline net: herring bottom trawls, GOV with groundgear A, porcupine baka
GOV GG	Demersal trawl with rock-hoppers or old bobbin disks and high headline net: GOV used in Scottish surveys above 57.5 and in Irish surveys, Norwegian Campbell
BAK CL	Demersal trawls with clean gear and low headline net: baka trawls
BAK GG	Demersal trawls with rock-hoppers/bobbins and low headline net: Aberdeen 48 foot
PEL	Midwater and pelagic trawls with limited bottom contact: Foto midwater and 'Pelagic trawlnet Kabeljaubomber'
OTT	Remaining trawl types

Table 3.1.1.4. Gear categories to be used in analysis.

Survey	Gear	Gear name	Gear category	Notes and references
BITS	TVL	Large TV Trawl	TV	A type of TV-3 trawl, with 930 meshes in circumference, for vessels with engine more than 600 KW. Denmark added a stone panel. On Latvian surveys the TVL is used with rock-hopper. (ICES, 2014)
BITS	TVS	Small TV Trawl	TV	A type of TV-3 trawl, with 520 meshes in circumference, for vessels with engine less than 600 KW. (ICES, 2014)
BTS	BT4	Beam Trawl 4 m	BT	UK-Cefas and Iceland 4-m beam trawls have a flip up rope, while Belgium 4-m beam trawl has no flip-up rope. (ICES, 2019f)
BTS	BT4A	Four m Beam trawl, aft	BT	(ICES, 2019f)
BTS	BT4AI	Four m Beam trawl, aft - in IrishSea q3 BTS	BT	(ICES, 2019f)
BTS	BT4P	Four m Beam Trawl, port	BT	(ICES, 2019f)
BTS	BT4S	Four m Beam Trawl, starboard	BT	(ICES, 2019f)
BTS	BT7	Seven m Beam trawl	BT	Ticklers. (ICES, 2019f)
BTS	BT8	Eight m Beam trawl	BT	Flip up rope, ticklers. (ICES, 2019f)
DYFS	BT3	Beam Trawl 3 m	BT	Beam trawls but these are shrimp trawls. Demersal Young Fish survey, so are gear more tailored to smaller fish (ICES, 2021b).
DYFS	BT6	Beam Trawl 6 m	BT	Beam trawls but these are shrimp trawls. Demersal Young Fish survey, so are gear more tailored to smaller fish (ICES, 2021b).

Survey	Gear	Gear name	Gear category	Notes and references
EVHOE	GOV	GOV Trawl	GOV_CL	Without exocet Kite which is replaced by 6 additional floats (ICES, 2010).
FR-CGFS	GOV	GOV Trawl	GOV_CL	Double sweeps (Moriarty *et al*., 2020).
IE-IGFS	GOV	GOV Trawl	GOV_GG for Irish West Coast Groundfish Survey (covering ICES Division VIa (south) and VIIb (north), VIIb and VIIj); GOV_CL for Irish Sea and Celtic Sea covers ICES Division VIIa and VIIg	Standard GOV survey gear (ICES, 2010; 2015; Moriarty *et al*., 2020).
NIGFS	ROT	Rock-hopper otter trawl	GOV_GG	Double sweep with 16-inch bobbins (ICES, 2010; Moriarty *et al*., 2020).
NS-IBTS	ABD	Aberdeen 18 ft trawl	BAK_GG	Used to collate info on age-0 fish so presumably effective at catching small fish
NS-IBTS	BOT	Bottom Trawl	OTT	
NS-IBTS	DHT	Dutch Herring Trawl	GOV_CL	
NS-IBTS	FOT	Foto midwater trawl	PEL	
NS-IBTS	GOV	GOV Trawl	GOV_CL	
NS-IBTS	GRT	Granton trawl	OTT	
NS-IBTS	H12	Herring Bottom Trawl 120 feet	GOV_CL	
NS-IBTS	H18	Herring Bottom Trawl 180 feet	GOV_CL	
NS-IBTS	HOB	High Opening Bottom Trawl	GOV_CL	
NS-IBTS	HOB	High Opening Bottom Trawl	GOV_CL	

Survey	Gear	Gear name	Gear category	Notes and references
NS-IBTS	HT	Herring Bottom Trawl	GOV_CL	Designed for herring. Used in International Young Fish Survey (ICES, 1999).
NS-IBTS	KAB	Pelagic trawlnet Kabeljaubomber	PEL	
NS-IBTS	SOV	SOV-NET	OTT	
NS-IBTS	VIN	Vinge trawl	GOV_CL	International Young Fish Survey (ICES, 1999)
PT-IBTS	CAR	Bottom trawl FGAV019	CAR	Without rollers in the groundrope. https://datras.ices.dk/Home/Descriptions.aspx
PT-IBTS	NCT	Norwegian Campell Trawl 1800/96	GOV_GG	Groundrope with bobbins, with a 20 mm codend mesh size. https://datras.ices.dk/Home/Descriptions.aspx
ROCKALL	GOV	GOV Trawl	GOV_GG	
SCOROC	GOV	GOV Trawl	GOV_GG	(ICES, 2017) https://www.ices.dk/data/Documents/DATRAS%20Manuals/Survey%20design%20for%20ROCKALL%20and%20SWC-IBTS.pdf
SNS	BT6	Beam Trawl 6 m	BT	
SP-ARSA	BAK	Baka trawl	BAK_CL	International Young Fish Survey (ICES, 1999)
SP-NORTH	BAK	Baka trawl	BAK_CL	International Young Fish Survey (ICES, 1999)
SP-PORC	PORB	Porcupine Baka	GOV_CL	With a footrope and a headline, codend is 20mm
SWC-IBTS	GOV	GOV Trawl	GOV_GG if above 57.5 lat; GOV_CL if below 57.5	

3.1.1.6 Dividing individuals into juveniles and adults

Individuals can be divided into juveniles and adults in several ways. A general approach which can be used for all species is to use the length at 50% maturity (L_{mat}) as a knife edge cutoff for mature fish. If needed, individuals smaller than the length at 50% maturity can be divided into early and late juveniles using the cutoff $0.5L_{mat}$. Length at maturity is available for all fish species in DATRAS is derived from Rindorf *et al.* (2021). For red mullet in the Mediterranean adults were separated using a cut-off of 11 cm total length that is the Minimum Conservation Reference Size (MCRS) and coincident with the size at 50% maturity estimated in the Data Collection Framework for the investigated GSAs.

3.2 Best practice for models

3.2.1 Accommodating statistical properties of data

Survey catch data often hold many zeros as well as occasional very high values (skewed distributions with substantial probability of attaining zeros). This characteristic should be accommodated by using appropriate treatment of skewed data with substantial proportion of zeros, for example by exploring different statistical error distributions. Commonly used statistical distributions include hurdle/delta distributions where the probability of non-zero catches are modelled as a binomial distributed variable and the number or biomass caught in non-zero hauls as e.g. lognormal, gamma or other skewed distributions. Hurdle/delta models do not intrinsically link the probability of attaining a non-zero catch to the catch in non-zero catches, which may make interpretation of parameter estimates derived from the model somewhat more complicated (e.g. the effect of depth is the combined effect of both submodels). Models with intrinsic links between the probability of non-zero catches with the number or biomass in non-zero catches include the negative binomial and Tweedie distributions. Distributions which are considered inappropriate due to their sensitivity to occasional high catches and substantial proportions of zeros include Poisson and normal distributions, as well as distributions assuming normal distribution of transformations such as square root and log(observation+1) transformed data.

3.2.2 Model quality control

The models should have demonstrated ability to reproduce distributions from data simulated from known distributions. Useful metrics of model performance can be derived from e.g. Zuur *et al.* (2016). To allow full transparency and validation, the model code should be implemented in an open-source package, preferably organized in an easy to use and stable package format.

3.2.3 Model complexity

Statistical models should be designed for the required purpose, with appropriate consideration of the run- and handling-time of different complexity models. While it is important to cover all potential causes of dependence in the survey data, higher complexity models will undoubtedly require considerable computing power and user resource, thus compromises are often required. Run-times have improved with technological advances, but when making comparisons between models, different methods and computer specifications may interact with model complexity in unpredictable ways. Using parallel cores is one way to address this, but even with this expansion, models of high complexity (many grid points, many years, many other variables to account for statistical distributions like negative binomial that take longer to fit) are slow to run and if complexity increases in one part of the model, model simplifications will have to be made in another to keep run times reasonable.

The aim in WKFISHDISH2 was to use models that have a large spatial and temporal coverages, encompassing as much of the available data as possible. It is likely that slight differences in the model predictions will be observed if the models are tailored to less complex situations (i.e. fewer years or smaller areas). To avoid spurious conclusions, it is also advisable to avoid extrapolating the model to areas or depths where the species is not observed (i.e. far from species observations). Utilizing existing knowledge of the species when setting up the model to detect errors in the data and deciding the modelling area a priori is recommended. Note that predicted density is specific to the gear/ time for observer data used as reference, so gear/time should be clearly stated. Estimating absolute abundance can be done as explained by Walker *et al.* (2017).

3.3 Best practice for validation of model specific fits

Relevant diagnostics of model fits include residual plots against included and excluded variables, QQ plots, cross validation (train/test removing 30% for test), correlations of residuals in space and time (look at residuals in space and time) and investigations of sensitivity of results to gear or knot assumptions. An additional diagnostic can be the observed vs. the simulated mean and/or frequency of zero observations. When interpreting residual plots, remember that raw residuals may be biased and OSA/simulated residuals therefore preferable for complex mixed models.

Relevant approaches to reducing models of a specific type (model selection within model type) include investigations of the deviance explained, AIC/DIC, RMSE, Mean absolute error and model specific diagnostics. Remember to include investigations of the effect of the number of knots, as knot number is a trade-off between running time and flexibility. Remember that models can always be improved. The models used in WKFISHDISH2 are best available given the limited time of the workshop.

3.4 Metrics to compare distributions from different models

A variety of metrics of difference between spatial distributions were discussed as well as desirable properties of such metrics (Table 3.3.1). With this in mind, the group decided to use an integrated indicator, the SPAtial EFficiency metric (SPAEF) of Koch *et al.* (2018) as well as indicators of the difference in spatial shifts and core areas. Before estimating the indicators, densities deemed to be highly uncertain (estimated CV> model specific limit) were removed.

Table 3.3.1. Differences which the model comparison should and should not reflect

Should reflect	Should not reflect
Differences in the location of high- and low-density grid points	Differences in the mean as these may be caused by differences in model approaches to bias correction
Differences in the variation in density between grid points	Differences in the mean in locations with high uncertainty in the prediction (CV > model specific limit)
Differences in the frequency of high- and low-density grid points	
Differences related to spatial shifts (e.g. individuals found further north or in deeper water in one model than in another)	
Differences in the extent of high-density/core areas	

SPAEF (Koch *et al.*, 2018) combines differences in three aspects: the Pearson correlation coefficient between density grid values predicted by two models (α), the coefficient of variation of density between grid values of one model divided by that of the other (β), and the histogram overlap between the grid values predicted by one model and that predicted by the other model

(γ). These three aspects reflect the degree to which models agree on the location of high- and low-density grid points, the variation between grid points and the probability density of different densities. The three aspects are combined in the indicator SPAEF as:

$$\mathrm{SPAEF}^{*} = \sqrt{(\alpha - 1)^2 + (\beta - 1)^2 + (\gamma - 1)^2}$$

SPAEF* is modified slightly from the original indicator to take values between 0 and ∞. It takes the value 0 when the predicted distributions agree completely and ∞ when the predicted distributions disagree completely.

Differences between models related to spatial shifts (e.g. individuals found further north or in deeper water in one model than in another) were analysed by estimating the centre of gravity in latitude, longitude and depth for each model in each year and then the ratio between the centre estimated by the two models. Differences in aggregation were investigated by estimating the minimum area containing 90% of the density and then calculating the ratio between the estimates from different models.

All indices were estimated by year and combination of models for each of the species analysed.

In addition to these comparisons, the estimated relative effects of the main gear types were also compared (e.g. TV relative to GOV-CL for cod).

4 ToR c: Implementation of best practice approaches to produce distribution maps

Implement best practice approaches to produce distribution maps and define and establish an efficient and transparent approach to producing updates of these maps (Science Plan codes: 4.2);

Among the models listed in section 2, seven were used in WKFISHDISH2 to predict the distribution of at least one species. The model configurations are described below in section 4.1 and methods used in the comparison of predicted distributions between models are described in section 4.2.

The presence of experts on a wide variety of models at WKFISHDISH2 provided a unique opportunity to compare the output from different models to determine if the choice of models presents a major structural uncertainty in the estimation of distributions of different species. To conduct this comparison, the workshop identified five species of interest. The species were chosen to represent species with a wide distribution across several survey areas in the east-west or north–south direction and abundant and less abundant/rare species. The five species chosen were red mullet, hake (all areas), cod, conger eel and turbot. The latter two are the less abundant species. The species were divided into juveniles and adults before analyses using either length at 50% maturity (Atlantic) or Minimum Conservation Reference Size (Mediterranean).

4.1 Model configurations, diagnostics and validation used to predict distributions

4.1.1 Model 1: Approximate Bayesian inference using integrated nested Laplace approximation (INLA)

The INLA model was applied first to adult cod biomass. For the adult cod, there was data available from surveys using seven different gears. The Tweedie distribution was chosen as the likelihood family for modelling the catches. This distribution has two parameters, p and Dispersion, that were estimated in INLA as hyperparameters. The model had a log link. To account for the effect of swept-area on the catches, swept-area was added to the model as offset after log transformation. This log transformation was needed because of the log link in the model. The resulting offset implies that catches proportionally increase with offset.

To account for the effect of gear on the catch efficiency (and thus the relationship between local abundance and catch), the gear was added to the model as a fixed effect. The effect of depth on the local abundances was modelled as a second order random walk of square-root transformed depth. To allow for trends in global fish biomass over time, the year in which the haul was done entered the model as a second order random walk. The parameters describing the distribution of the second order increments are estimated as hyperparameters of the precision of a normal distribution.

The variance in spatial distribution of catches that was not explained by the depth effect was modelled using spatially correlated gaussian random field. This approach required a mesh of vertices (Figure 4.1.1.1). The final mesh has 1377 vertices. This size was chosen to be sufficiently

fine-scaled for allowing appropriate estimates of spatial correlation while being sufficiently course-grained to have model runs within one hour.

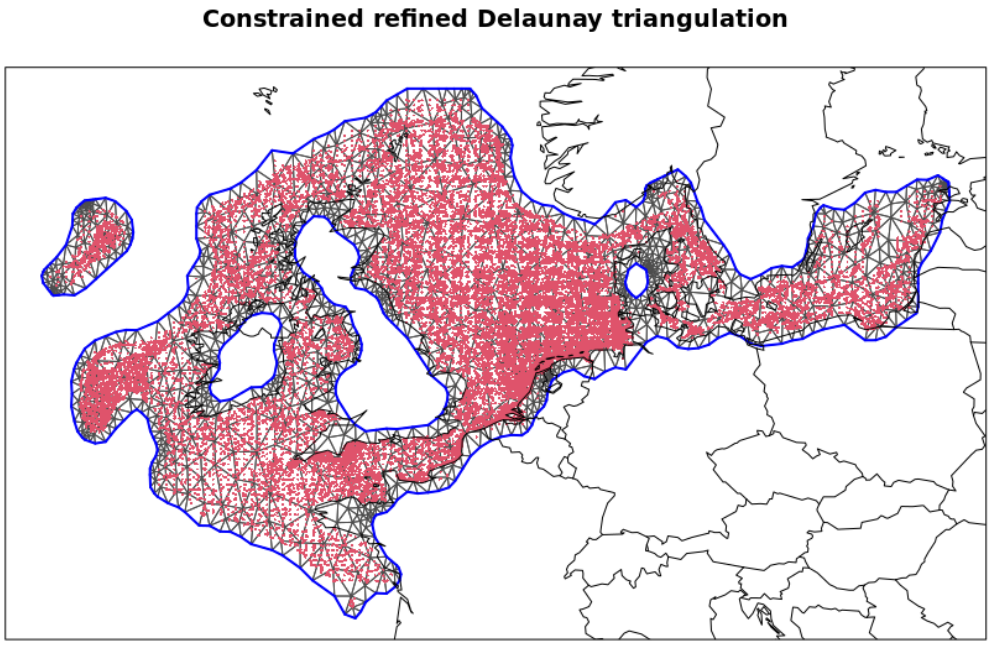

Figure 4.1.1.1. Mesh used for the INLA approach. The mesh is bounded by the blue polygon. Red dots within the mash depict the hauls and the prediction grid.

The INLA model was built in three steps, to compare the effects of long-term and seasonal changes in the distribution of the species. First, a model was tested where the spatial correlation in observations was included without any temporal effect on this spatial distribution. Then, to allow for changes in the spatial distribution over time, the spatial gaussian random field was modelled to change over the years as an autoregressive AR1 process. The 1d mesh over the years that allows for this modelling has a single node for every third year in the time-series. Finally, a second AR1 process was included, but this time for the four seasons in which the surveys are categorized.

From these models, predictions on the prediction grid used for the workshop were generated by taking 500 samples from an approximated posterior of a fitted model, and taking the values estimated by the model for each grid cell, season, gear type and year for each sample. Means, SDs, and CV values can then be calculated from the 500 drawn estimates.

INLA modelling was done using the experimental mode of INLA version 21.11.22 in R 4.1.2.

4.1.1.1 Results

The p parameter for the Tweedie distribution was estimated to be 1.61, and the dispersion parameter was estimated to be 58.35 (Table 4.1.1.1).

Table 4.1.1.1: estimates of hyperparameters for the INLA model for adult cod biomass. Estimates of mean and SD are given, as well as 0.025, 0.5, and 0.975 quantiles. The precision for the square root of depth was 49.96, while the precision for the random walk of year of the observation was 61.69.

	mean	sd	0.025quant	0.5quant	0.975quant
p parm Tweedie	1.61	0.0012	1.61	1.61	1.62
Dispersion parm Tweedie	58.35	0.1831	57.98	58.35	58.71
Precision for sqrtDepth	49.96	10.3508	31.88	49.01	73.65
Precision for Year	61.69	14.5850	38.56	59.63	97.48
Theta1 for w.y	-1.10	0.0389	-1.18	-1.10	-1.02
Theta2 for w.y	-0.51	0.0343	-0.58	-0.51	-0.44
GroupRho for w.y	0.94	0.0062	0.92	0.94	0.95

A closer look at the estimates for the individual gears reveals that the BT gear category had the lowest gear efficiency, being (((1- exp(-2.142))*100%=) 88% lower than the BAK_GG reference gear (table 4.1.1.2). While the mean gear efficiency of the gear with the highest gear efficiency, being GOV_CL, was estimated to be ((exp(0.457)-1)*100%=) 58% more efficient, credible intervals for this estimate crossed zero, suggesting that this estimate is quite uncertain.

Table 4.1.1.2: estimates of gear effects for the INLA model for adult cod biomass. Note that the BAK_GG gear type is in the intercept. Hence these is no estimate for this gear type presented. Estimates of mean and SD are given, as well as 0.025, 0.5, and 0.975 quantiles as:

	mean	sd	0.025quant	0.5quant	0.975quant
fGearBT	-2.142	0.304	-2.7384	-2.142	-1.545
fGearGOV_CL	0.457	0.276	-0.0852	0.457	1.000
fGearGOV_GG	0.101	0.357	-0.6006	0.101	0.801
fGearTV	-0.127	0.369	-0.8502	-0.127	0.596

The second order random walk of the catches over the year suggests a period with great uncertainty about this trend at the beginning of the time-series, in the period 1965- 1980 (Fig 4.1.1.2, marginal effects year rw). From the 1990s onwards there is a downward trend into the 2000s. The effect of depth on catches has a "dome shape", where there seems to be an optimum depth for cod catches around 150 meters depth.

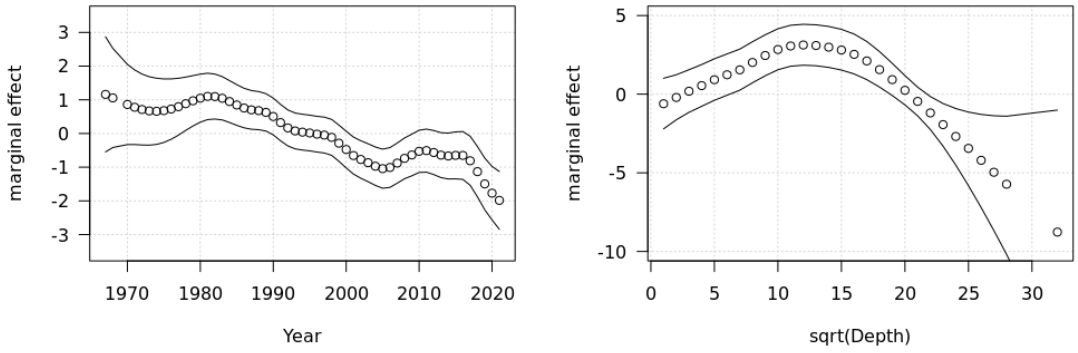

Figure 4.1.1.2. Marginal effect of the year on the adult cod biomass (left panel) and marginal effect square root transformed depth (right panel). Dots indicate means, lines indicate the credible intervals.

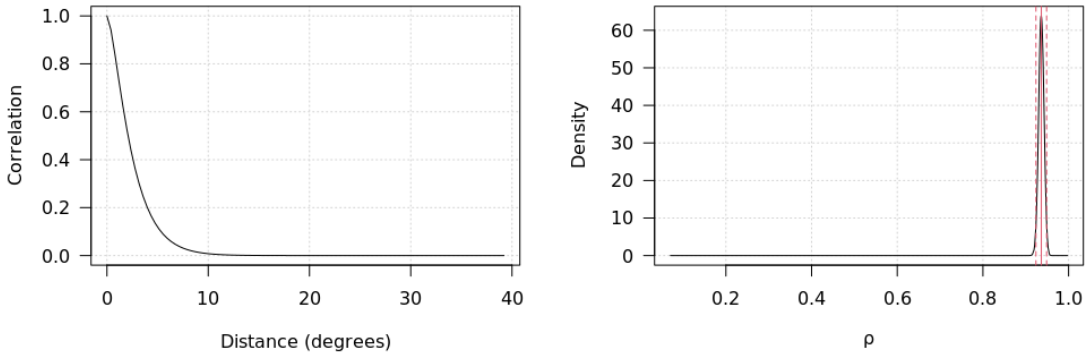

Figure 4.1.1.3. Correlation as a function of distance in the observations, following the Matérn correlation function (left panel). Density distribution of rho estimate (right panel). Vertical lines indicate mean and credible intervals in the right panel.

The catches are clearly spatially correlated. The range of the correlation, where the correlation is approximately 0.1, is about 4.7 degrees (Figure 4.1.1.3). Meanwhile, although there are clear changes in the distribution of adult cod biomass observed, these changes have occurred gradually: the rho parameter in the AR1 process describing the changes in the spatial distributions over the years is estimated to be 0.94.

The gradual change in the spatial distribution can be seen in Fig 4.1.1.4. The posterior mean of the spatial random field depicts only the change in the relative distribution: the long-term changes in the overall abundance are estimated in the second order random walk for year. The precision of the estimates should be considered, however, and these are seen in Figure 4.1.1.5. The standard deviation of the spatial random field shows is high for areas and years where survey information is lacking, for instance on the Porcupine bank in the 1960s and 1970s.

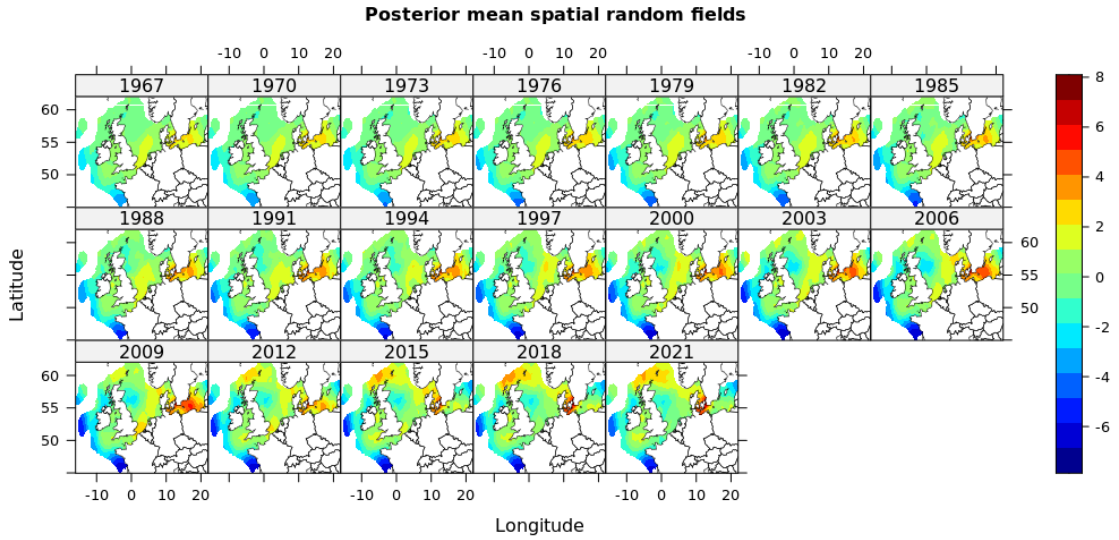

Figure 4.1.1.4. Posterior mean of the spatial random field of the INLA model for adult cod biomass. Note that the posterior means are given only at the 1d mesh nodes that were used to model the changes in the spatial random field as an AR1 process.

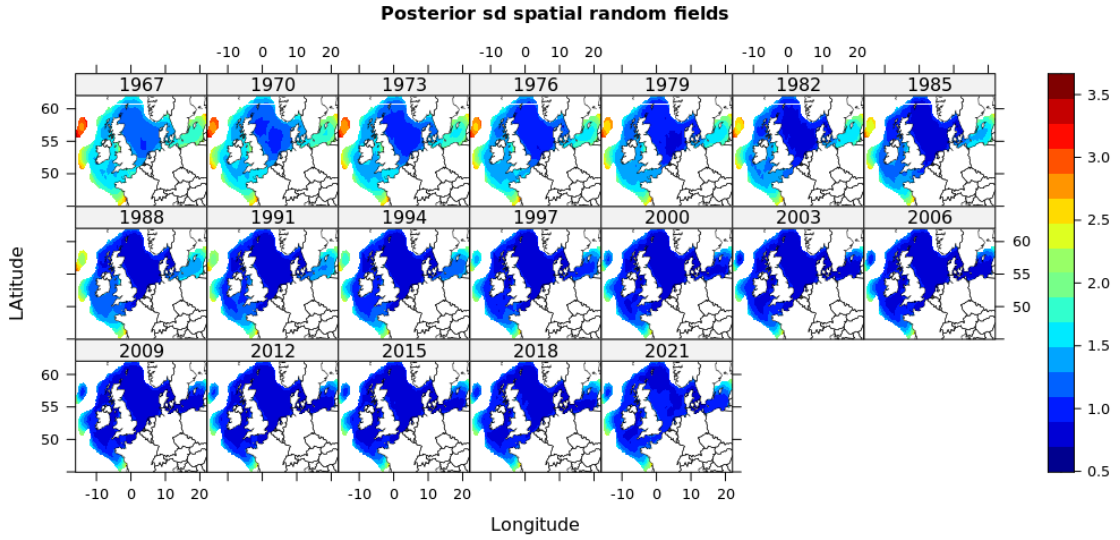

Figure 4.1.1.5. Posterior s.d. of the spatial random field of the INLA model for adult cod biomass. Note that the posterior means are given only at the 1d mesh nodes that were used to model the changes in the spatial random field as an AR1 process.

Estimates of the full model for the years and cells in the prediction grid clearly showed the combined effects of year, depth, and the spatial random field (Figure 4.1.1.6). Estimates in the prediction grid in the 1970s and 1980s were clearly higher than those in the later years. Estimates for the deeper areas are all lower than those in shallower waters. Meanwhile, in the North Sea, the distribution of the adult cod biomass has shown a distinct shift northward.

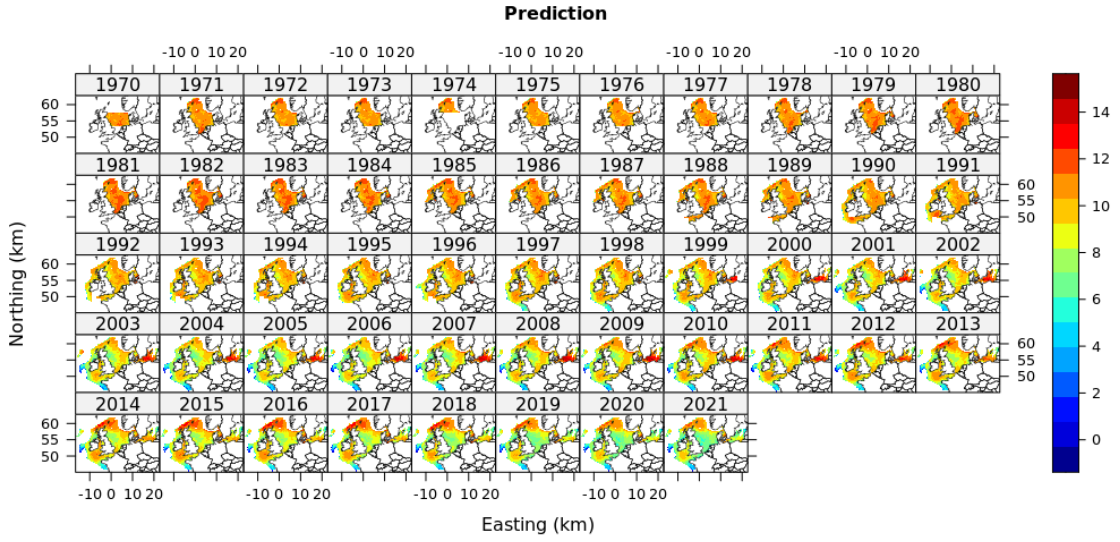

Figure 4.1.1.6. Predicted means for the prediction grid. The predictions were made for the reference gear, in quarter 1.

4.1.2 Models 3: GAM model with random effects and train/test approach

The GAM approach with random effects and train/test was applied in the following Mediterranean Geographical Sub-Areas (GSA, GFCM) and species:

1. GSA 18–19–20 M. merluccius (biomass index, kg/km^2);
2. GSA 17–18–19 M. barbatus (biomass index, kg/km^2);

3. GSA 18 M. barbatus (adults abundance index, N/km2, individuals with total length >= 11 cm);
4. GSA 6 M. barbatus (adults abundance index, N/km2, individuals with total length >= 11 cm);
5. GSA 9 M. merluccius (biomass index, kg/km2).

GSA 17 corresponds to Northern Adriatic Sea, GSA 18 to Southern Adriatic, GSA 19 to Western Ionian Sea, GSA 20 to Eastern Ionian Sea, GSA 6 to Northern Spain and GSA 9 to Ligurian Sea and Northern Tyrrhenian Sea (Figure 4.1.2.1). Geo-referred observations available from MEDITS trawl survey for the time-series 1996–2021 have been used to model the distribution of the above-mentioned species in the considered areas. For red mullet the bathymetrical range considered was 0–200 m.

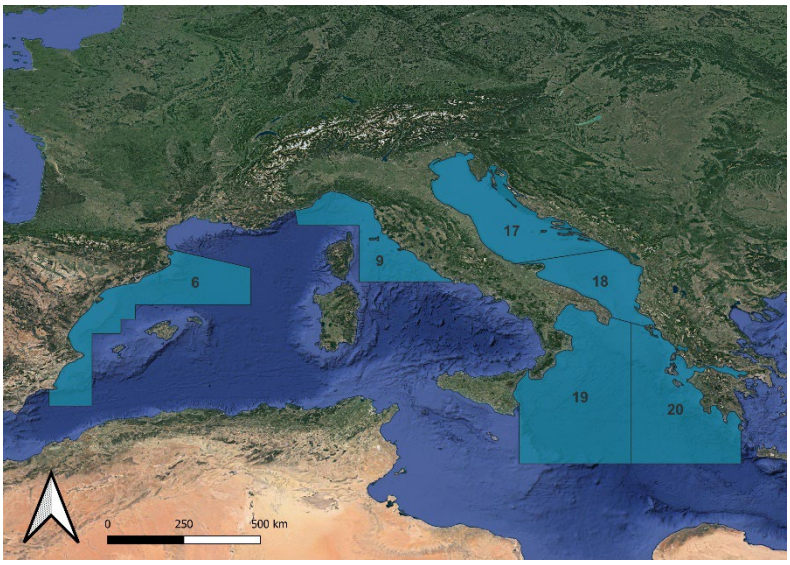

Figure 4.1.2.1 Geographical Sub-Areas (GSA) considered in the comparison among the models.

The explanatory variables selected for these applications were latitude, longitude, depth and year. Four different error distributions on response variable were explored: Gaussian, Tweedie, Negative Binomial and Delta distributions, through canonical link functions. In particular, in the Delta approach the error distribution is a Gaussian for the positive observations, while a binomial for presence/absence submodel, the latter accounting for 0-observations. 0-observations can also be treated assuming a Tweedie error distribution of the response variable. For all the case studies, the Tweedie probability distribution was selected according to the residuals diagnostic, explained deviance and comparability with observed spatial distribution.

Interactions among the significant variables was explored through tensors and random effects. The canonical thin plate smoothers on latitude, longitude and depth, as well their interactions are included (e.g. bidimensional smoothers, tensors). Furthermore, the possibility to account for landmasses was explored through the use of soap film smoothers (Wood *et al.*, 2008; Baudron *et al.*, 2020).

REstricted Maximum Likelihood (REML) was applied as automatic criterion for the selection of the k of the smothers for each explanatory variable, in order to reduce the risk of over-fitting. The significance of the smoothers on explanatory variables was evaluated through the pvalue and the reasonability of the partial effect (splines) on the dependent variable (biomass/adults abundance).

A train/test procedure with 20 iterations was conducted to explore the predictive capability of the best model, refitting it on 70% of the data and testing its performance on the left 30%. The

model was then validated by the MAE (Mean Absolute Error, Willmott and Matsuura, 2005), AIC and explained deviance.

From the best model, predictions on a spatial grid with 0.04° resolution were generated, taking the values estimated by the model in each cell and year. Parametric bootstrapping was carried out to get the standard deviation in each cell, resampling the parameters on the basis of covariance matrix (1000 drawn estimates); finally the CV was derived for each cell.

GAM fitting was carried out using mgcv R package 1.8–36 in R 4.1.1.

For European hake in GSAs 18–19–20 the biomass index (kg/km²) from 1996 to 2021 was modelled through the use of soap film smoothers to account for landmasses, according to the following equation:

$$kg/_{km^2} = s(Lat, Lon, bs = \text{"sw"}) + s(Lat, Lon, bs = \text{"sf"}) + s(depth) + s(year)$$

where the first addend sets up the wiggly component of a soap film (zero on the boundary) and the second one sets up just the boundary interpolating soap film. The Tweedie power parameter estimated by tw() argument was 1.479. For European hake the comparison was carried out between models of the same type (GAM) with different configurations. For model 3 it was defined a base configuration without interactions (see equation above), while for model 4 a more complex equation was explored (see chapter 4.1.3).

For red mullet in GSA17–18–19 the biomass index (kg/km2) from 1996 to 2020 was modelled through the use of soap film smoothers, including spatial-temporal interactions, according to the following model:

$$kg/_{km^2} = ti(Lat, Lon, year, bs = c(\text{"sw"}, \text{"cr"}), d = c(2,1)) + ti(Lat, Lon, year, bs = c(\text{"sf"}, \text{"cr"}), d = c(2,1)) + s(Lat, Lon, bs = \text{"so"}) + s(depth) + s(year)$$

The estimated Tweedie power parameter was 1.658. The predicted distribution from model 3 was compared with model 9.

The comparison between the model 3 and model 6 (VAST) were carried out for red mullet in GSA18 and GSA6. In GSA18 the abundance indices (N/km2) of adults (individuals with total length >= 11 cm) from 1996 to 2021 were fitted, taking into account spatial-temporal interactions and combination of month and year, according to the following equation:

$$N_{adult}/_{km^2} = te(Lat, Lon, year, bs = c(\text{"sw"}, \text{"cr"}), d = c(2,1)) + te(Lat, Lon, year, bs = c(\text{"sf"}, \text{"cr"}), d = c(2,1)) + te(month, year, bs = c(\text{"cc"}, \text{"cr"})) + s(depth))$$

The estimated Tweedie power parameter is 1.558.

For red mullet in GSA 6 the abundance indices (N/km2) of adults (individuals with total length >= 11 cm) from 1996 to 2019 were fitted taking into account spatial-temporal interactions and combination of depth and year, according to the following equation:

$$N_{adult}/_{km^2} = te(Lat, Lon, year, bs = c(\text{"sw"}, \text{"cr"}), d = c(2,1)) + te(Lat, Lon, year, bs = c(\text{"sf"}, \text{"cr"}), d = c(2,1)) + te(depth, year, bs = c(\text{"tp"}, \text{"cr"}))$$

The estimated Tweedie power parameter was 1.503.

For European hake in GSA 9 the biomass index (kg/km2) from 1996 to 2021 were fitted taking into account spatial-temporal interactions and combination of depth and year, according to the following equation:

$$kg/_{km^2} = te(Lat, Lon, year, bs = c(\text{"sw"}, \text{"}cr\text{"}), d = c(2,1)) + te(Lat, Lon, year, bs = c(\text{"sf"}, \text{"}cr\text{"}), d = c(2,1)) + ti(depth, year, bs = c(\text{"tp"}, \text{"}cr\text{"})) + ti(year, month, bs = c(\text{"tp"}, \text{"}cc\text{"})) + s(depth) + s(year)$$

The estimated Tweedie power parameter is 1.556.

4.1.2.1 Results

For European hake in GSAs 17–18–19–20 the best model explained the 43.2% of deviance and AIC was 35879 (Table 4.1.2.1). Figure 4.1.2.2 shows the partial effects of the explanatory variables on the biomass index: the wiggly component of the soap identifies two hot spots in the area, one close to Sicily coasts and another one offshore Patras, while the sf component detects higher biomass in deeper areas in Western Ionian Sea.

Several maxima of biomass were highlighted by the spline on the depth around 100, 350 and 600 m; generally corresponding to the distributional range of European hake. The smoother on the year described an oscillating pattern with higher biomass values around 2010 and then in recent years, in line with observed temporal trends for this species. The residuals of the model are shown in Figure 4.1.2.3.

Table 4.1.2.1. European hake GSAs 18–19–20. Summary table of the best GAM model results.

Smoothers	edf	F	p-value
s(x,y)	78.533	5.797	<2e-16
s(x,y)	7.771	36.541	<2e-16
s(depth)	7.739	58.286	<2e-16
s(year)	7.343	27.002	<2e-16
Expl Dev		AIC	
43.20%		35879	

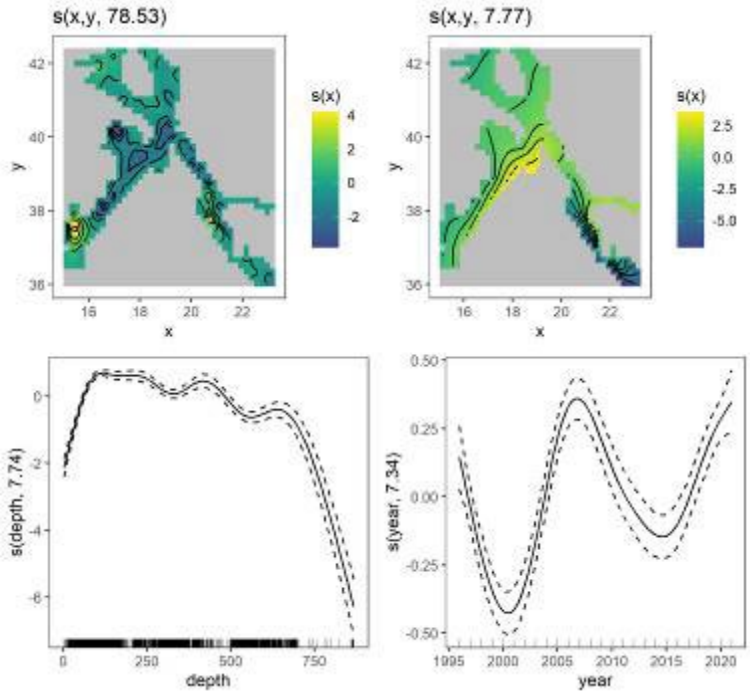

Figure 4.1.2.1. European hake GSAs 18–19–20. Partial effects on explanatory variables as described by the smoothers estimated by the Tweedie GAM.

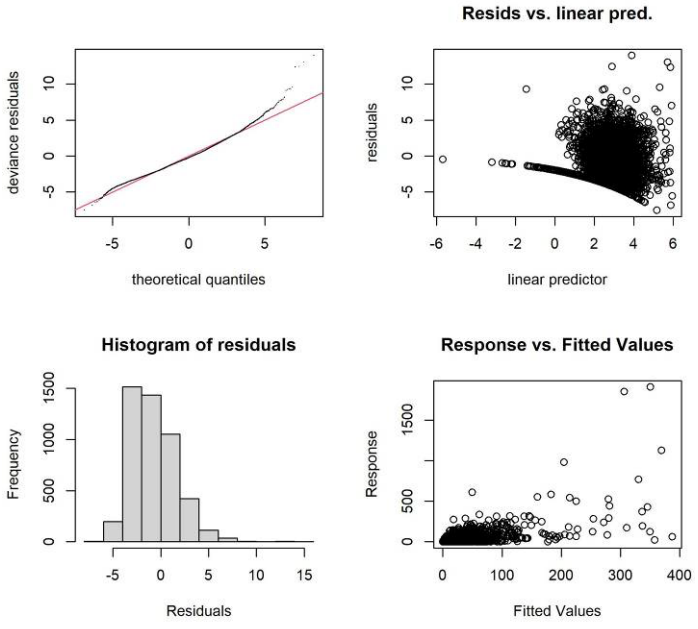

Figure 4.1.2.2. European hake GSAs 18–19–20. Residuals diagnostic plots. In the top left panel: normal Q-Q plot; Top right panel: residuals vs. linear predictor; Bottom left panel: histogram of residuals; Bottom right panel: response vs. fitted values.

Figure 4.1.2.3 reports the estimates of the selected model for all the years and cells in the prediction grid, showing a higher concentration of the biomass in higher depth ranges, generally inhabited by bigger individuals. Estimates in the prediction grid in the years 2005–2009 and 2019–2021 are higher than those in the other years.

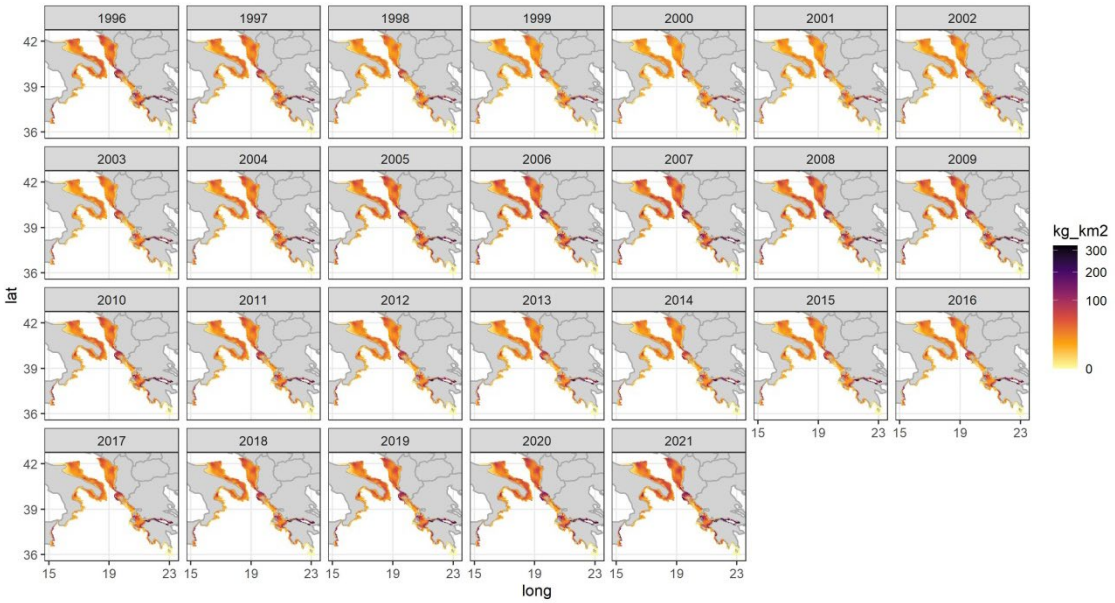

Figure 4.1.2.3 – European hake GSAs 18–19–20. Predicted biomass index for the prediction grid in the years 1996–2021.

Figure 4.1.2.4 shows the spatial distribution of the coefficient of variation (CV) of the predictions. A poorer precision is shown by the mapped CV in the area offshore Corfu and in the South of Peloponnese, corresponding to areas where the survey information is lacking.

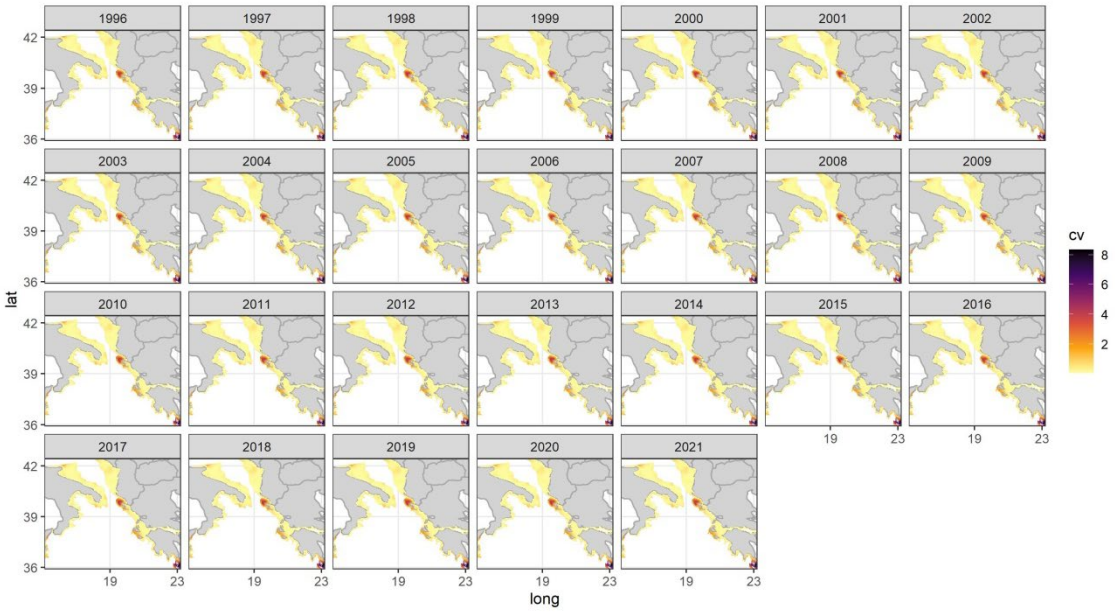

Figure 4.1.2.4 European hake GSAs 18–19–20. Spatial distribution of the CV by year.

The results of the train/test (Figure 4.1.2.5) show a quite narrow range for AIC and MAE indicators as well as for the explained deviance, showing an acceptable stability of the model.

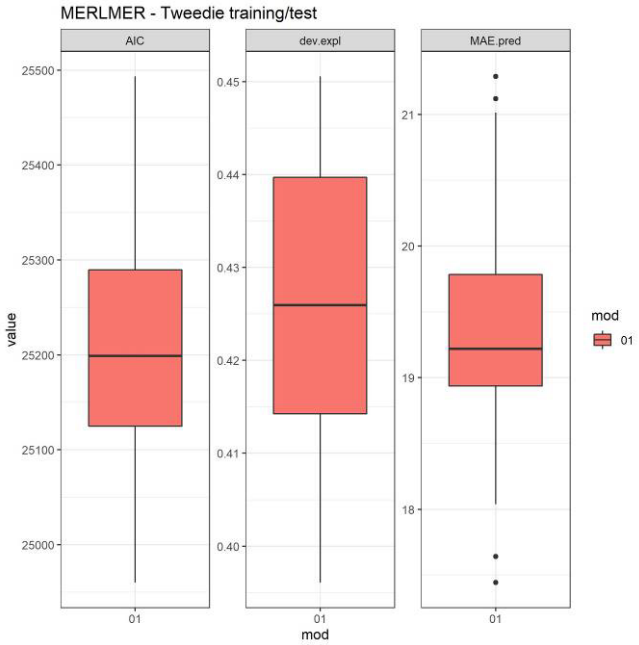

Figure 4.1.2.5. European hake GSAs 18–19–20. Train/test results: AIC, explained deviance and MAE.

For red mullet in GSAs 17–18–19 the best model explained the 52.3% of deviance and AIC was 36491 (Table 4.1.2.2). Figure 4.1.2.6 shows the partial effects of the explanatory variables on the biomass index: the interaction between the wiggly component of the soap and the year identifies a hot spots along Apulian coasts in the middle of the time-series, while another one is highlighted in the Northern part of GSA 17 in recent years. The interaction of the sf soap film component and the year detects a recent shift of the biomass from greater depths toward the areas closer to the coasts.

Table 4.1.2.2. Red mullet GSAs 17–18–19. Summary table of the results of the best GAM model.

Smoothers	edf	F	p-value
ti(x,y,year)	40.91	0.626	<2e-16
ti(x,y,year)	20.47	2.539	<2e-16
s(x,y)	66.892	24.7	<2e-16
s(depth)	6.616	55.647	<2e-16
s(year)	7.752	59.436	<2e-16
Expl Dev		AIC	
0.523		36491	

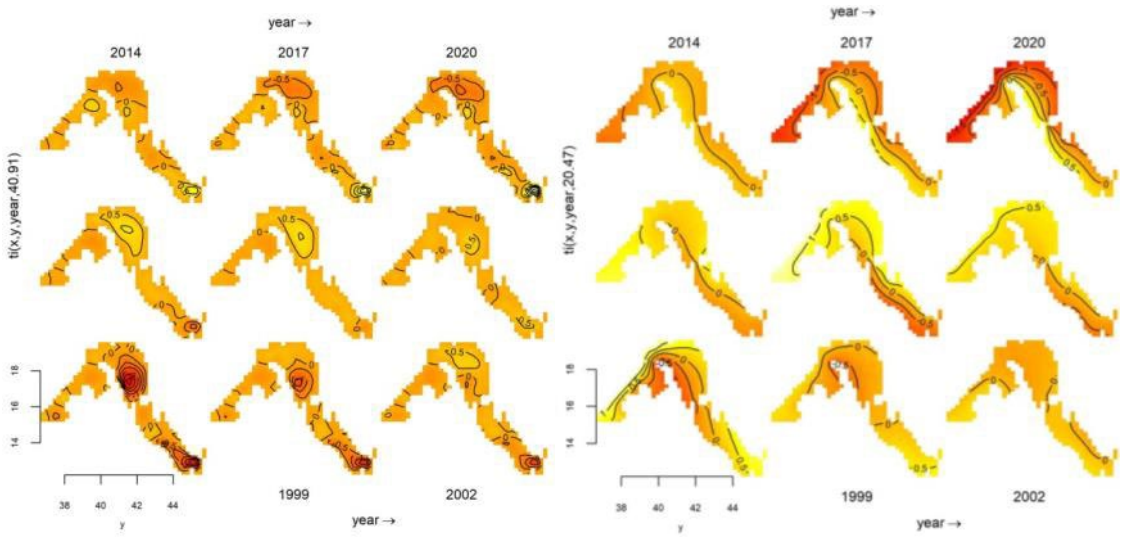

Figure 4.1.2.6 Red mullet in GSAs 17–18–19. Partial effects of the spatial-temporal interaction: wiggly (left) and sf (right) component of the soap.

The partial effect of depth indicates a decreasing biomass with increasing depth, consistently with the biology of this species. The smoother on the year described an oscillating pattern with higher biomass values in recent years consistently with the observed biomass index (Figure 4.1.2.7). The residuals of the model are shown in Figure 4.1.2.8.

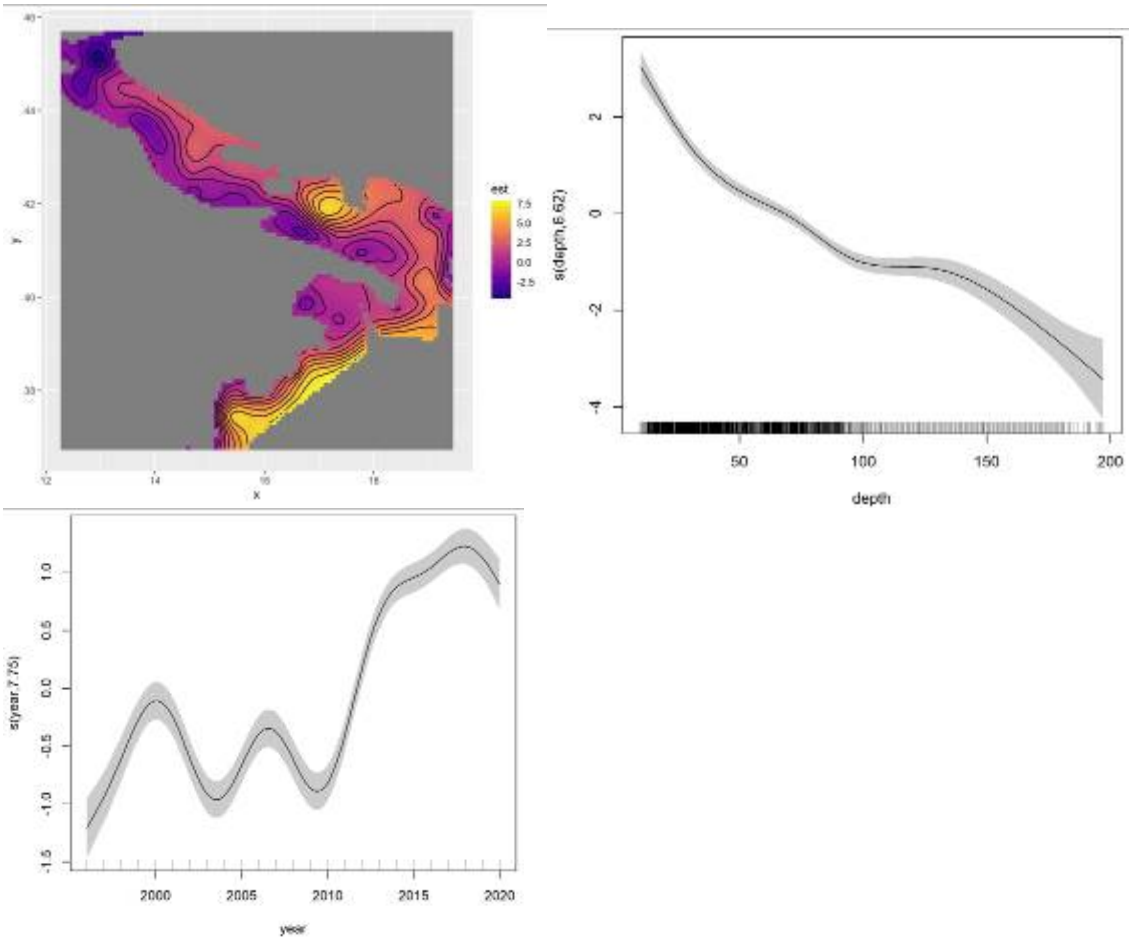

Figure 4.1.2.7. Red mullet in GSAs 17–18–19. Partial effects on Latitude-Longitude (soap film), depth and year.

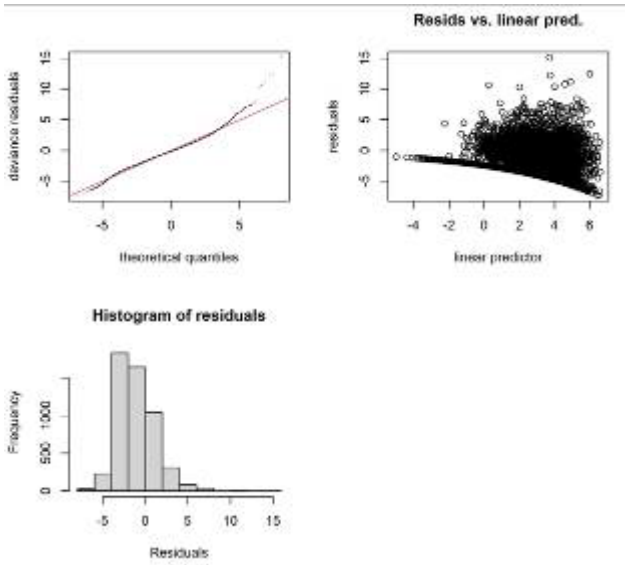

Figure 4.1.2.8. Red mullet GSAs 17–18–19. Residuals diagnostic plots. In the top left panel: normal Q-Q plot; Top right panel: residuals vs. linear predictor; Bottom left panel: histogram of residuals; Bottom right panel: response vs. fitted values.

Figure 4.1.2.9 reports the estimates of the selected model for all the years and cells in the prediction grid, showing an overall higher concentration of the biomass in coastal areas and, in Northern Adriatic, also close to the Croatian 12 NM boundary. The estimated spatial distribution highlights also in this case an increase in the biomass in the last years, a phenomenon observed in the area from surveys and commercial catches. The model returns a spatial distribution quite similar to the one observed in survey data along the years, also in terms of absolute values.

Figure 4.1.2.9. Red mullet in GSAs 17–18–19. Predicted biomass index for the prediction grid in the years 1996–2020.

Figure 4.1.2.10 shows the spatial distribution of the coefficient of variation (CV) of the predictions. A worse precision is shown by the mapped CV in the area along the Apulian cost in the Western Ionian Sea and in the southern Sicilian coast, corresponding to areas where the survey information is very scant or missing.

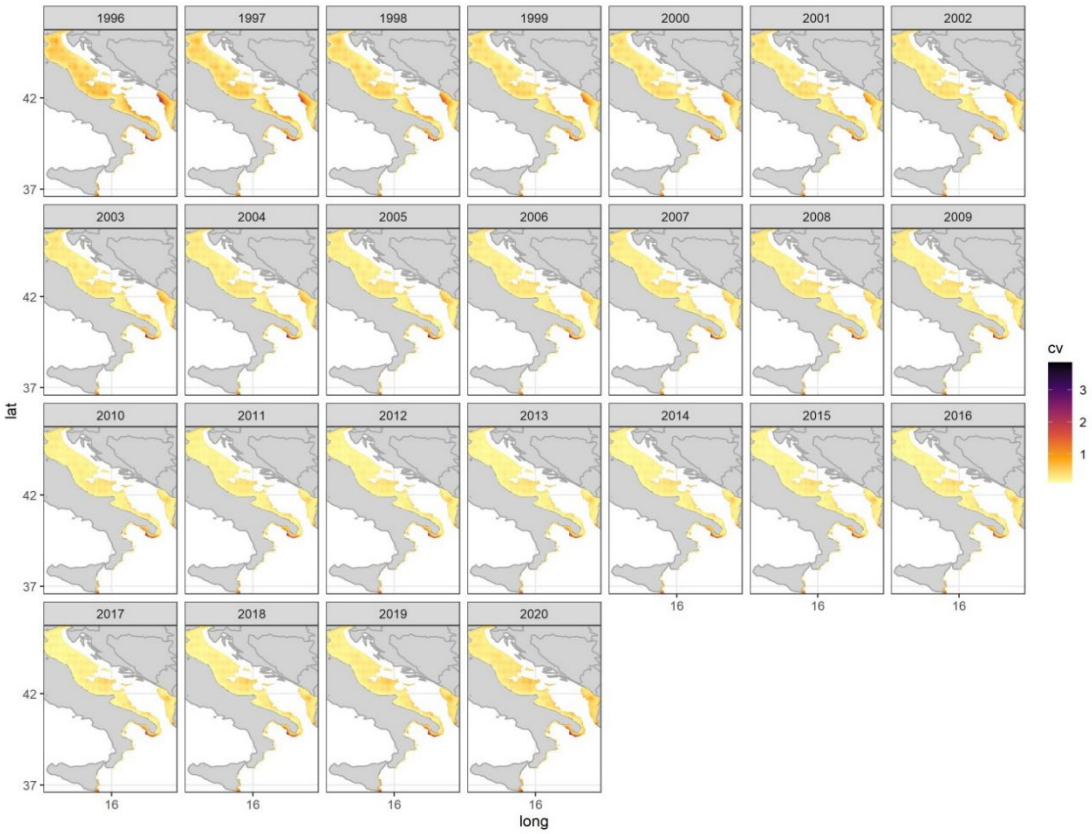

Figure 4.1.2.10. Red mullet in GSAs 17–18–19. Spatial distribution of the CV by year.

The train/test results (Figure 4.1.2.11) show a quite narrow range for AIC and MAE indicators as well as for the explained deviance, showing an acceptable stability of the model.

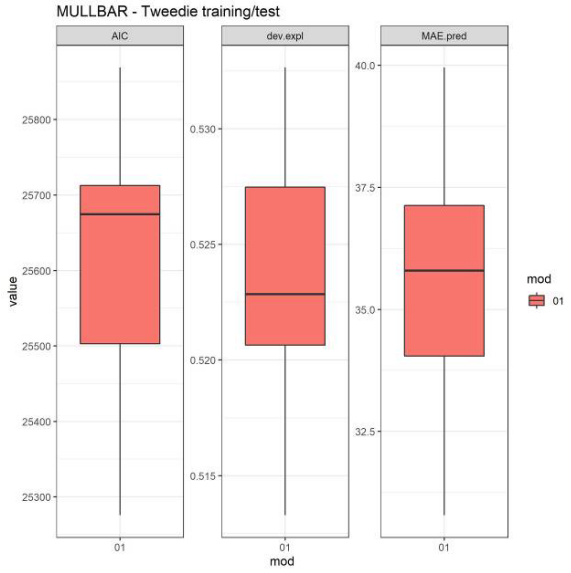

Figure 4.1.2.11. Train/test results: AIC, explained deviance and MAE.

For the abundance of red mullet adults in GSA 18 the best model explained the 64.6% of deviance and had an AIC of 16980 (Table 4.1.2.3). Figure 4.1.2.12 shows the partial effects of the explanatory variables on the adult density index: the interaction between the wiggly component of the soap and the year identifies several hot spots of adults along western side of the area along the time-series, with the one in the Northern part more pronounced in recent years. On the other hand, the interaction of the sf soap film component and the year detects less marked density of adults on the soap film boundary in recent years respect to the first part of the time-series that is consistent with the observed data.

Table 4.1.2.3. Red mullet GSA 18. Summary table of the best GAM model results.

Smoothers	edf	F	p-value
te(x,y,year)	42.316	2.557	<2e-16
te(x,y,year)	22.494	1.935	<2e-16
te(month,year)	9.514	6.455	<2e-16
s(depth)	6.105	14.254	<2e-16
Expl Dev		AIC	
64.6%		16980	

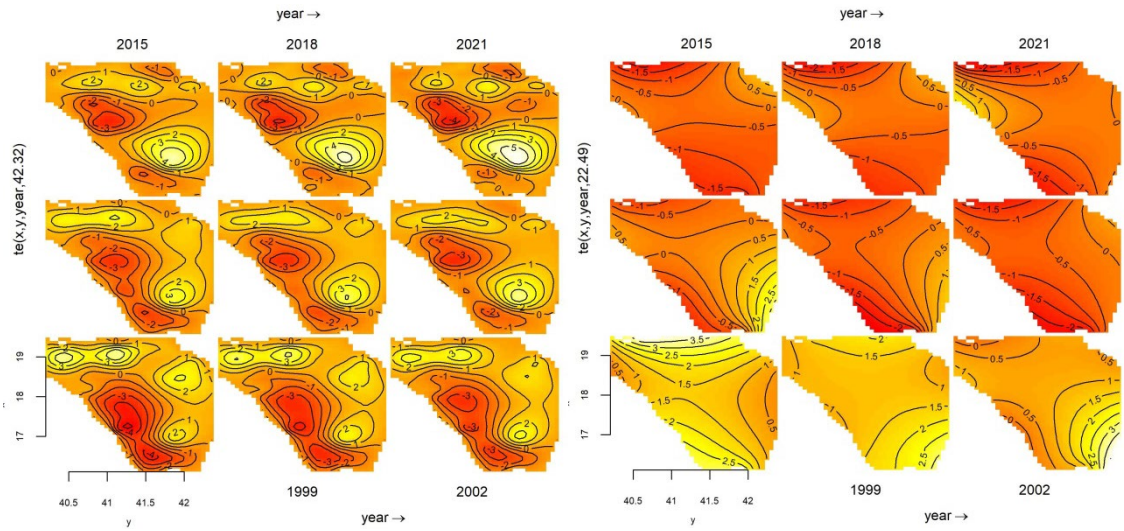

Figure 4.1.2.12. Red mullet in GSAs 18. Partial effects of the spatial-temporal interaction: wiggly (left) and sf (right) component of the soap.

The partial effect of depth indicates a decreasing abundance of adults with increasing depth, while the tensor on year and month indicates higher abundance of adults in recent years regardless the sampled month (Figure 4.1.2.13). The residuals of the model are shown in Figure 4.1.2.14.

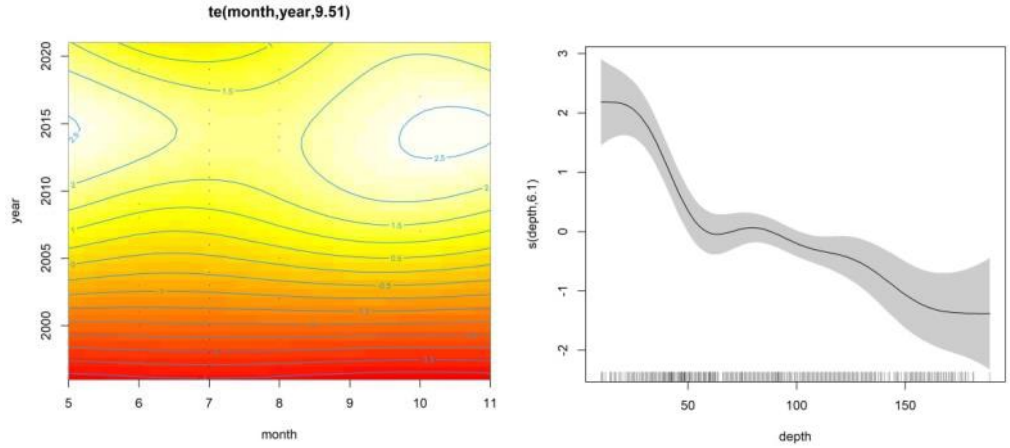

Figure 4.1.2.13. Red mullet in GSA 18. Partial effects on month-year and depth.

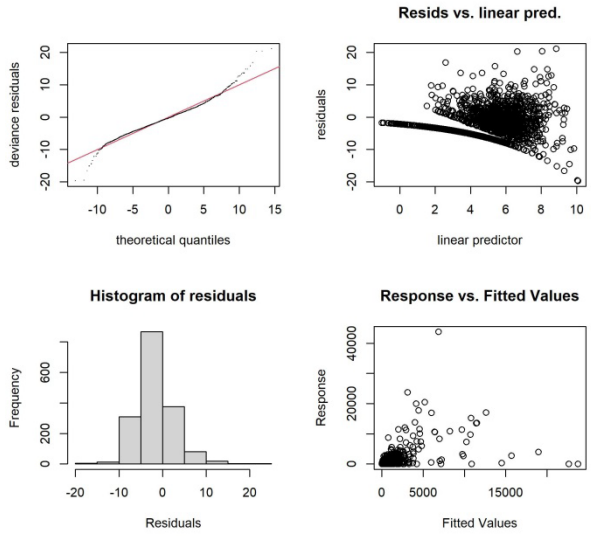

Figure 4.1.2.14. Red mullet GSA 18. Residuals diagnostic plots. In the top left panel: normal Q-Q plot; Top right panel: residuals vs. linear predictor; Bottom left panel: histogram of residuals; Bottom right panel: response vs. fitted values.

Figure 4.1.2.15 reports the estimates of the selected model for all the years and cells in the prediction grid, showing an overall higher concentration of the adult abundance in coastal areas around Gargano promontory, offshore Brindisi and along the eastern side of the area. The estimated spatial distribution highlights a widening of the area with higher adults' density.

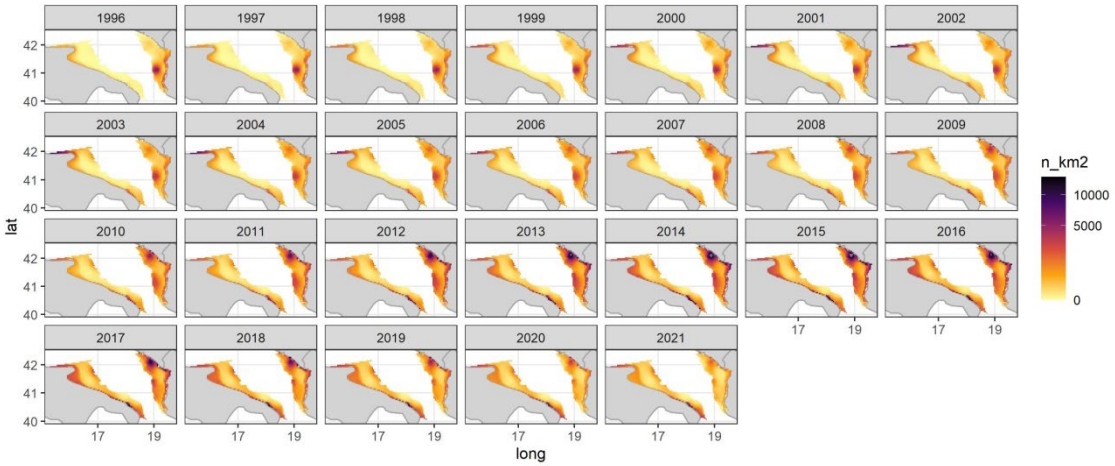

Figure 4.1.2.15. Red mullet in GSA 18. Predicted adult abundance index for the prediction grid in the years 1996–2021.

Figure 4.1.2.16 shows the spatial distribution of the coefficient of variation (CV) associated to the predictions. A worse precision is shown by the mapped CV at the beginning of the time-series, especially at depth where the species is less present (e.g. depths around 150–200 m) and where the survey information is very scattered or missing.

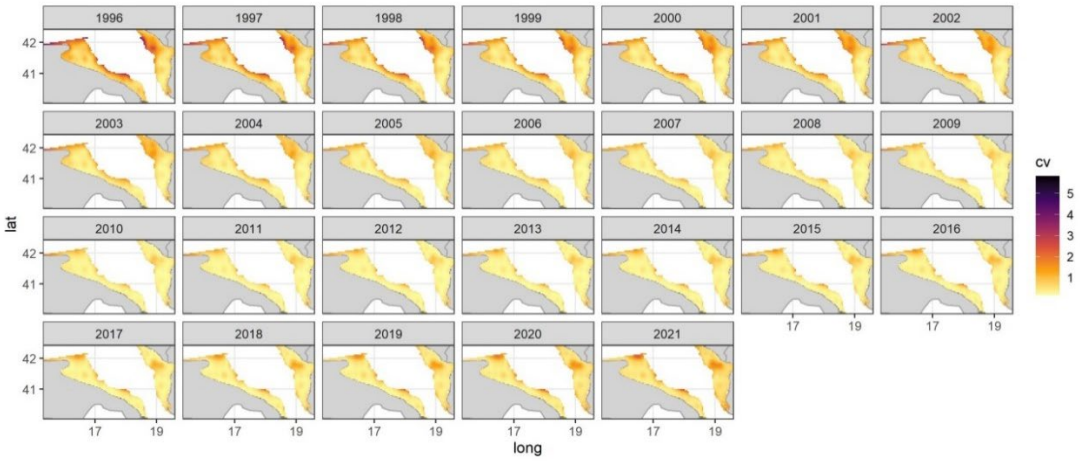

Figure 4.1.2.16 Red mullet in GSA 18. Spatial distribution of the CV by year.

The train/test results (Figure 4.1.2.17) show a quite narrow range for AIC and MAE indicators as well as for the explained deviance, showing an acceptable stability of the model.

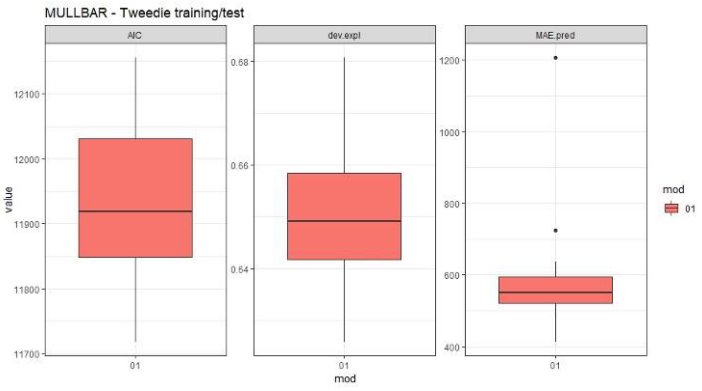

Figure 4.1.2.17 Train/test results: AIC, explained deviance and MAE.

For red mullet in GSA 6, the best model explained the 54.8% of deviance and AIC was 17206 (Table 4.1.2.4). Figure 4.1.2.18 shows the partial effects of the explanatory variables on the adult density index: the interaction between the wiggly component of the soap and the year identifies several hot spots of adults along Spanish costs along the time-series, in particular around latitude 39, latitude 40 and 42. On the other hand, the interaction of the sf soap film component and the time detects higher density in the centre of the area in recent years, consistently with observed data.

Table 4.1.2.4. Red mullet GSA 6. Summary table of the best GAM model results.

Smoothers	edf	F	p-value
te(x,y,year)	84.8	1.98	<2e-16
te(x,y,year)	17.13	0.624	<2e-16
te(depth,year)	12.62	5.246	<2e-16
Expl Dev		AIC	
54.8%		17206	

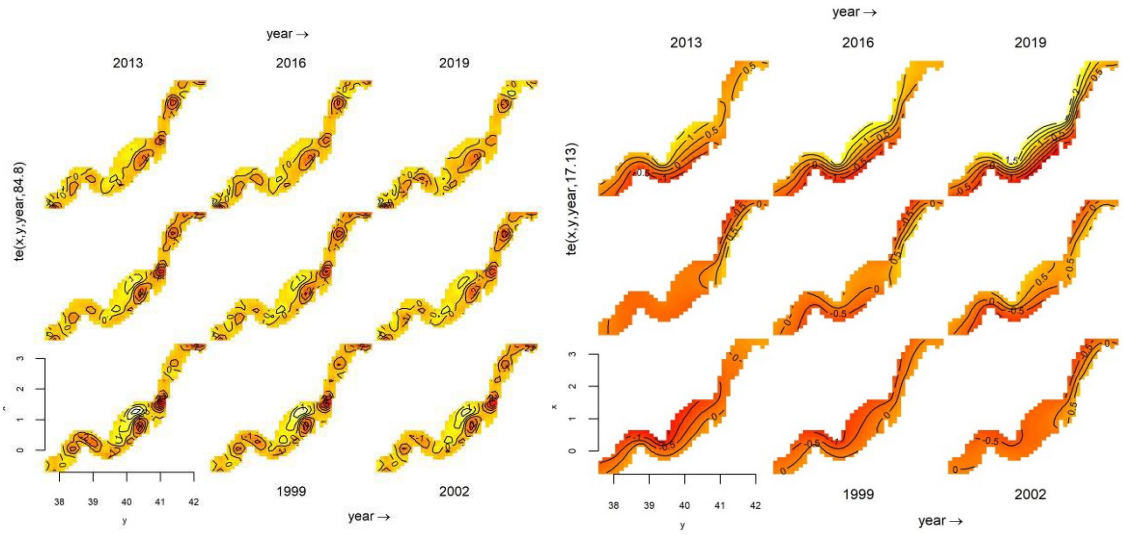

Figure 4.1.2.18 Red mullet in GSA 6. Partial effects of the spatial-temporal interaction: wiggly (left) and sf (right) component of the soap.

The combined effect of depth and year indicates a higher abundance of adults within 50–70 m depth in recent years (Figure 4.1.2.19). The residuals of the model are shown in Figure 4.1.2.20.

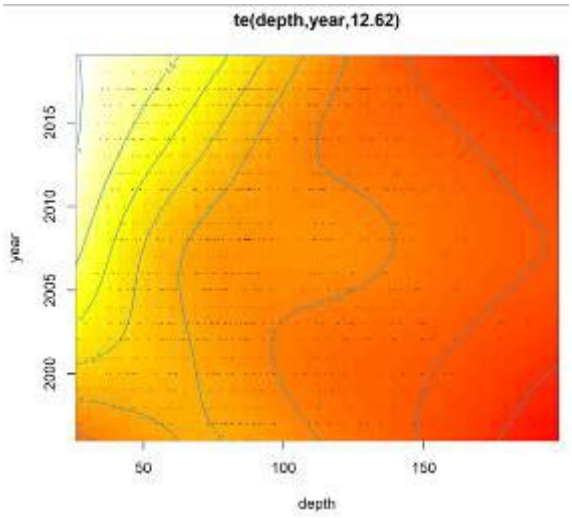

Figure 4.1.2.19 Red mullet in GSA 6. Partial effects on depth-year.

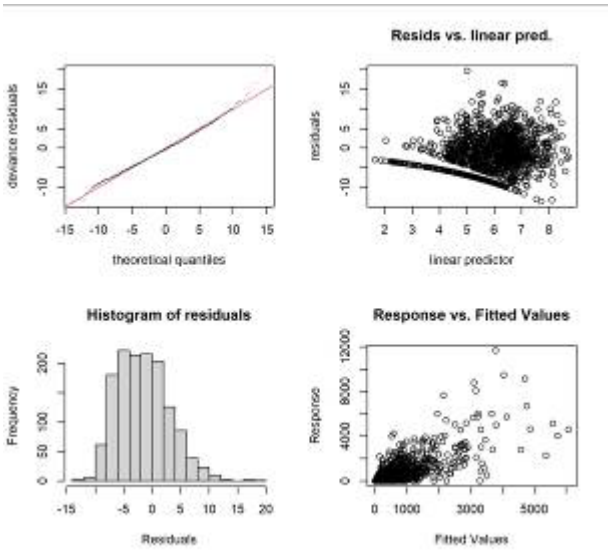

Figure 4.1.2.20. Red mullet GSA 6. Residuals diagnostic plots. In the top left panel: normal Q-Q plot; Top right panel: residuals vs. linear predictor; Bottom left panel: histogram of residuals; Bottom right panel: response vs. fitted values.

Figure 4.1.2.21 reports the estimates of the selected model for all the years and cells in the prediction grid, showing an overall higher concentration of the adult abundance in coastal areas and an increasing abundance of adult in the Northern part of the area in the last years.

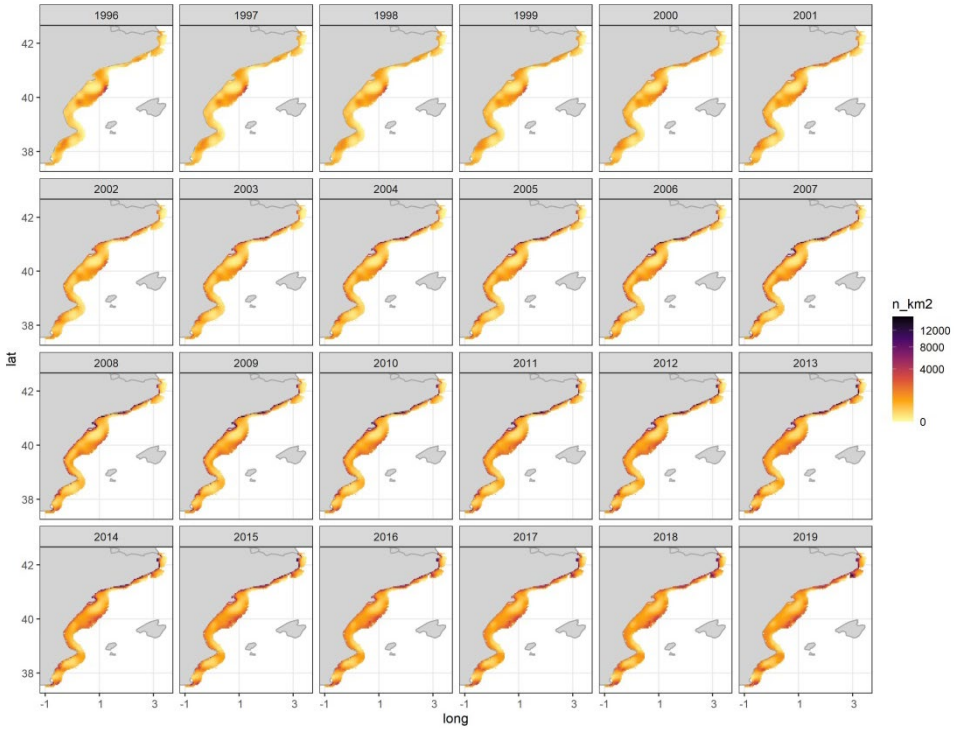

Figure 4.1.2.21. Red mullet in GSA 6. Predicted adult abundance index for the prediction grid in the years 1996–2019.

Figure 4.1.2.22 shows the spatial distribution of the coefficient of variation (CV) associated to the predictions. A poorer precision is shown by the mapped CV at the beginning of the time-series, where the survey information was more scattered. In the last years available a higher CV is shown in the areas where survey information is missing (e.g. offshore Valencia and offshore Barcelona).

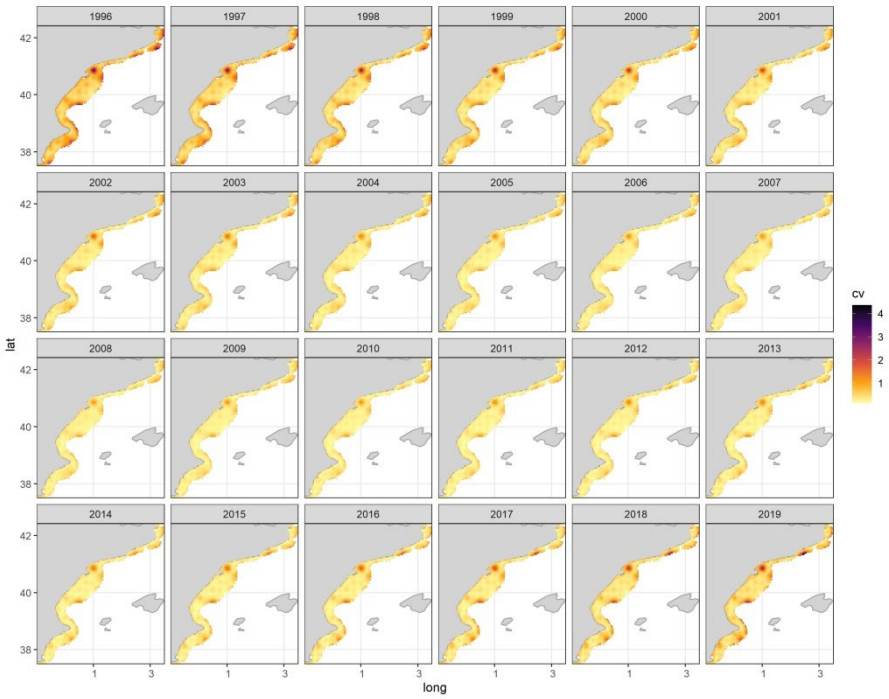

Figure 4.1.2.22. Red mullet in GSA 6. Spatial distribution of the CV by year.

The train/test results (Figure 4.1.2.23) show a quite narrow range for AIC and MAE indicators as well as for the explained deviance, showing an acceptable stability of the model.

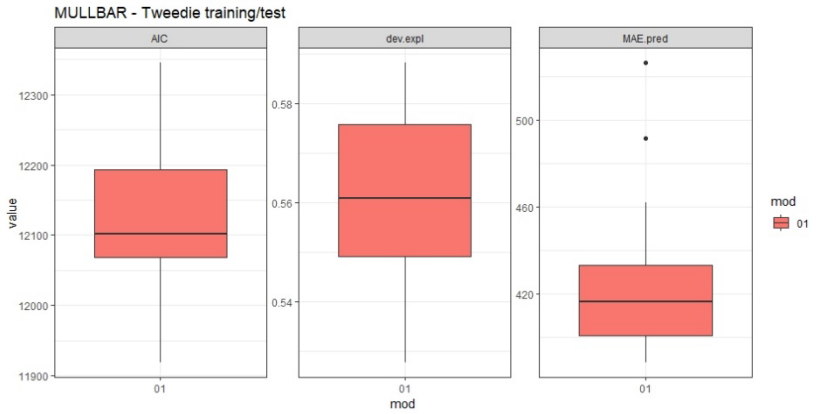

Figure 4.1.2.23 Train/test results: AIC, explained deviance and MAE.

For European hake in GSA 9, the best model explained the 50.9% of deviance and AIC was 25386 (Table 4.1.2.5). Figure 4.1.2.24 shows the partial effects of the explanatory variables on the biomass index: the interaction between the wiggly component of the soap and the year identifies several hot spots of biomass, in particular around latitude 42 and latitude 43 along the years. In 1996 and in the last years, another hot spot is present at latitude 41. The interaction of the sf soap film component and the time detects higher biomass in 2021 in the coastal areas and an overall higher biomass in the previous years.

Table 4.1.2.5. European hake GSA 9. Summary table of the best GAM model results.

Smoothers	edf	F	p-value
te(x,y,year)	61.057	0.651	<2e-16
te(x,y,year)	12.91	0.593	<2e-16
ti(depth,year)	8.7	3.701	<2e-16
ti(year,month)	5.394	2.848	<2e-16
s(depth)	8.205	158.605	<2e-16
s(year)	6.21	5.104	<2e-16
Expl Dev		**AIC**	
50.90%		**25386**	

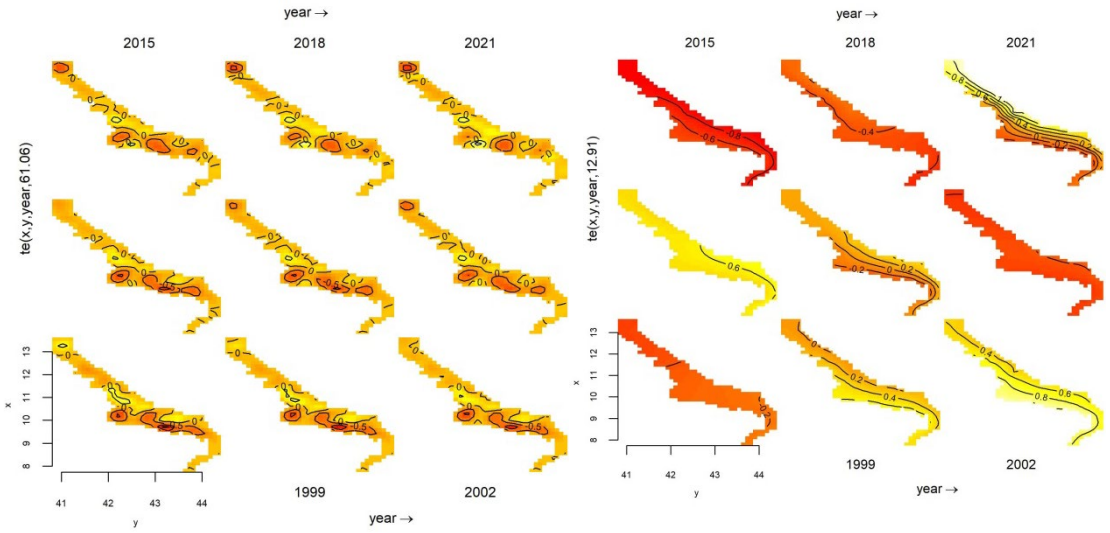

Figure 4.1.2.24. European hake in GSA 9. Partial effects of the spatial-temporal interaction: wiggly (left) and sf (right) component of the soap.

The spline on depth highlights higher biomass around 200 m of depth, while the spline on the year indicates an increasing trend in recent years (Figure 4.1.2.25). A similar pattern is shown by the tensor depth-year. The residuals of the model are shown in Figure 4.1.2.26.

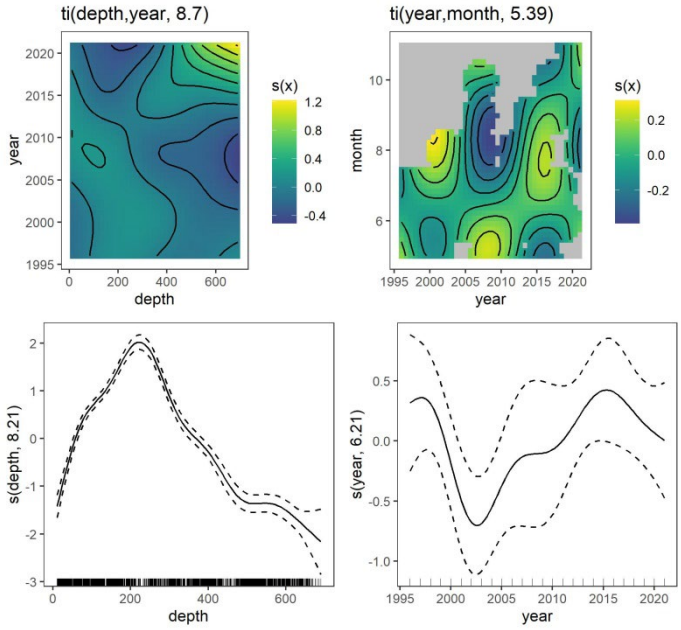

Figure 4.1.2.25. European hake in GSA 9. Partial effects on depth-year, year-month, depth (only) and year (only).

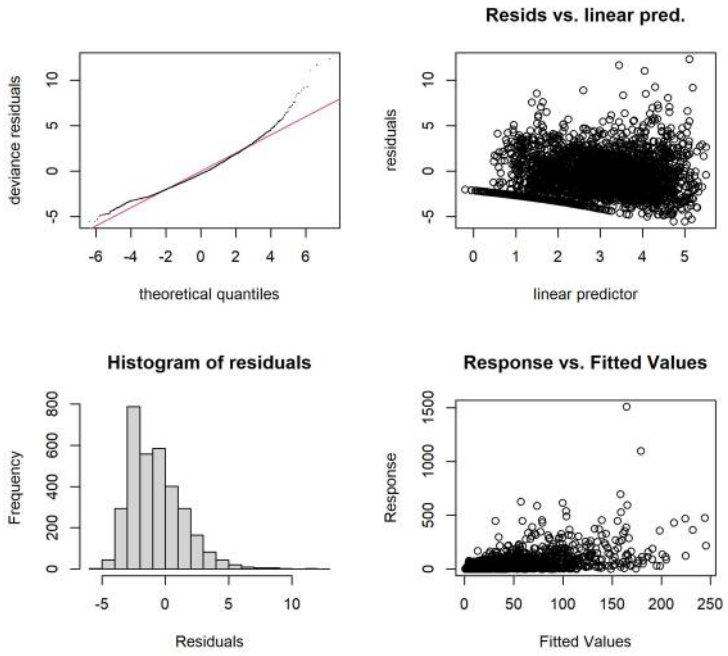

Figure 4.1.2.26. European hake GSA 9. Residuals diagnostic plots. In the top left panel: normal Q-Q plot; Top right panel: residuals vs. linear predictor; Bottom left panel: histogram of residuals; Bottom right panel: response vs. fitted values.

Figure 4.1.2.27 reports the estimates of the selected model for all the years and cells in the prediction grid, showing an overall higher concentration of the biomass in the Ligurian Sea and in the Tuscan Archipelago (northern Tyrrhenian Sea) in the first part of the time-series. In recent years, the model predicts a southeastern shift of the biomass, consistently with the observed data.

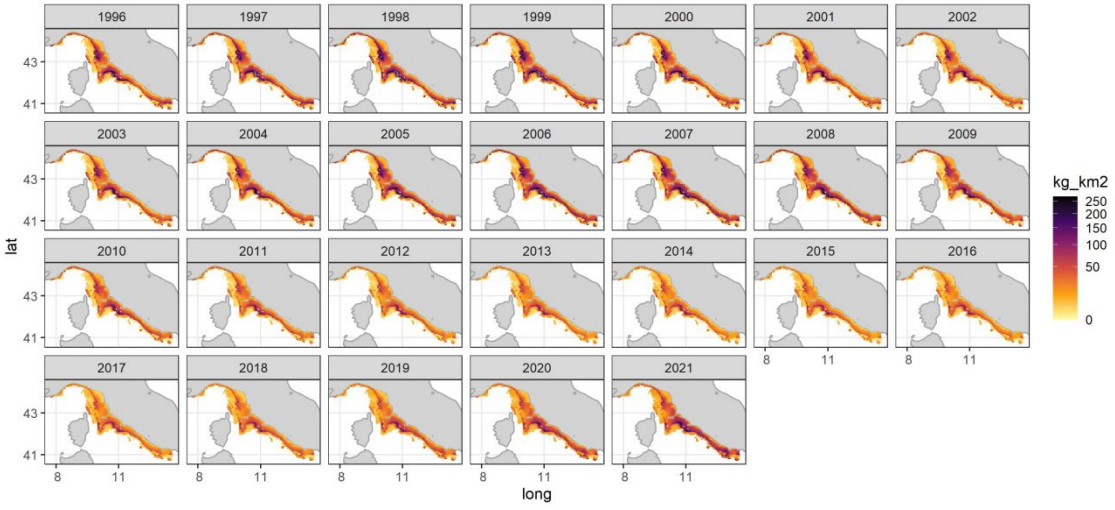

Figure 4.1.2.27. European hake in GSA 9. Predicted biomass index for the prediction grid in the years 1996–2021.

Figure 4.1.2.28 shows the spatial distribution of the coefficient of variation (CV) associated to the predictions. In general, the CV is quite small along the time-series. A worse precision is shown by the mapped CVs at the beginning of the time-series and in recent years, in particular offshore.

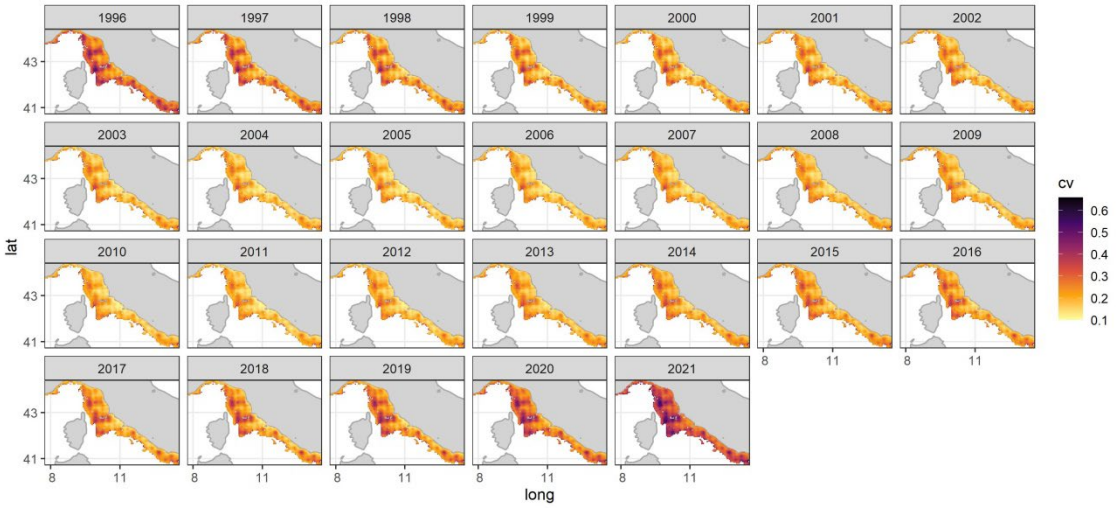

Figure 4.1.2.28. European hake in GSA 9. Spatial distribution of the CV by year.

The train/test results (Figure 4.1.2.29) show a quite narrow range for AIC and MAE indicators as well as for the explained deviance, showing an acceptable stability of the model.

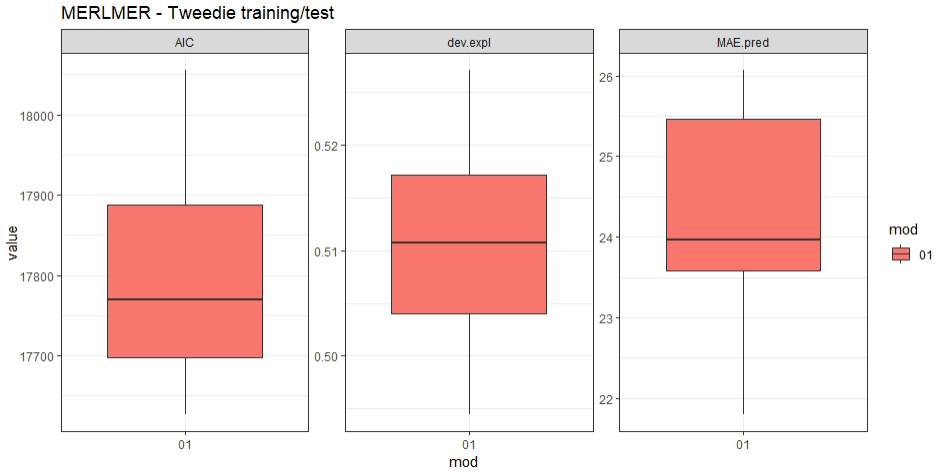

Figure 4.1.2.29. Train/test results: AIC, explained deviance and MAE.

4.1.3 GAM model 4 with random effects

Hake biomass data (expressed in kg/km2) for the Mediterranean Sea (GSAs 18, 19 and 20) were analysed using Generalized Additive Modelling (GAM). The data were based on MEDITS surveys for the period 1996–2021. The GAM incorporated a spatio-temporal soap film smoother, an interaction term and a random effect. The explanatory variables used in the model were depth, year, geographic coordinates and vessel code.

Biomass data (including 0-observations) were modelled using a Tweedie error distribution with a logit link function. A Tweedie index parameter set to 1.417 as estimated by argument tw() and considered as the most appropriate based on residual plots. For the interaction term, the thin plate regression spline (tp) was used for the variable depth along with a cubic (cr) regression spline for year. Additionally, a three-dimensional space–time smooth (easting; northing; year) which is the soap film smoother for space, and the one dimensional, cr, smoother for year was included in the models (this is performed by using two singly penalized components, see Augustin *et al.*, 2013; Wood, 2017). The geographic coordinates, easting and northing, are longitude

and latitude expressed in meters and were estimated using the projected system ETRS89-LAEA. The vessel to vessel variability was included as random variable in the model using the argument bs="re". To avoid over-fitting and to simplify the interpretation of the results, the degree of smoothing of each predictor was chosen based on the REstricted Maximum Likelihood (REML). The original values for depth were log-transformed to achieve normal distributions.

GAM selection was based on the Root Mean Squared Prediction Error (RMSPE) and AIC. In order to examine whether the final selected model has eliminated spatial and temporal autocorrelation in residuals, semivariograms of the Pearson residuals (detecting spatial autocorrelation) and Partial Auto-Correlation Function (PACF) plots (detecting temporal autocorrelation) were produced.

The temporal trends were estimated along with 95% Bayesian credible intervals. This is achieved by repeatedly sampling predictor vectors from a multivariate normal distribution where the mean is the estimated predictor vector and the variance matrix is the Bayesian posterior covariance matrix. From the sampled predictor vectors, samples of fitted values were obtained and the temporal trend of fitted values was then estimated. The mean, 2.5% and 97.5% percentile of the distribution are the required summary statistics for the annual time-trends displayed along with the 95% Bayesian credible intervals. In addition, maps showing the Coefficient of Variation (CV = Standard Deviation / Mean) were calculated based on the mean and standard deviation of hake biomass (by grid cell and year) estimated for each sample of 1000 simulated fitted values.

The model with a three-dimensional spatio-temporal smoother, depth and interaction of depth and year had the lowest RMSPE and AIC (Tables 4.1.3.1, 4.1.3.2; Figure 4.1.3.1) and was selected for performing annual predictions. Additionally, no pronounced patterns were observed in the standard diagnostic, semivariogram and PACF plots for Pearson residuals (Figs 4.1.3.2; 4.1.3.3). The above suggest that the final model is able to describe the underlying data. The spatial outcomes varied by year and revealed that the main areas with pick hake biomass (kg/km2) were indicated in southern part of western Ionian (along Sicily coasts) and in the central part of eastern Ionian Sea (Patraikos gulf) (Figure 4.1.3.4). Maps of CV revealed higher values in areas with less or lacking data from surveys suggesting that the model predictions are more uncertain in those areas (fig 4.1.3.5). The predicted trends among years for the hake biomass are shown in figure 4.1.3.6 along with credible intervals.

Table 4.1.3.1: Results for factors affecting EU hake biomass (kg/km2) based on the final Generalized Additive Model.

Smooth terms	edf	F	p-Value	R-sq (adj)	DE%
te(x, y, year) ("sf")	26.88	4.089	<0.001	0.444	46.4
te(x, y, year) ("sw")	103.37	0.948	<0.001		
s(lndepth)	3.46	8.081	<0.01		
te(lndepth, year)	49.53	2.738	<0.001		
s(vessel)	0	0	ns		

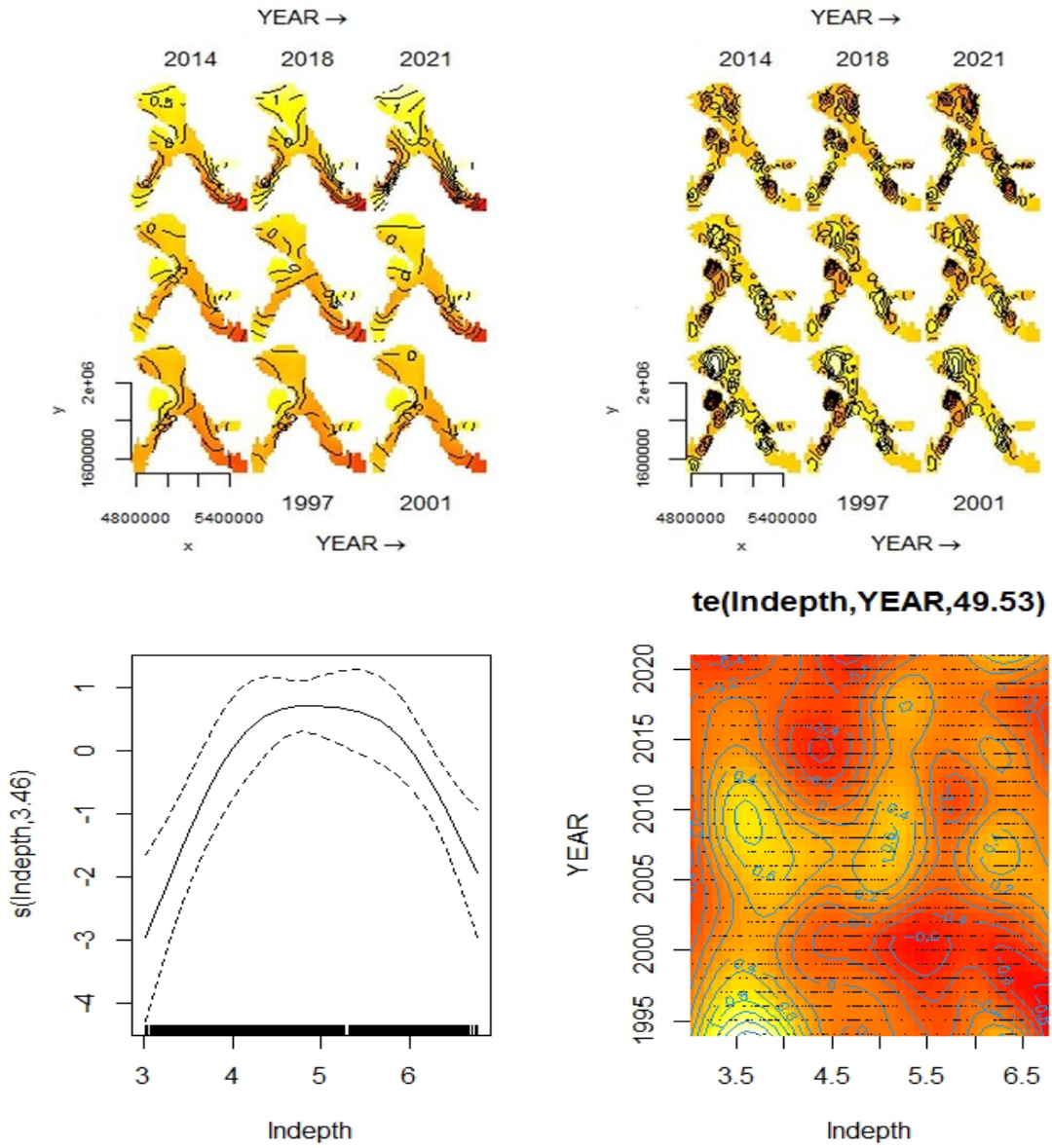

Figure 4.1.3.1. Estimated smooth terms for the best GAM for hake biomass in Mediterranean GSAs 18, 19 and 20. For the main effect of depth the corresponding 95% confidence intervals are indicated with dashed lines. For the 2-D interactions between depth and year the lines are the contours of the fitted function plotted on a grid. Red indicates lower fitted values and yellow higher otherwise. For the space-time soap film smoother the estimated degrees of freedom are shown in Table 4.1.3.1.

Table 4.1.3.2: Estimated RMSPE and AIC for GAMs tested. Model 1 indicated lower AIC and RMSPE values and selected as final. (x: easting, y: northing).

Model (number)	GAM (formula)	AIC	RMSPE
(1) includes a three-dimensional space-time smooth (easting, northing, year) and a soap spatial smoother expressed as two singly penalized components the“sf” (soap film) and the “sw” (soap wiggly)	kg_km2 ~ te(x, y, YEAR, bs = c("sf", "cr"), k = c(20, 3), d = c(2, 1), xt = list(list(bnd = fsb), NULL)) + te(x, y, YEAR, bs = c("sw","cr"), k = c(40, 3), d = c(2, 1), xt = list(list(bnd = fsb),NULL)) + s(Indepth, k=5) + te(Indepth, YEAR, bs = c("tp","cr"),k=c(10,9)) + s(vessel, bs="re") , knots=soap_knots, data=mydata, family =Tweedie(p=1.417), method="REML")	25855.9	58.36

Model (number)	GAM (formula)	AIC	RMSPE
(2) includes a two dimensional spatial smooth (easting, northing) and a doubly penalized soap spatial smoother: "so"	kg_km2 ~ s(x,y,k=25,bs="so",xt=list(bnd=fsb)) + s(YEAR, bs="cr", k=15) + s(lndepth, k=5) + te(lndepth, YEAR, bs = c("tp","cr"),k=c(10,10)) +s(vessel, bs="re") , knots=soap_knots, data=mydata, family =Tweedie(p=1.417) , method="REML")	25975.9	60.29
(3) includes a three-dimensional space-time smooth (easting, northing, year) and a thin-plate regression spline spatial smoother	kg_km2 ~ te(x, y, YEAR, bs = c("tp", "cr"), k = c(30, 3), d = c(2, 1)) + s(lndepth, k=5) #+ te(lndepth, YEAR, bs = ("tp","cc"),k=c(10,10)) +s(vessel, bs="re") , data=mydata, family =Tweedie(p=1.417), method="REML")	26119.3	62.09
(4) includes a two dimensional spatial smooth (easting, northing) and a thin-plate regression spline spatial smoother	kg_km2~ te(x, y, bs = c("tp"), k = c(30, 3), d = c(2)) + s(YEAR,bs="cr",k=10) + s(lndepth, k=5) + te(lndepth, YEAR, bs = c("tp","cc"),k=c(10,10)) + s(vessel, bs="re") , data=mydata, family =Tweedie(p=1.417), method="REML")	26382.2	63.20

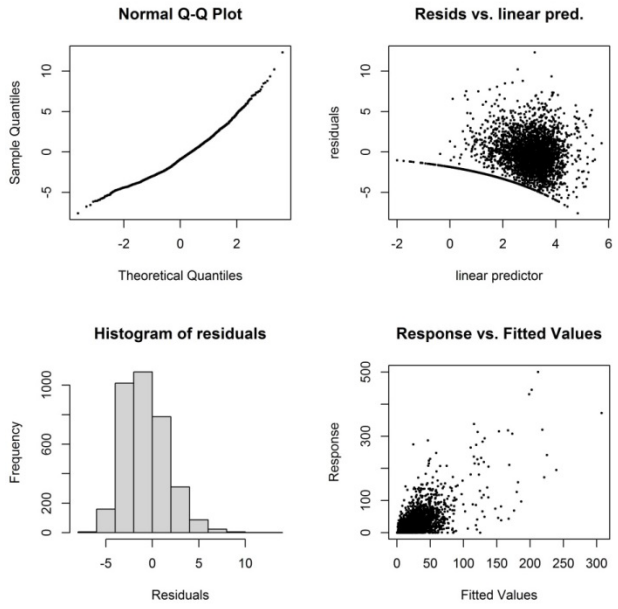

Figure 4.1.3.2: Standard diagnostic plots (residual plots) based on the final GAM. In the top left panel: normal Q-Q plot; Top right panel: residuals vs. linear predictor; Bottom left panel: histogram of residuals; Bottom right panel: response vs. fitted values.

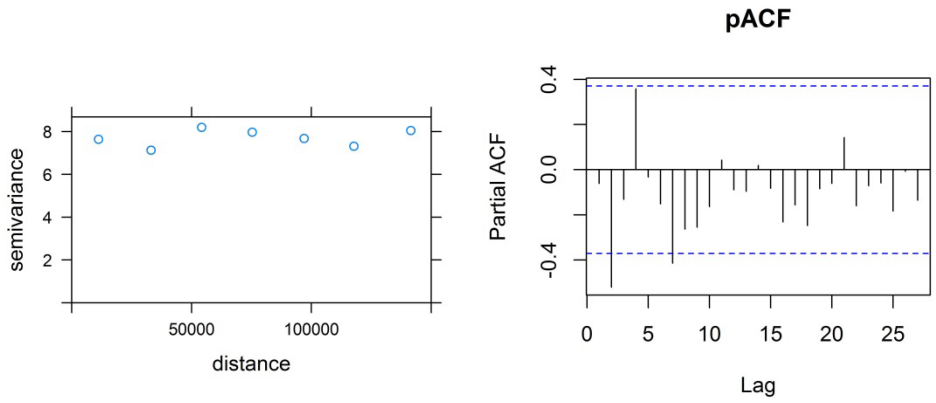

Figure 4.1.3.3. Semivariogram based on the residuals of the final GAM and Plots of the Partial Auto-Correlation Function (PACF) for the residuals of the final GAM.

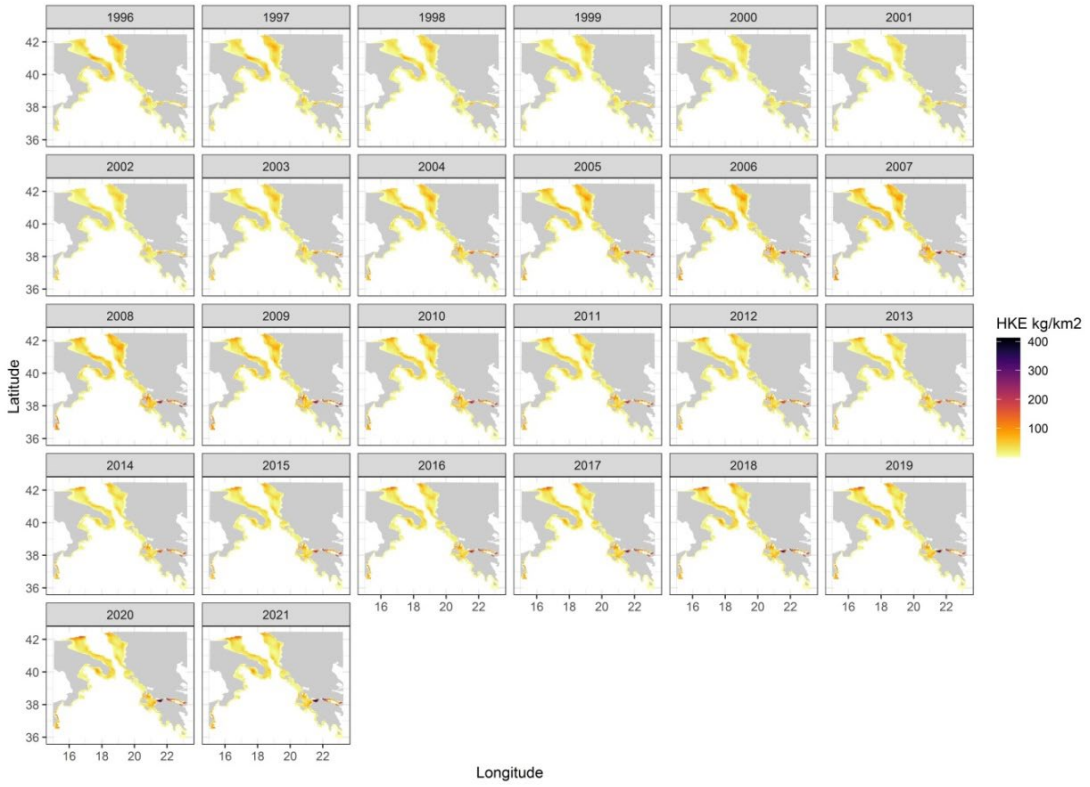

Figure 4.1.3.4 Annual predictions for hake biomass based on the final GAM.

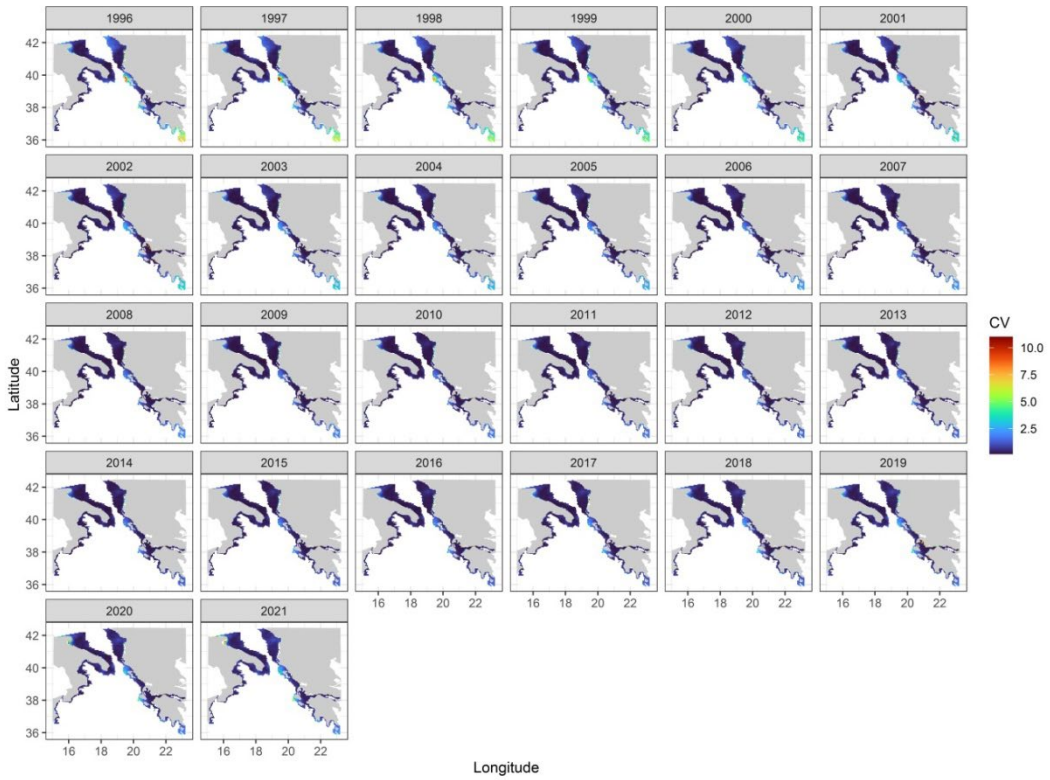

Figure 4.1.3.5 Annual CV based on the final GAM calculated based on the mean and standard deviation of hake biomass estimated for each sample of 1000 simulated fitted values.

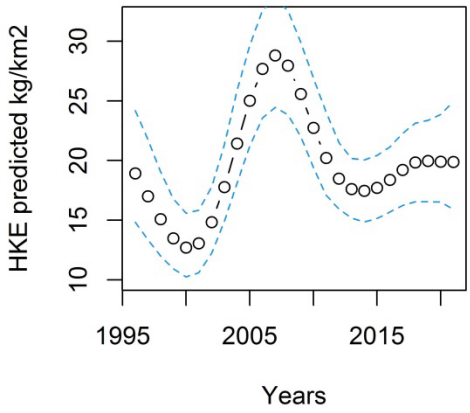

Figure 4.1.3.6. Time-trends of mean hake biomass values for the years 1996–2021. The round dots are the mean kg/km2 by year for each sample of 1000 simulated fitted values (based on the final model's predictions) averaged over all locations of the grid used for prediction in the study area (0.04 * 0.04 decimal degrees). The dashed lines are the 95% Bayesian credible intervals.

4.1.4 Model 5: Spatio-temporal generalized additive models

The GAM used here models all ICES DATRAS data and includes the following 8 terms and specifications (number of knots, type of spline, and penalty; corresponding to the R code):

1. s(lon,lat,bs='ds',k=256,m=c(1,0.5)) +
2. s(ctime,bs='ds',k=ny,m=c(1,0)) +
3. ti(ctime,lon,lat,d=c(1,2),bs=c('ds','ds'),k=c(ny,10),m=list(c(1,0),c(1,0.5))) +
4. te(timeOfYear,lon,lat,d=c(1,2),bs=c('cc','ds'),k=c(6,30),m=list(c(1,0),c(1,0.5))) +

5. Gear +
6. s(ShipG,bs='re') +
7. s(Depth,bs='ds',k=5,m=c(1,0)) +
8. offset(log(SweptArea))

Where ny is the number of years for each species (see Table 4.1.4.1).

Table 4.1.4.1: First year used for analysis and number of hauls with and without observations.

	Gadus morhua		Merluccius merluccius		Scophthalmus maximus		Conger conger	
	juv	adult	juv	adult	juv	adult	juv	adult
First year	1967	1967	1979	1979	1979	1979	1985	1985
Number of years (ny)	54	54	42	42	42	42	36	36
Length at 50% maturity (cm)	59		50		46		135.65	
Number of hauls bio > 0	39807	14955	24059	7792	10319	852	8409	373
Number of hauls bio == 0	48441	73293	46230	62497	83481	92948	42628	50664

Besides the spatial and temporal component (first two terms), the model includes a spatio-temporal interaction, that is two-dimensional smooth surface with 10 knots for each year and similarly, a two-dimensional smooth surface with 30 knots for different times of the year. The model also includes a parametric gear effect and random ship-gear effect, a smooth effect of the depth and the swept-area as offset. The response variable was the biomass of the juvenile and adult part of the population of the following 4 species: Cod (Gadus morhua), Hake (Merluccius merluccius), Turbot (Scophthalmus maximus), and Conger eel (Conger conger). The size at 50% maturity was used to split the data into the juvenile and adult part (Table 4.1.4.1). The Tweedie distribution with a log link function was used as the likelihood family of the model.

The estimation of the abundance and uncertainty are based on the methodology described in Berg *et al.* (2014). The abundance was predicted for the longitude and latitude values corresponding to the centroid of a regular sized grid based on the ICES statistical subrectangles with 20′ longitudinal and 10′ latitudinal dimensions. The extensions of the grid were constrained to be within a distance of 0.5° to the location of the hauls included in the ICES DATRAS database. The depth for each of the grid cells was downloaded from the NOAA database (Figure 4.1.4.1).

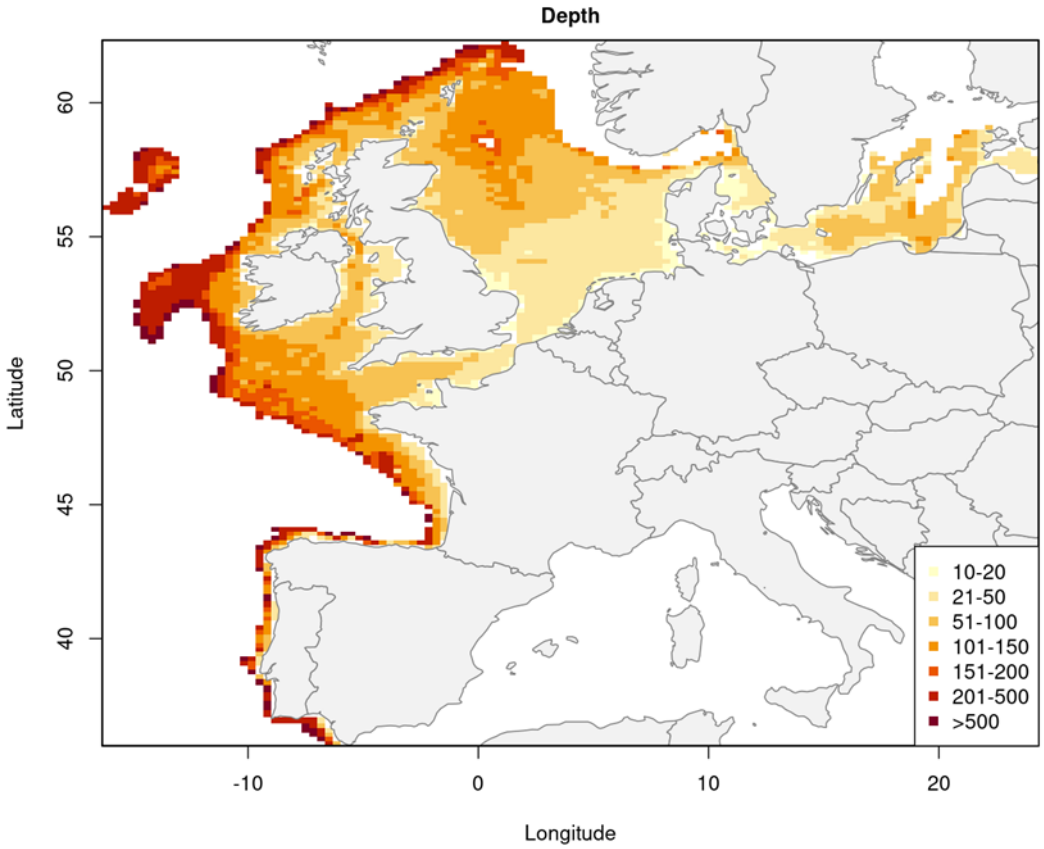

Figure 4.1.4.1. Depth in each grid cell of the prediction grid.

The abundance was not predicted for the whole prediction grid as presented in Figure 4.1.41, but a subset thereof dependent on the locations where a species was observed in order to minimize required extrapolation. Therefore, the prediction grid for each species and each year was defined as the ICES subareas in which a species was observed at least once. That means that all subrectangles of a certain subarea were included for a given year if the species was observed at least in one of these subrectangles. Figure 4.1.4.2 shows the ICES statistical subrectangles with corresponding ICES subareas for the maximum extension of the prediction grid as defined above. This also implies that the prediction grid for a single species can vary over time. The reference gear was defined as the gear with the largest number of hauls in which the respective species was observed. The time of year was defined as the median time of the year over all samples for a given species and for each quarter.

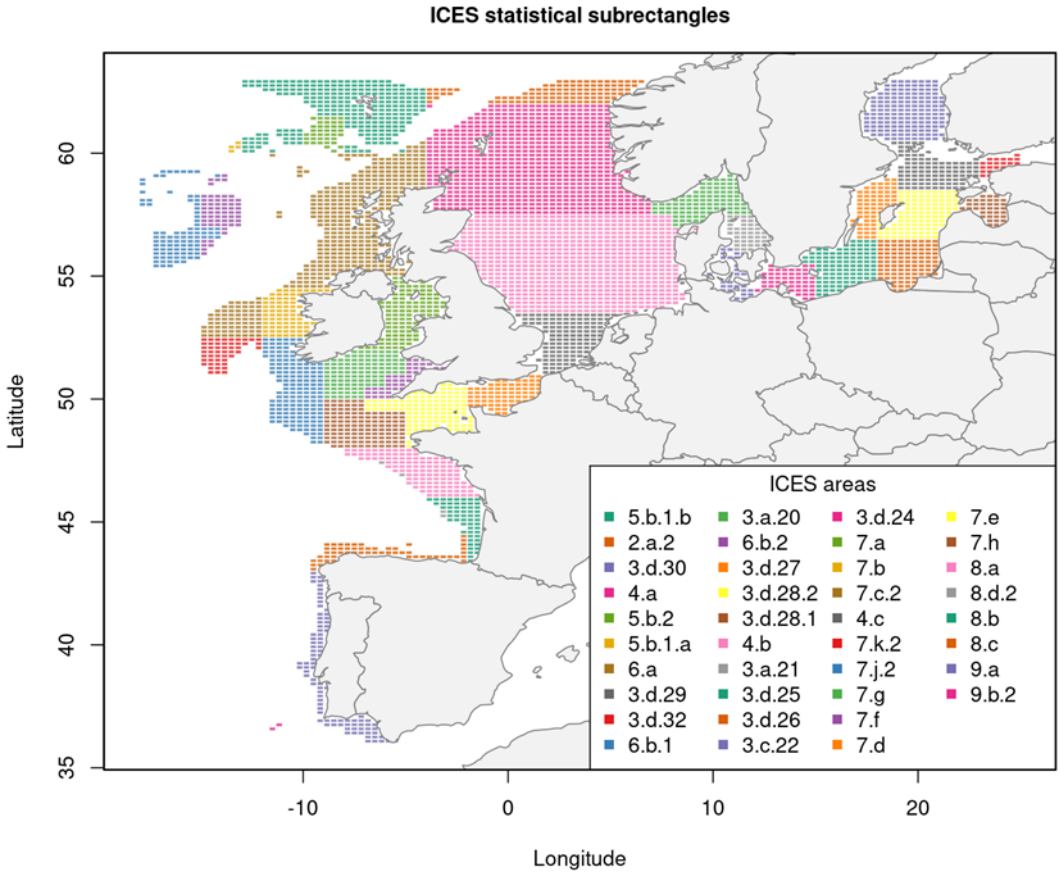

Figure 4.1.4.2. ICES statistical subrectangles in relevant depth range with associated ICES area.

The uncertainty was estimated based on parametric bootstrapping with 1000 samples.The model fitting and abundance estimation was done in R and by means of the following R packages: mgcv (Wood, 2011), surveyIndex (Berg, 2014), marmap (Pante and Simon-Bouhet, 2013) and fishdist.

4.1.4.1 Results

The model was able to estimate parameters and predict abundances for all species and datasets (juveniles and adults), although for some years and species the number of hauls with observations was very low (Table 4.1.4.1). In particular, the adult datasets of Conger eel and turbot had a very low sample size with 373 and 852 hauls with observations over the whole period. The results for these datasets should, thus, be interpreted with caution. While the estimated gear effects show similar patterns for juvenile cod and hake, overall the gear effects vary substantially between juveniles and adults and between the different species (Table 4.1.4.2).

Table 4.1.4.2: Estimated parametric gear effects (reference gear for all species GOV_CL)

Gear	*Gadus morhua*		*Merluccius merluccius*		*Scophthalmus maximus*		*Conger conger*	
	juv	adult	juv	adult	juv	adult	juv	adult
GOV_CL	1	1	1	1	1	1	1	1
BT	0.46	0.28	0.5	0.33	2.23	2.11	0.19	0.3
TV	3.64	0.77	2.55	0.1	1.21	2.96		

Gear	*Gadus morhua*		*Merluccius merluccius*		*Scophthalmus maximus*		*Conger conger*	
	juv	adult	juv	adult	juv	adult	juv	adult
GOV_GG	0.54	0.73	0.88	0.42	1.4	1.18	0.24	0.72
BAK_GG	0.38	0.99	0.37	0.31	0.67	0.29		
BAK_CL			0.32	0.21	0.11	0.86	1.76	0.59
CAR			0.4	0.43	16.08	0	0.21	1.43

The estimated abundance for the 4 species (Figures 4.1.4.3–10) shows distinct core areas of the distribution for each species as well as how these core areas change over time by 3 maps corresponding to the beginning, middle, and end of the period. While juvenile cod and turbot appear to be abundant in the southwest Baltic Sea (Figure 4.1.4.3 and 4.1.4.7), adult cod and turbot show a wide distribution throughout the North Sea and Celtic Seas (Figure 4.1.4.4 and 4.1.4.8). The distribution of adult cod indicates a higher abundance in more northern waters in more recent years (Figure 4.1.4.4). Juvenile and adult hake, on the other hand, shows a higher abundance in deeper areas and at the border of the sampled areas (Figure 4.1.4.5 and 4.1.4.6). Juvenile and adult conger eel show a high abundance northwest of France and in the English channel (Figure 4.1.4.9 and 4.1.4.10). The coefficient of variation (CV) maps reveal the uncertainty associated with the predicted abundance for each grid cell and reveal that in particular for early years across all species and for conger eel as well as adult hake and turbot large parts of the distribution are associated with high CV > 1 (purple areas).

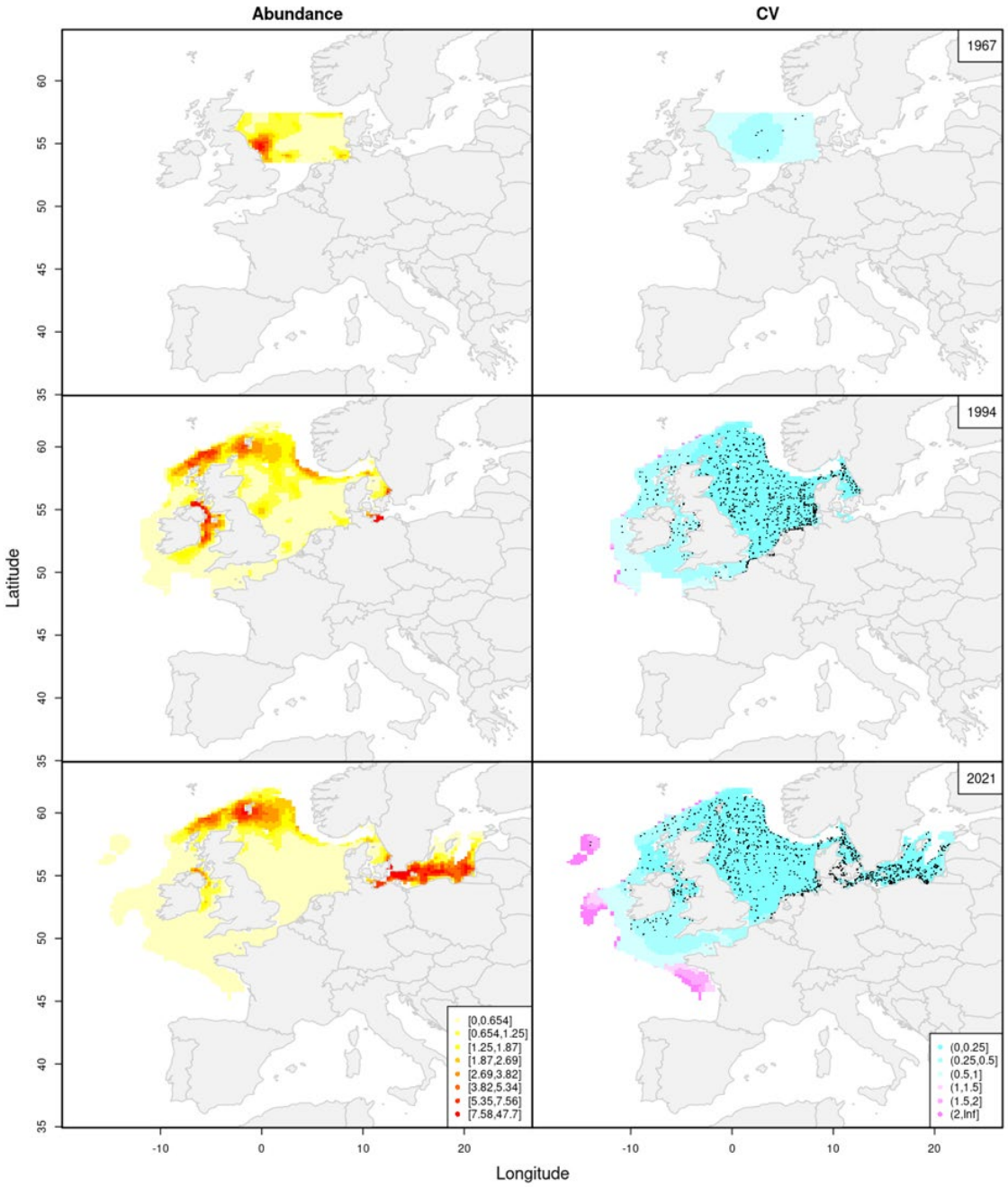

Figure 4.1.4.3: Distribution (left column) and uncertainty maps (right column) of juvenile *Gadus morhua*.

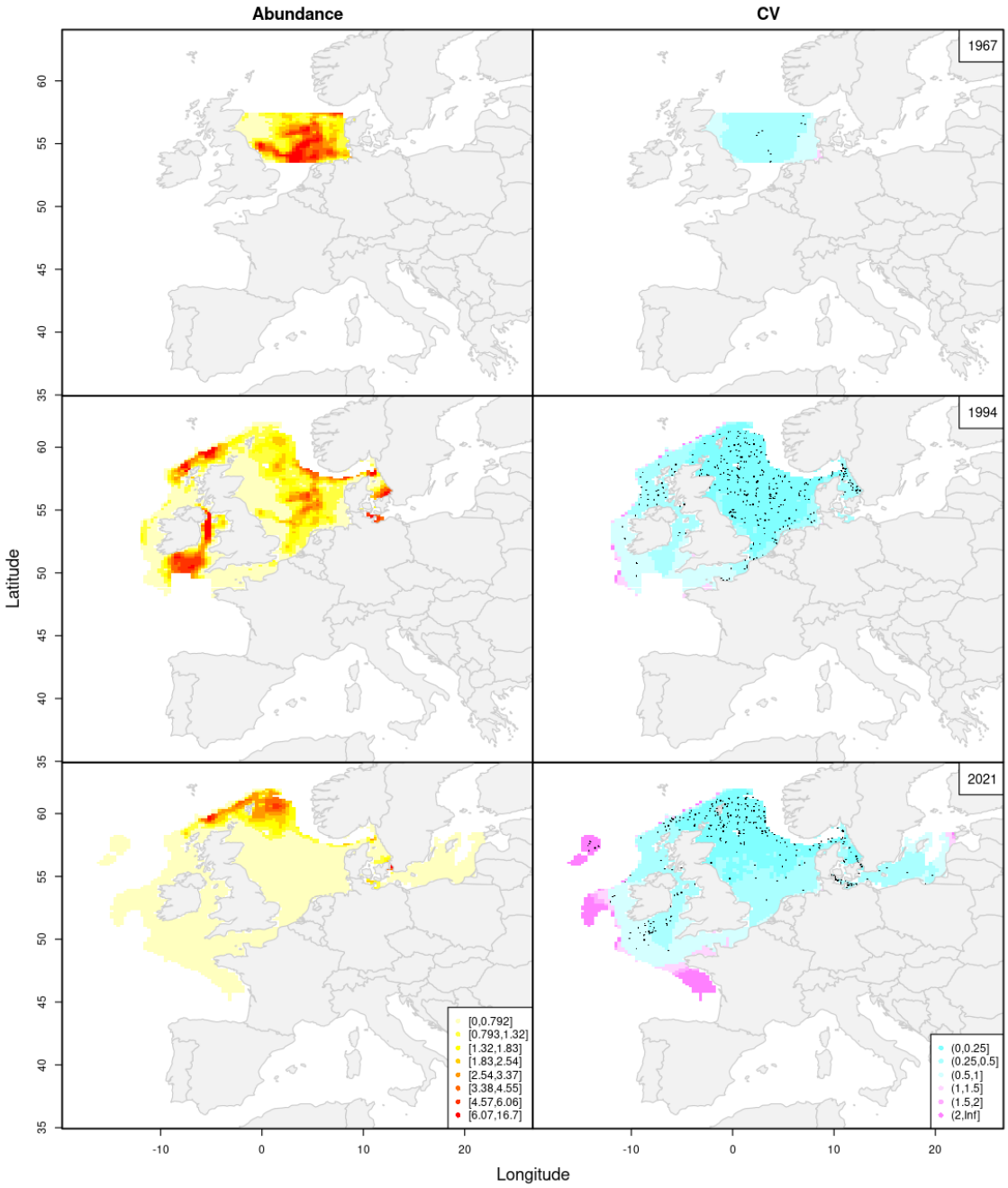

Figure 4.1.4.4: Distribution (left column) and uncertainty maps (right column) of adult *Gadus morhua*.

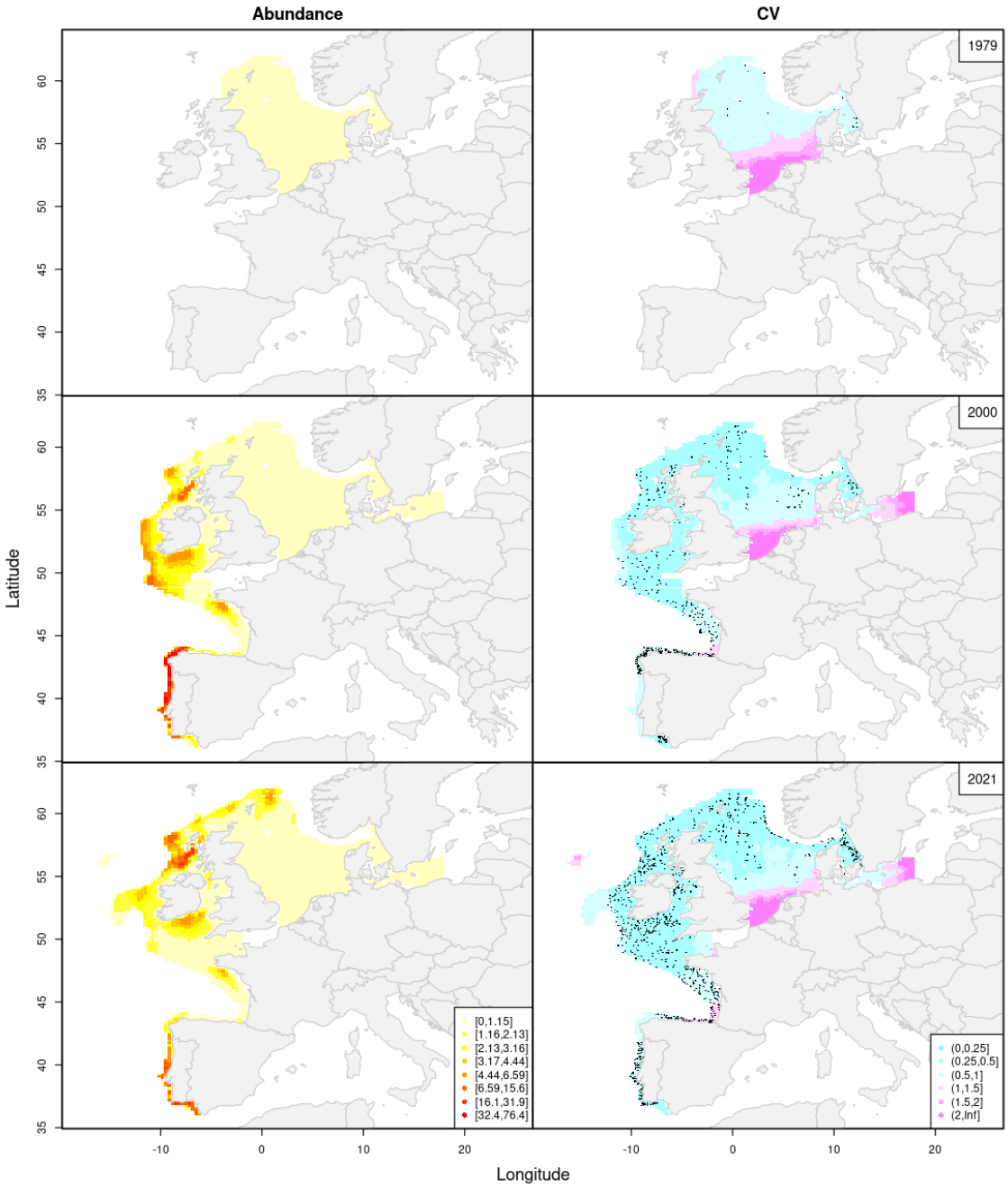

Figure 4.1.4.5: Distribution (left column) and uncertainty maps (right column) of juvenile *Merluccius merluccius.*

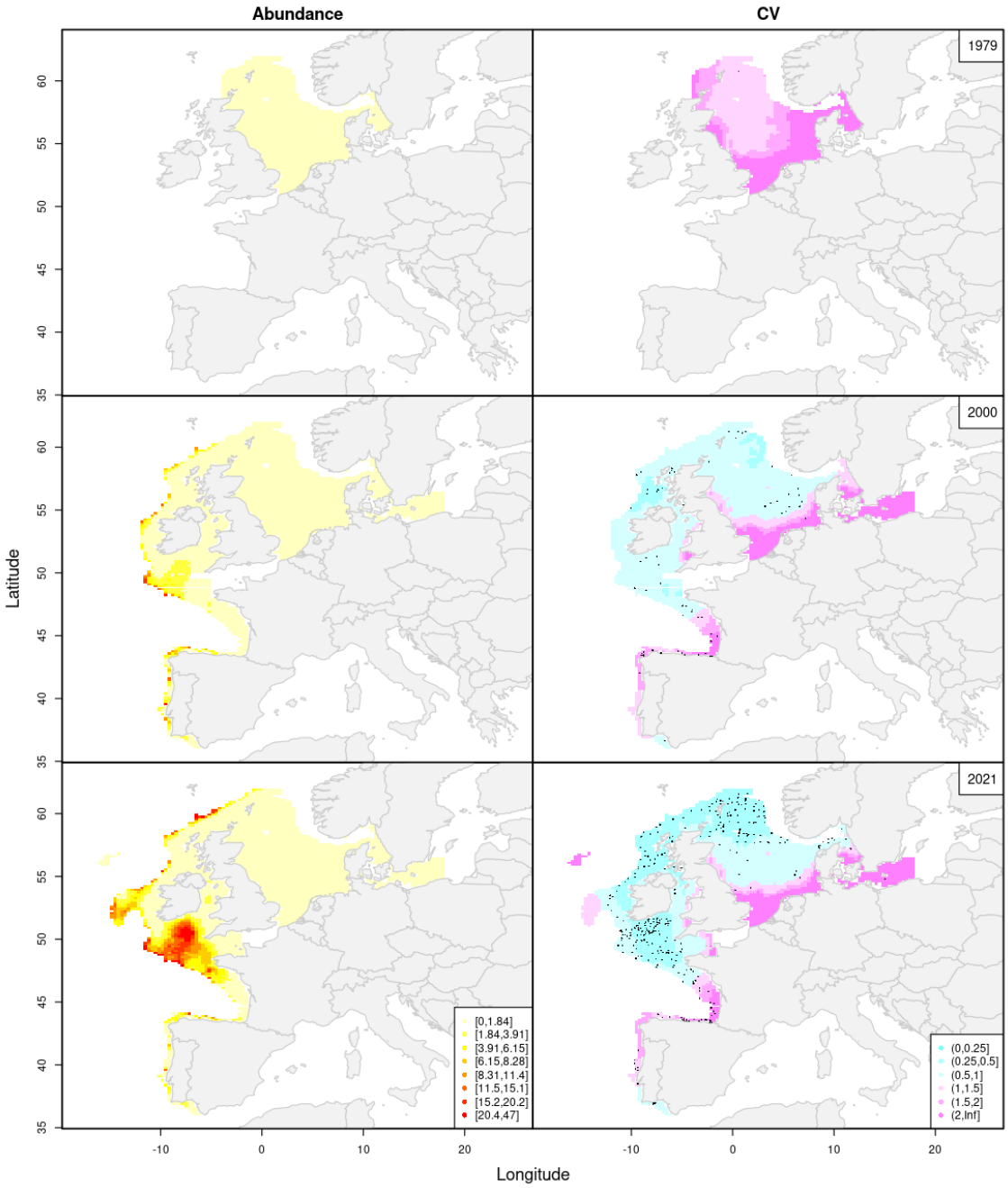

Figure 4.1.4.6: Distribution (left column) and uncertainty maps (right column) of adult *Merluccius merluccius.*

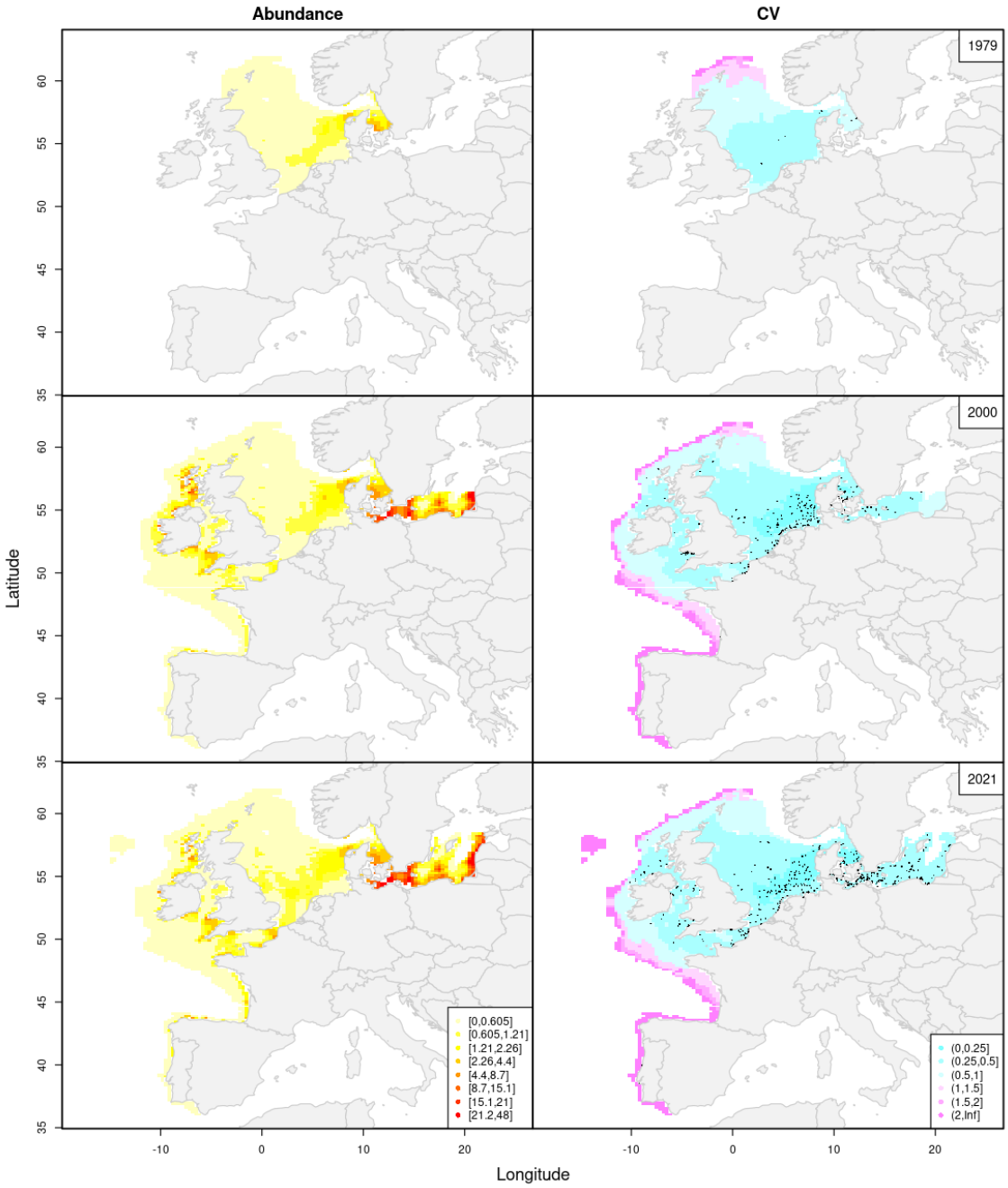

Figure 4.1.4.7. Distribution (left column) and uncertainty maps (right column) of juvenile *Scophthalmus maximus.*

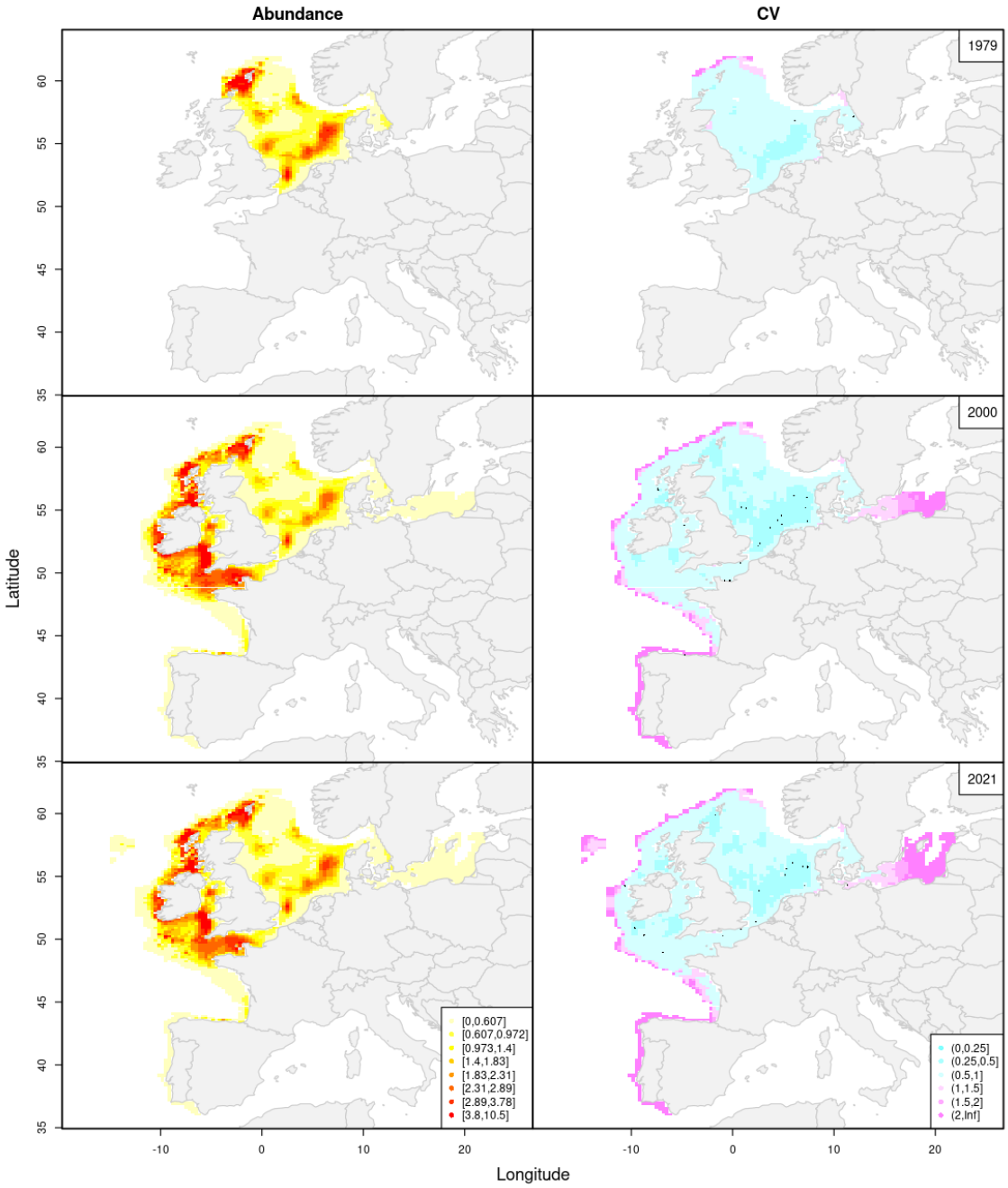

Figure 4.1.4.8. Distribution (left column) and uncertainty maps (right column) of adult *Scophthalmus maximus.*

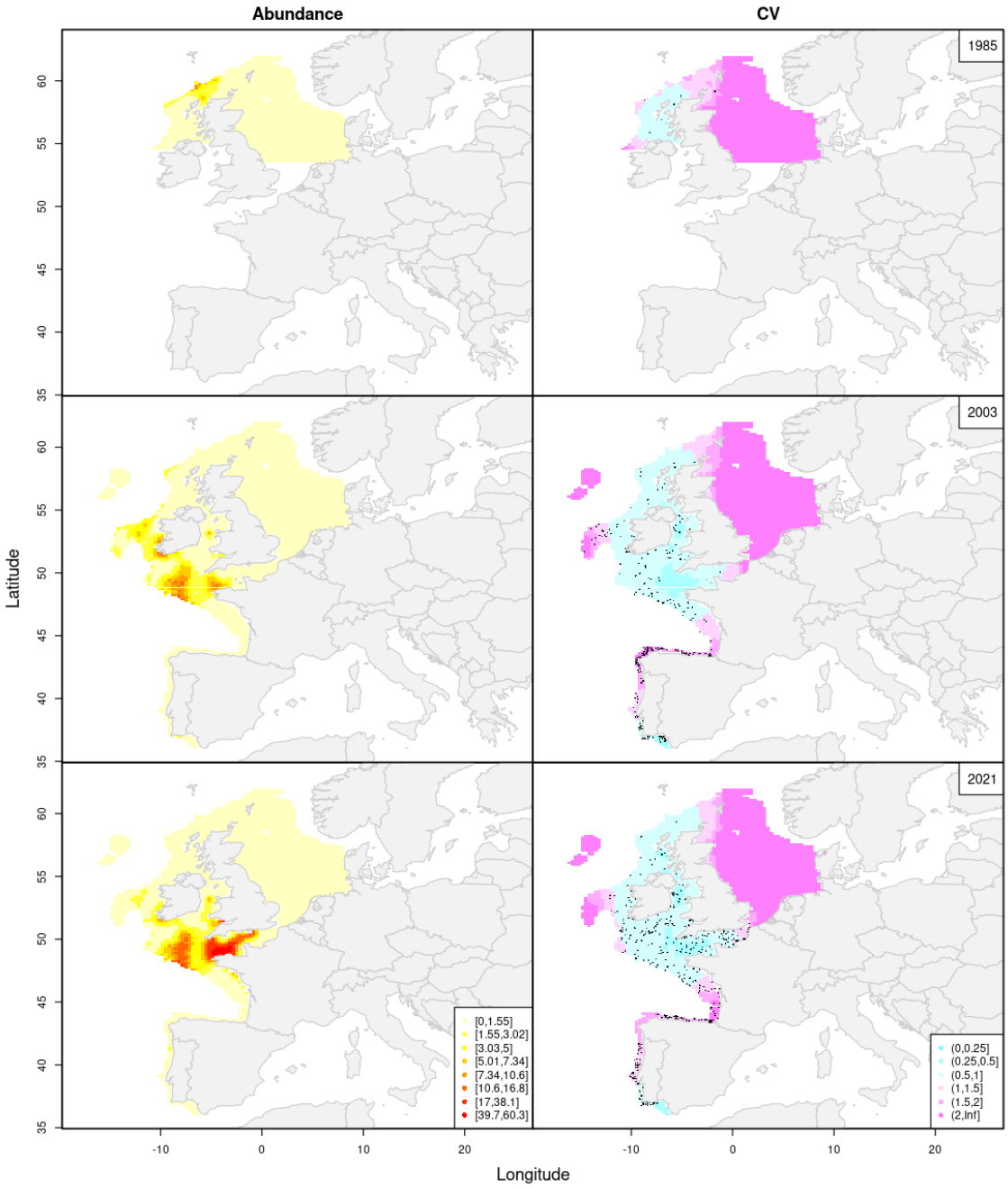

Figure 4.1.4.9. Distribution (left column) and uncertainty maps (right column) of juvenile *Conger conger.*

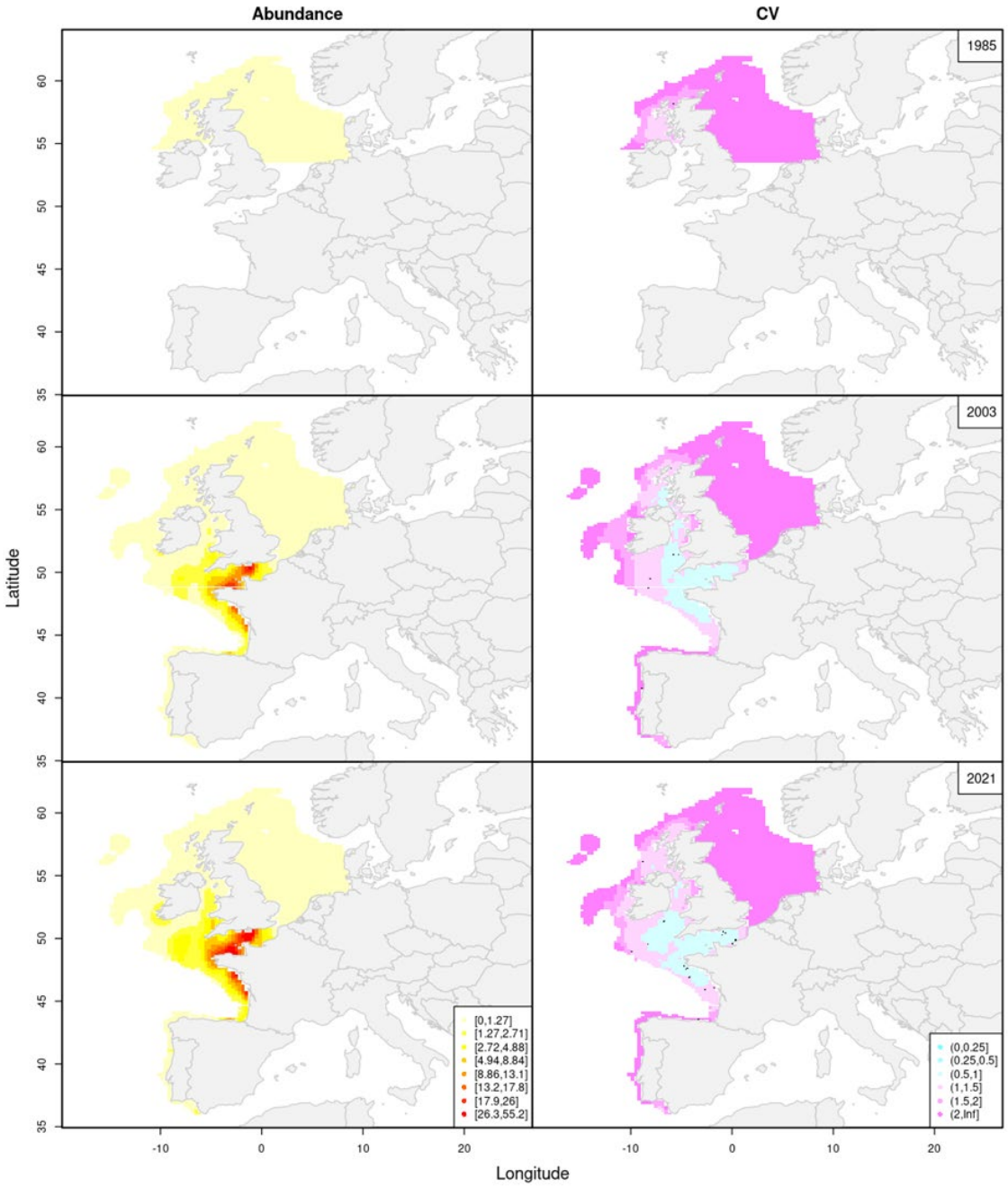

Figure 4.1.4.10. Distribution (left column) and uncertainty maps (right column) of adult *Conger conger*.

4.1.4.2 Discussion and Conclusion

Future work should compare these models with models that include a time of day effect and environmental variables. Furthermore, it should be evaluated whether the specified number of knots is sufficient and whether the knots are optimally distributed between the various terms. The residuals looked reasonable for the models presented here, however, further work should include model validation by cross validation. In particular, gear and ship effects tend to be confounded with space and time effects (due to limited overlap of samples) so these should be compared with results from other models as well as different formulations of the GAMs to check for such problems.

The length at 50% maturity is arguably not the best metric to split the datasets as the values might vary substantially between regions (e.g. cod and turbot in the North and Baltic Sea) or between sexes (e.g. Conger eel). Alternatively, the median of the length distribution could be used to split the datasets. Using the median would have two further advantages: 1) datasets with very few positive hauls are avoided when length-at-maturity specimens are rare and 2) size-dependent gear effects are likely better captured. However, the median is highly affected by mortality and will thus differ between species. Further, the median has no biological equivalent in terms of relationship with e.g. spawning areas.

The extent to which the abundance in very uncertain grid cells (e.g. CV > 0.5) should be presented in the final maps needs to be considered. Values above 0.25 could be considered as thresholds. However, especially low CV thresholds might lead to neglecting large parts of the distribution for less abundant species, such as Conger eel in this case (see Figure 4.1.4.9 and 4.1.4.10).

4.2 Model 6: VAST

Two VAST models were fitted during the workshop, one for adult cod and another for red mullet.

4.2.1 Model configuration for cod

The model was fitted to adult cod catches in biomass. In VAST, all spatial processes are assumed to be Gaussian Processes with a Matérn correlation so that the SPDE routine, as implemented in the INLA software, can be used for estimation. Note that a VAST model by default includes 2 linear predictors, a linear predictor for presence/absence, and a linear predictor for the positive catch rate.

To model the adult biomass of cod, the following model was setup:

First linear predictor:

Tweedie($catch_i > 0) \sim \beta_0 + offset(\log(SweptArea))$,

indicating that presence/absence is only driven by a single fixed effect, the intercept β_0. A Tweedie link (see VAST documentation) function was imposed so that SweptArea can be included as an offset variable.

Second linear predictor:

$\log(catch_i) \sim \beta_0 + \beta_{1_g} xgear_i + s(depth_i, k = 3) + f(\omega_{(x,y)_i}) + f(\gamma_{(x,y,q)_i})\ x\ Quarter_i + f(\varepsilon_{(x,y,t)_i}) + offset(\log(SweptArea)) + \sigma$,

where the catch of observation i is a function of an intercept, represented by the coefficient of β_0, a fixed gear effect where β_{1_g} is the coefficient of gear g, and gear is a dummy variable. For reasons of numerical stability, the depth covariate was scaled, and included in the model as a spline with 3 knots. The functions $f(\omega_{(x,y)_i}), f(\gamma_{(x,y,q)_i})\ x\ Quarter_i, f(\varepsilon_{(x,y,t)_i})$, represent the value of i at location x,y in the spatial fields ω, γ and ε, which are a fixed spatial field, a fixed spatial field for each quarter, and a spatio-temporal field with first order autocorrelation, respectively. Finally, the SweptArea was included as an offset variable in the model. The observation error, denoted by σ, is assumed to follow a Tweedie distribution. In summary, the model included 72469 parameters, of which 19 fixed and 72450 random effects parameters. The spatial models were defined on a triangulated mesh with 322 knots (Figure 4.1.5.1). Furthermore, a Barrier constrained was imposed to break down the spatial correlation process in case of land masses.

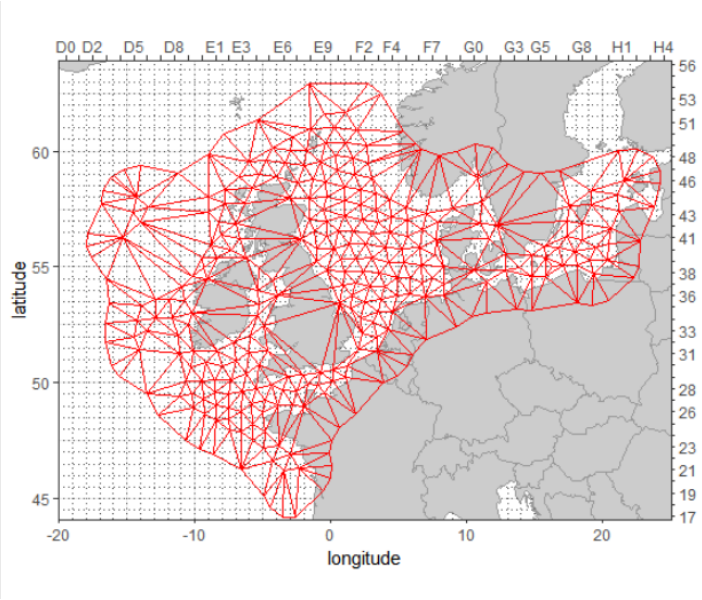

Figure 4.1.5.1. Mesh used to model spatial processes using the INLA approach.

4.2.2 Model fitting

To reduce runtime, the model was fitted with the Microsoft R Open software (4.0.2), this R distribution is similar to R 4.0.2 but includes additional capabilities for improved performance. More specific, the software uses MKL (Math Kernel Libraries) from IBM which provides multi-threaded implementation of many math operations. The total runtime of the model was 9460 seconds resulting in an AIC of 170588.2.

All parameters could be estimated and the maximum gradient in the final iteration was 8.2315e-08. Fixed effect parameters are given in Table 4.1.5.1. The covariate effects are shown in Figure 4.1.5.2. The depth effect is dome shaped with highest catches found between 100 and 300 m depth. The GOV-CL trawl has the highest catchability for cod, followed by the BAK_GG, GOV_GG and TV gears that are all designed for round fish. The beam trawl surveys (BT) have, as expected, the lowest catchability for cod. Remark that the gear effects (including the intercept) have a high uncertainty.

-0.06340116 0.220660576

Table 4.1.5.1. Parameter estimates, standard error and final gradient of the fixed effects. Parameters above, below the dotted line refer to the first, second linear predictor, respectively.

	Estimate	Std.Error	final_gradient
β_0	4.9964545	6.42E-03	-1.50E-08
β_0	4.95710619 0.371342553	4.95710619 0.371342553	-8.41E-10
β_{2_q}	0.129985	8.57E-01	5.78E-10
β_{2_q}	-2.1854855	3.99E-01	4.77E-09
β_{2_q}	-0.5868717	3.73E-01	-1.05E-09
$s(depth_i, k{=}1)$	14.8070033	5.05E-01	-1.90E-10

	Estimate	Std.Error	final_gradient
$s(depth_i, k=2)$	-26.3200555	1.69E+00	-3.29E-11
$s(depth_i, k=3)$	6.650868	4.00E+00	3.40E-10
β_{1_g} GOV_GG	-0.06340116 0.220660576	-0.06340116 0.220660576	9.74E-11
β_{1_g} BT	-1.51218029 0.189191029	-1.51218029 0.189191029	1.76E-09
β_{1_g} BAK_GG	0.06999124 0.165116554	0.06999124 0.165116554	-1.38E-09
β_{1_g} TV	-0.91031168 0.189135216	-0.91031168 0.189135216	-6.84E-10
$\log(\omega_\sigma)$	-1.3235248	1.41E-01	1.07E-08
$\log(\varepsilon_\sigma)$	-0.89104	2.81E-02	-7.77E-09
$\log(\kappa)$	-5.7521505	3.55E-02	1.61E-08
ρ	0.7754755	1.56E-02	-8.46E-08
$\log(\gamma_\sigma)$	0.449124	6.81E-02	-1.41E-08
$\log(\sigma)$	-0.6609258	1.07E-02	-6.30E-09

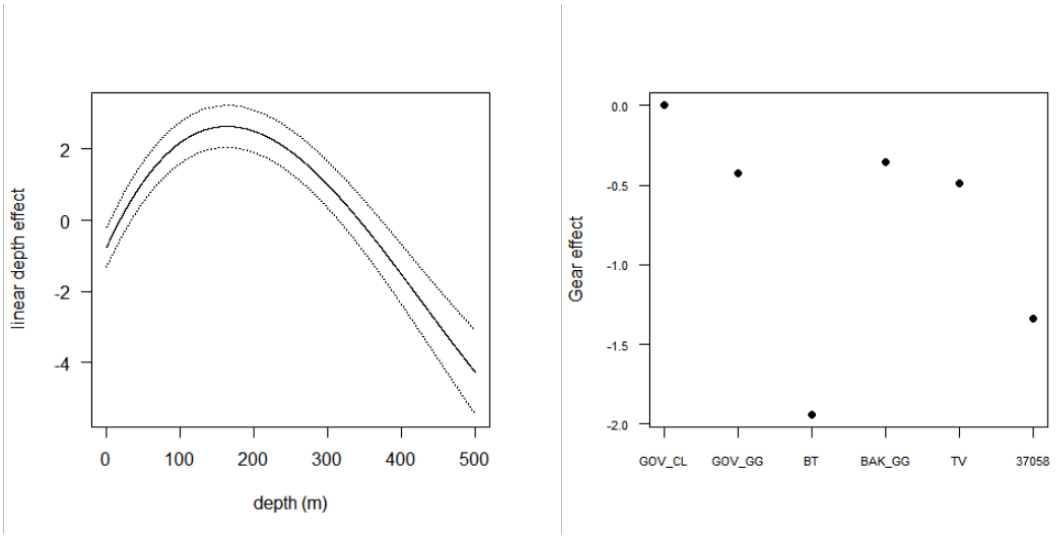

Figure 4.1.5.2. Predicted depth effect using a basis spline with 3 knots (left). The dotted lines represent the 95% confidence intervals. Predicted gear effect (right).

All spatial fields share the same kappa parameters of the Matèrn correlation function (Figure 4.1.5.3) which predicts that spatial correlation declines from 0.9 to 0.1 when the distance between two points increases from 70 to 890 km. Spatial variation is lowest for the fixed spatial and spatio-temporal fields, but is estimated to be higher for the seasonal spatial fields.

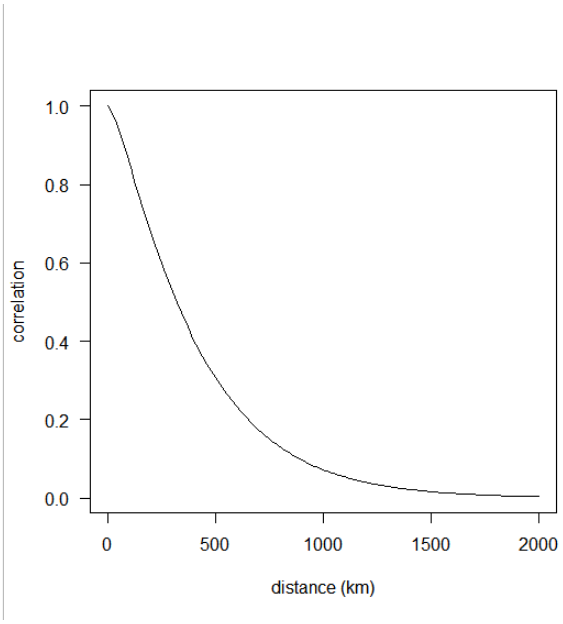

Figure 4.1.5.3. Development of the spatial correlation with respect to the distance as given by the Matérn correlation function.

The resulting spatial fixed effect, seasonal effect and density maps (Q1) are shown in Fig 4.1.5.4–6, respectively.

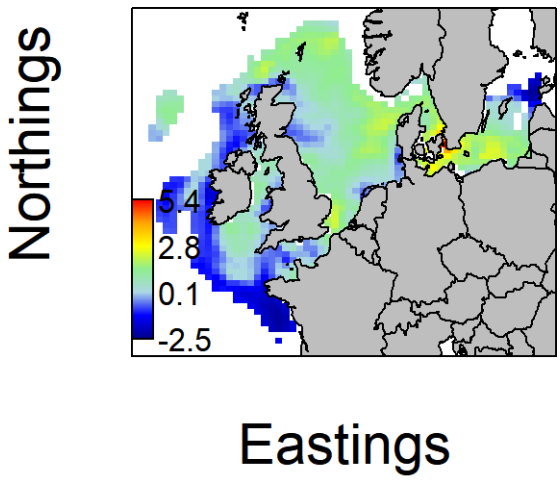

Figure 4.1.5.4. Static spatial field (omega 2).

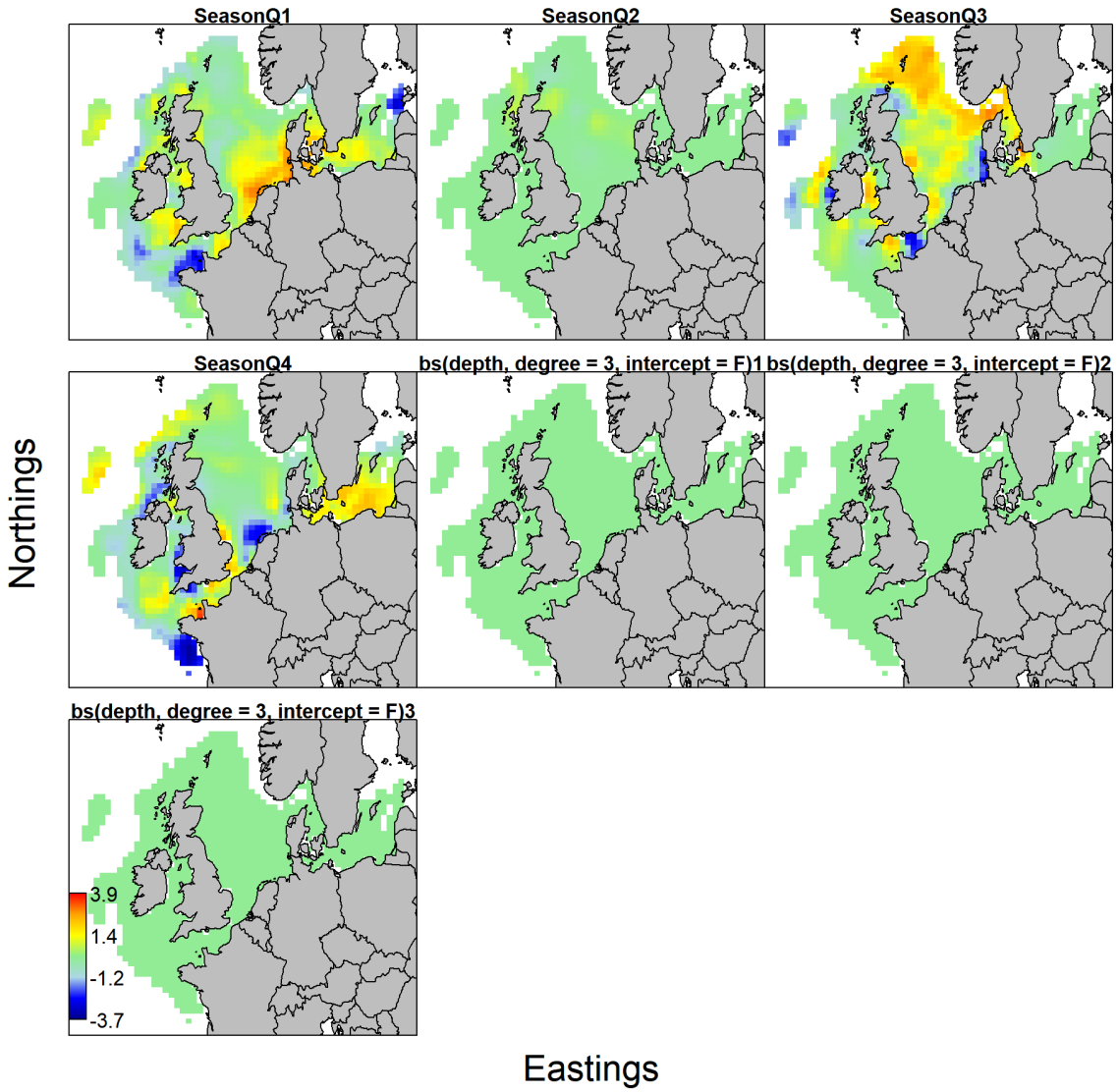

Figure 4.1.5.5. Spatial effect of the covariates. Remark that only the quarters are spatially varying, and that depth effects are constant in space.

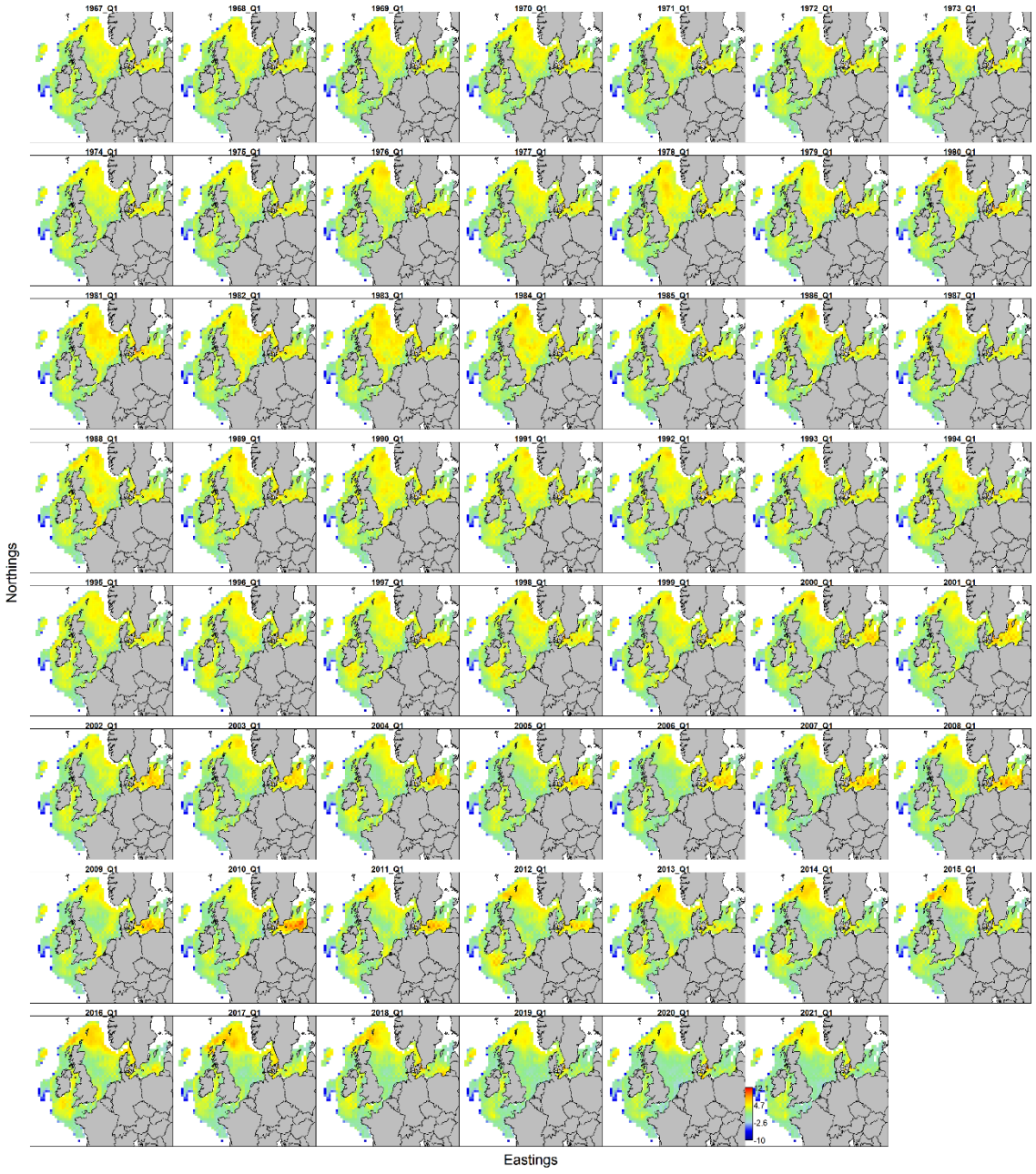

Figure 4.1.5.6. Log density of cod as predicted by the model (only Quarter 1).

4.2.3 Model validation

The VAST software computes the residuals using the approach of the DHARMa package (Hartig, 2022). To assess model performance, simulated (n = 250) new observations where drawn from the fitted model to construct an empirical cumulative distribution for each observation. The value of the ECDF at the real observation is then defined as the scaled residual. As such all residuals fall in the interval [0; 1] and are easy to interpret.

The residuals (Fig 4.1.5.7) show that there is an overdispesion effect. As a result of the large number of observations this was found to be significant, however, as the magnitude of the dispersion is low, this is not considered problematic. The overdispersion effect can also explain why the predicted number of zeros is slightly below the observed number of zeros in the data (Fig 4.1.5.8).

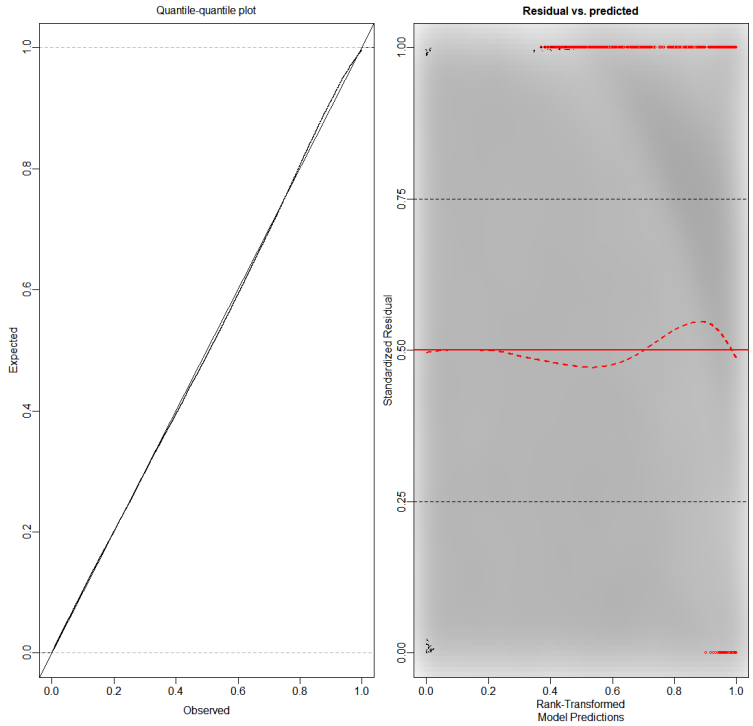

Figure 4.1.5.7. QQ plot of the residuals (left panel) and residuals vs. predicted (right panel).

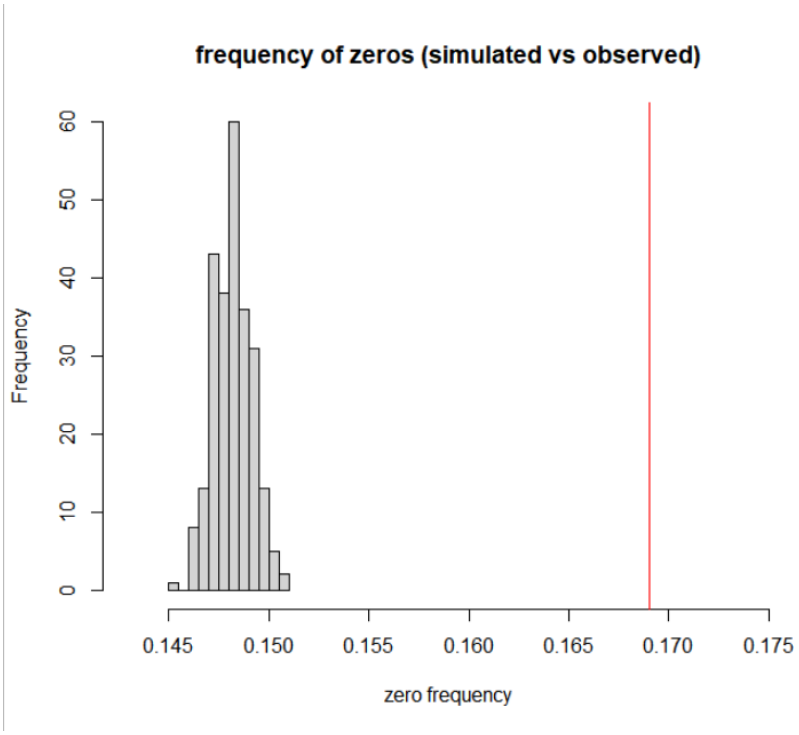

Figure 4.1.5.8. Histogram of the predicted number of zeros against the observed number of zeros in the data (red line).

Plotting the residuals against covariates (depth) did not show any problems of misspecification of the depth effect (Figure 4.1.5.9).

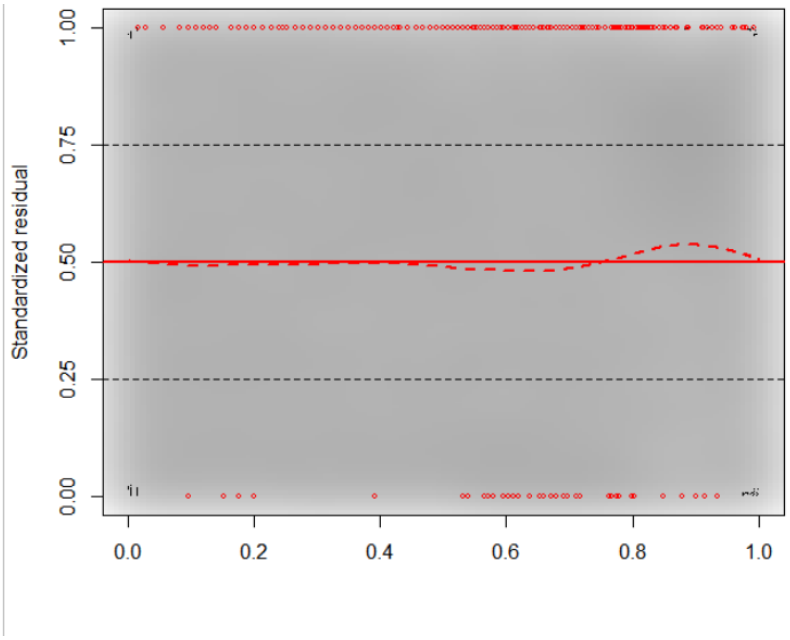

Figure 4.1.5.9. Residuals against depth covariate.

4.2.4 Model configuration for red mullet

VAST (v. 3.9.0) was used to fit a generalization of empirical orthogonal function (EOF) analysis to adult red mullet abundance data in GSA06 and GSA18 in depths of up to 200m. The two models included one linear predictor for presence/absence data:

$$\text{Log}\left(\text{catch}\,(s_i, t_i)\right) = \beta(t_i) + \omega(s_i) + \sum_{f=1}^{N_f} \lambda(t_i, f)\varepsilon(s_i, f) + \text{Depth}(s_i),$$

where ω is the spatial variation, representing unmeasured variation that is stable over time, β is the temporal variation representing a proportional increase or decrease at all locations from one year to another, ε is one or more dominant modes of spatio-temporal variation, representing unmeasured spatial variation that changes among years, as well as associated maps which represent the spatial response for the abundance to the estimated modes of variability. Furthermore, si and ti are, respectively, the location and year associated with sample i while Nf is the number of estimated modes of spatio-temporal variability. Finally, the λ(ti, f) estimate indicates whether a given year t has a positive phase λ(ti, f) > 0) or a negative phase (λ(ti, f) < 0) during the positive phase of mode f. The ε(si, f) estimate provides the map associated with the time-series λ(ti, f) and represent whether a given location s has a positive or negative value. Only depth was included as a covariate. The number of modes of variability were specified to 2 for either of the fitted models and the number of knots was set to 200.

Model fitting

Models were executed in R 3.6.3 for red mullet of GSAs 6 and 18, with AIC values for each GSA yielding 11255 and 11172, respectively.

In GSA06, two EOF modes representing the spatio-temporal variability were obtained. The first mode of density (n/km^2) variability explains 68.2% of the total spatial and spatio-temporal covariance and is characterized by high interannual variability while the second mode of variability (var. exp. 31.8%) represents a more pronounced long-term trend, possibly multidecadal, and shows less interannual variability (Figure 4.5.1.10a). The associated maps with the positive phases of the 2 modes of variability show areas with high variability of density of the red mullet (yellow and dark blue areas) across GSA06 (Figure 4.5.1.10b). The long-term spatial trend shows

density “hot spots”, i.e. yellow-coloured cells, of the species during the period that was examined in this analysis (1994–2019) (Figure 4.5.1.11). Some hot spots can be detected off Ebro Delta and in the central part of the Gulf of Valencia and below Ibiza Channel near the southern limit of GSA06. In Figure4.1.5.12, the log-densities for each year are displayed.

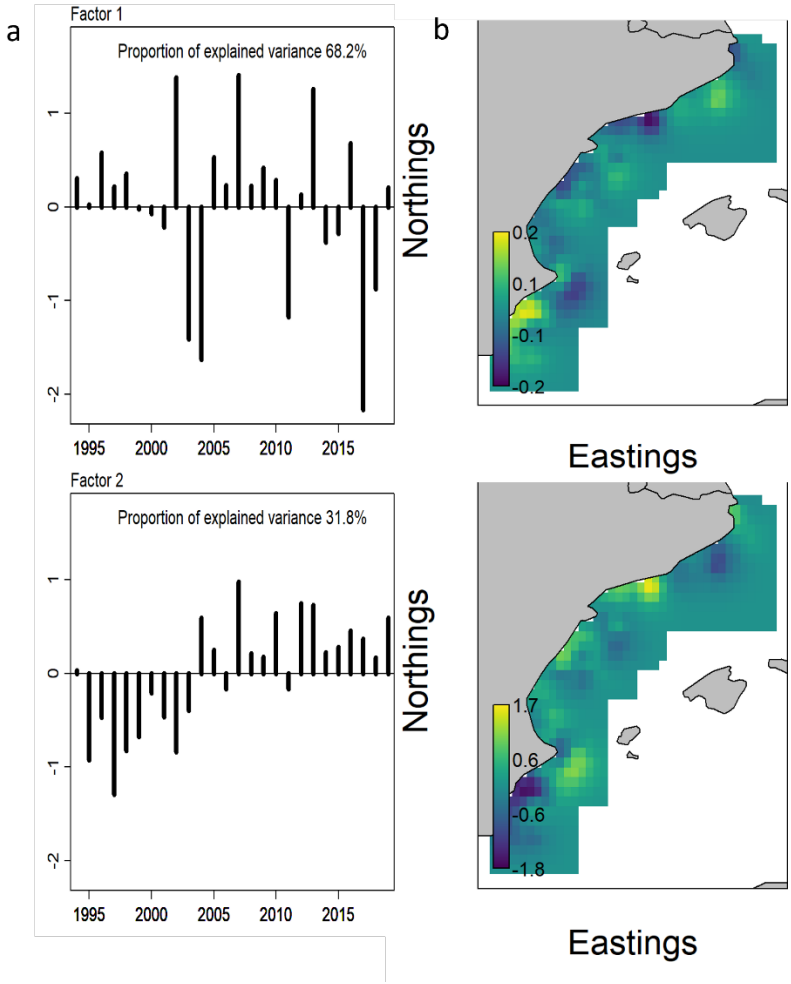

Figure 4.5.1.10. (a) Visualization of the two modes of variability and (b) variability of abundance expected during a positive phase of the first (up) and the second (down) mode of variability of GSA06.

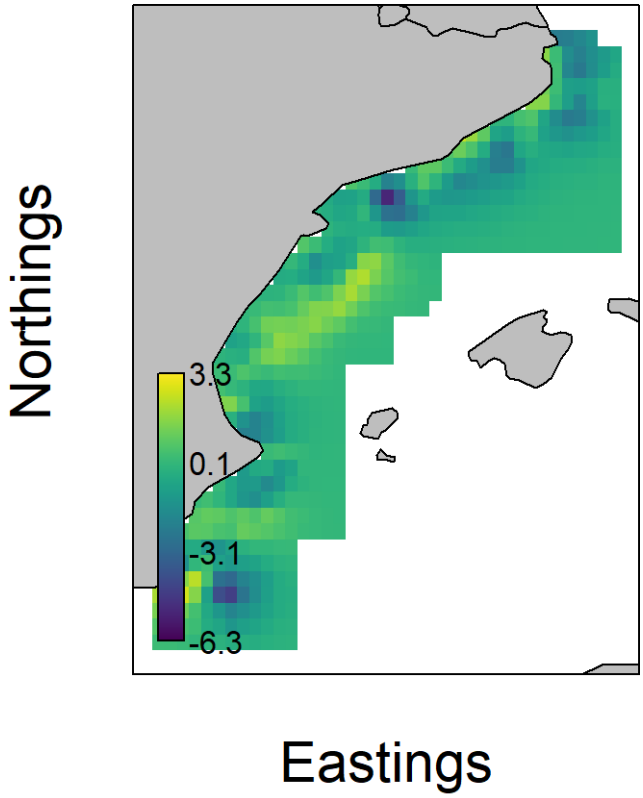

Figure 4.5.1.11. Long-term average value in spatial variation (ω) in GSA 6.

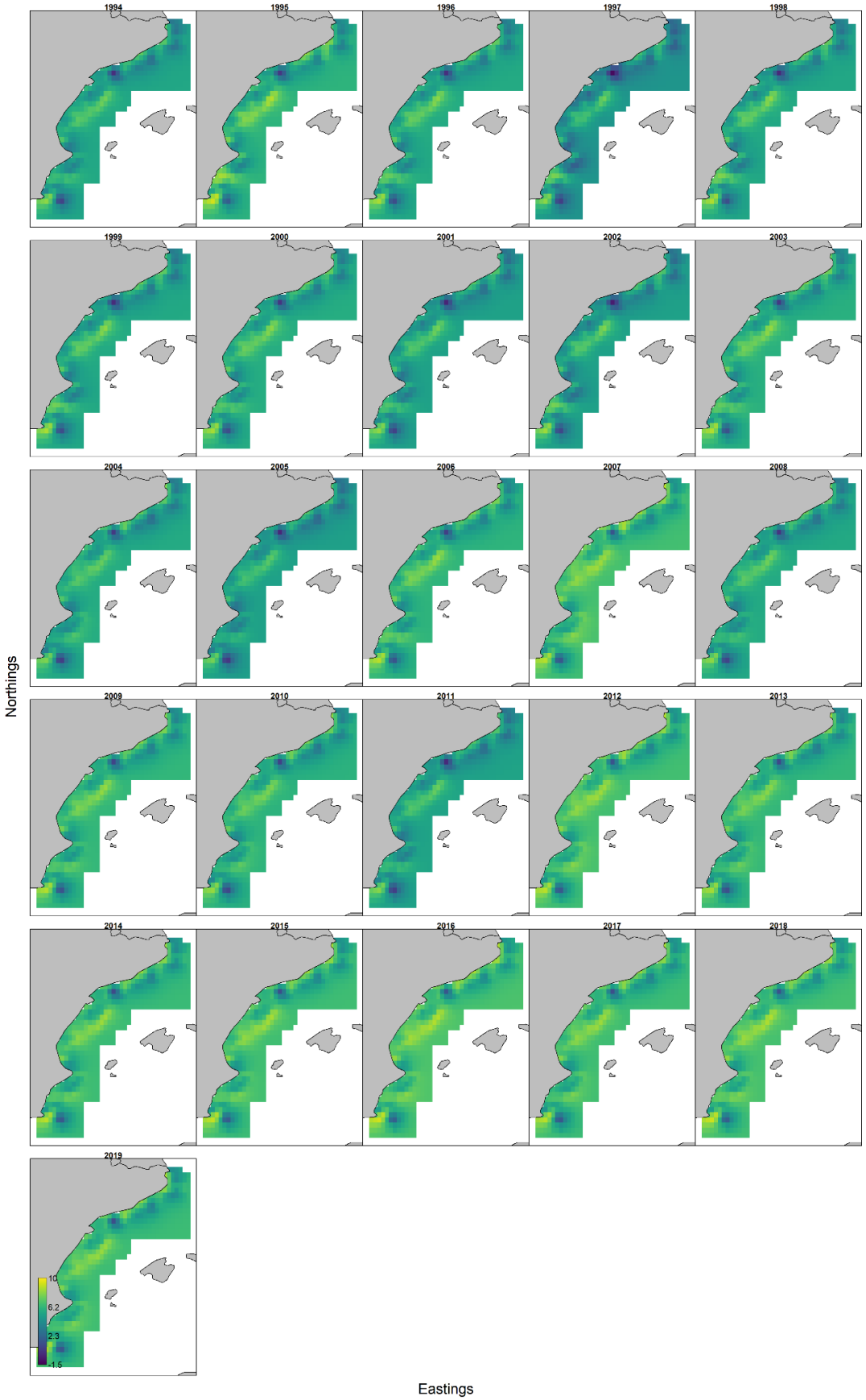

Figure 4.5.1.12. Log-densities of red mullet in GSA 6 as predicted by the model.

In GSA18, the two modes of density (n/km^2) variability explain 50.8% and 49.2% of the total spatial and spatio-temporal covariance, respectively (Figure 4.5.1.13a). The associated maps with the positive phases of the 2 modes of variability show areas with high variability of density of the red mullet in the SE Italian coast and off the coast of Albania (Figure 4.5.1.13b). The long-term spatial trend shows density "hot spots" of the species during 1994–2019 which are mainly found near the coast of Central-Northcentral Albania and off the coast of Montenegro (Figure4.5.1.14). The log-density for each year that was examined is displayed in Figure4.5.1.15.

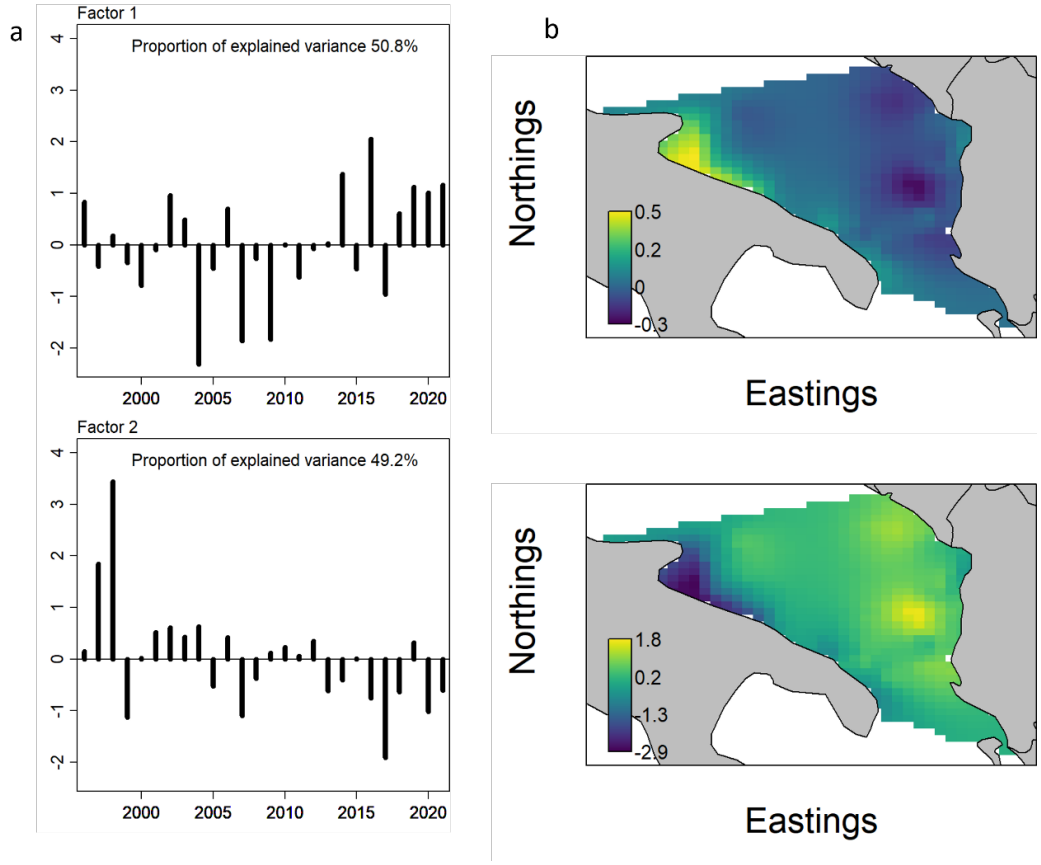

Figure 4.5.1.13. (a) Visualization of the two modes of variability and (b) variability of abundance expected during a positive phase of the first (up) and the second (down) mode of variability of GSA18.

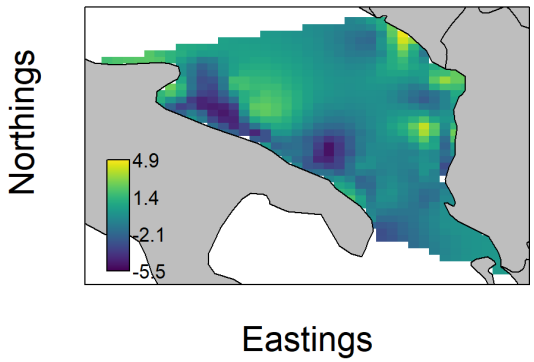

Figure 4.5.1.14. Long-term average value in spatial variation (ω) in GSA18.

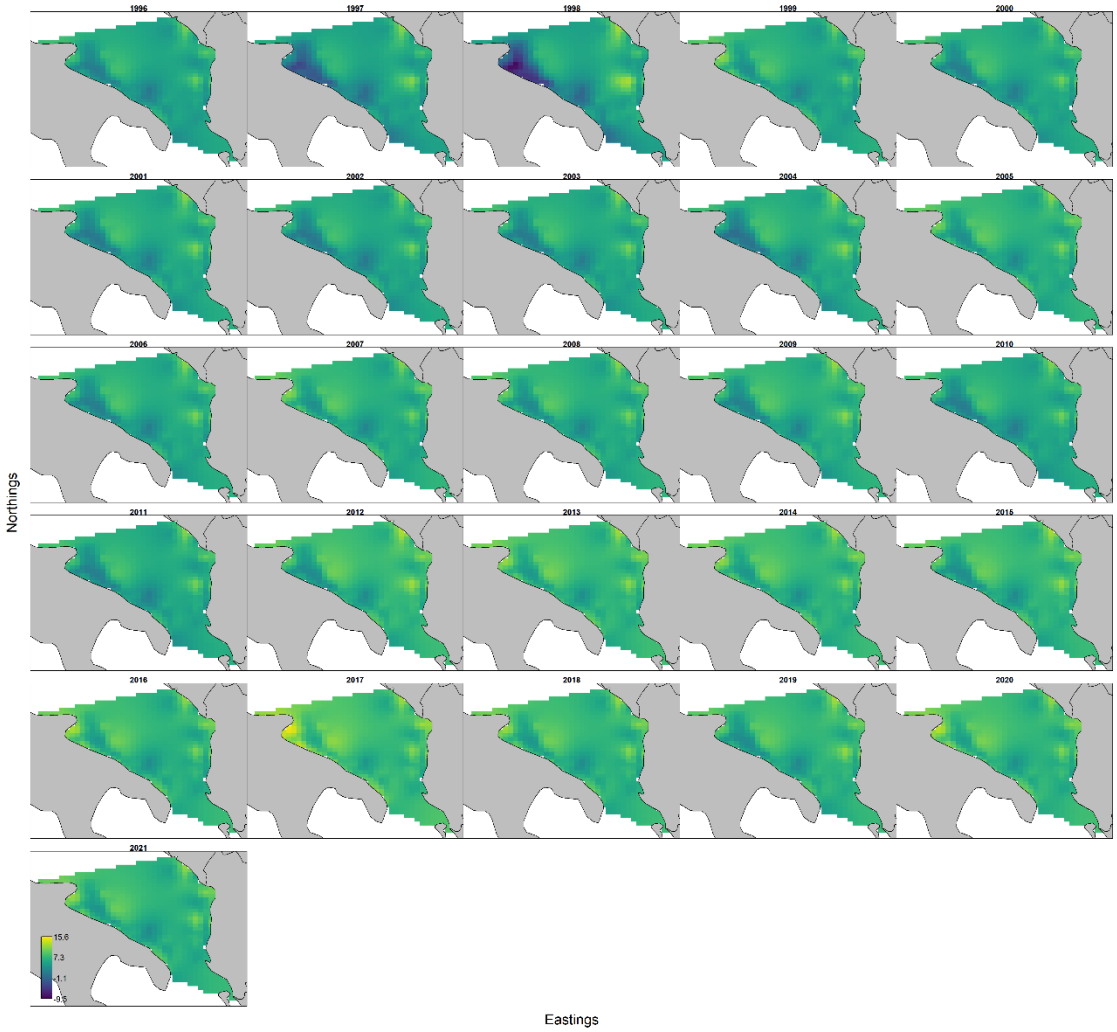

Figure 4.5.1.15. Log-densities of red mullet in GSA18 as predicted by the model.

4.2.5 Model 8: Log-Gaussian Negative Binomial Species Distribution Model (LGNB-SDM)

LGNB-SDM was applied to reconstruct and map the density distribution of both juvenile and adult cod (in numbers) in the greater North Sea area (Figure 4.1.7.1) over the most recent decade (2010- 2020). Although the LGNB-SDM can boost the reconstruction by using commercial catch data, only scientific survey data has been used during the workshop to align with other model approaches when using the exact same input dataset (i.e. DATRAS surveys data).

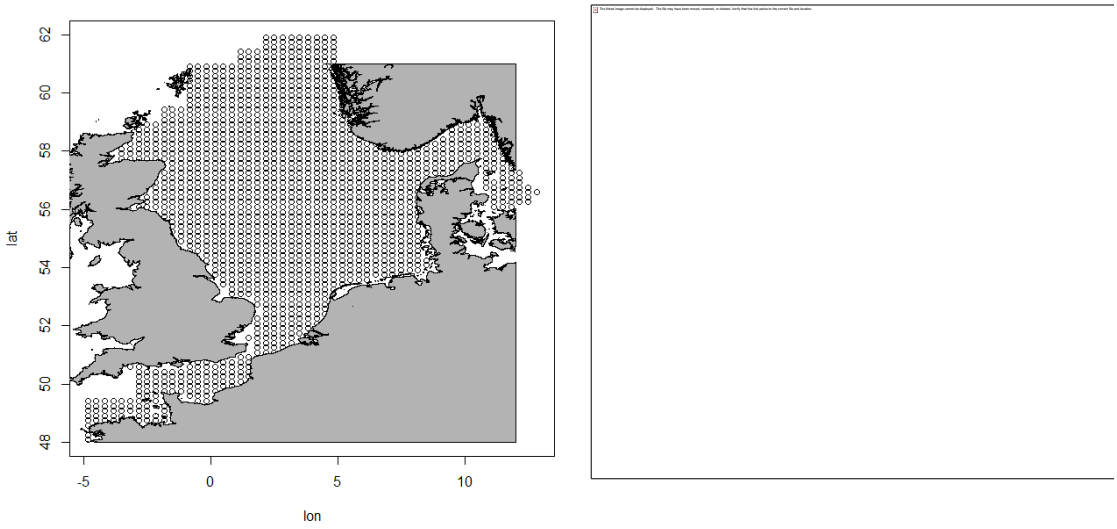

Figure 4.1.7.1. Left. Long/lat vertices of the underlying grid of interconnected discrete positions used for the LGNB-SDM approach at the geographical resolution applied during the WK. In the LGNB-SDM, the species' abundance fields are predicted on the grid in both space and time. and include spatial and temporal correlation structures on the connected graph. Right: survey points from the DATRAS data restricted to the greater North Sea area. Note the absence of sampling in the Norwegian Trench.

Albeit capable, the model used for the WK did not include environmental covariates and had the following formulation in R (see https://github.com/mcruf/LGNB/wiki/model.R for details):

m1 <- buildModelMatrices(fixed = ~ -1 + YearQuarter + Gear + Survey, random = ~ -1 + ShipTime, offset = quote(log(HaulDur)), data = datatot)

Hence, in this North Sea model are included Gear and Survey type as fixed effects as a direct way to account for differences in catchabilities across survey and gear types.

4.2.5.1 Results

Ctrl+Click on the pictures in Figure 4.1.7.2 to follow the link and see the animated abundance fields per year-quarter reconstructed over the 2010–2020 period (also stored on this data repository).

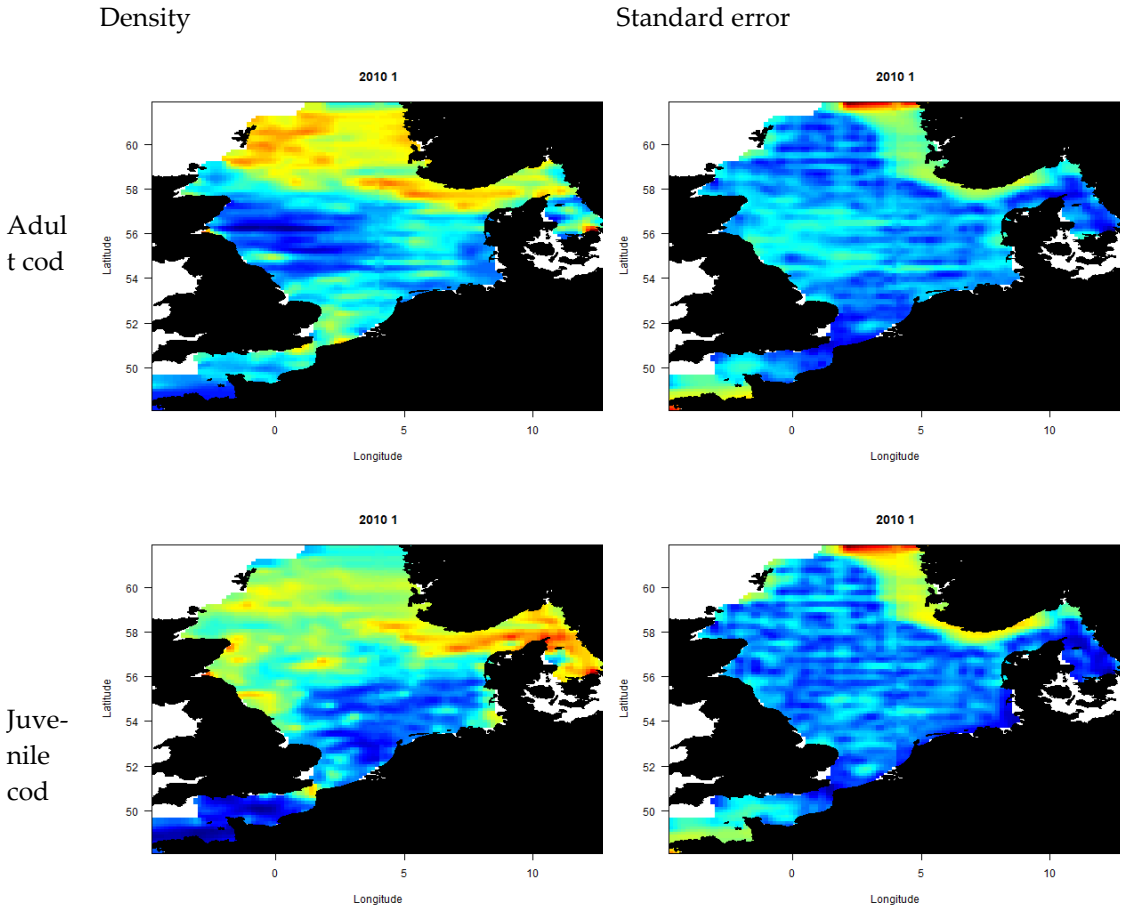

Figure 4.1.7.2. Outcomes of the spatial distribution for juvenile and adult cod over the 2010–2020 period estimated by running the LGN-SDM on the DATRAS data provided during the WK and restricted to the greater North Sea area. Left- the predicted abundance, right- the corresponding standard error. See Figure 4.1.6.3 for a more robust prediction.

As expected, the reconstruction is highly uncertain in the Norwegian Trench as seen on the Standard error mapping and hot coloured areas, where there are hardly any survey points. The Norwegian Trench is avoided by the demersal trawl surveys not designed to sample on deep bottom areas of the North Sea. Hence, the large abundance modelled by the LGNB-SDM here is a boundary effect and should be disregarded. The LGNB-SDM parameters (as described in Rufener *et al.*, 2021) were obtained for 2010–2020 adult cod (Table 4.1.7.1) and juvenile cod (Table 4.1.7.2).

The spatial correlation (logdelta) appears slightly more important for juveniles than adults while the spatial variability is low for both (logscale close to 0). Exponentiating the estimates of the fixed parameters (Tables 4.1.7.3 and 4.1.7.4) shows that the SNS survey is particularly a poor contributor in reconstructing the abundance field for cod, which is expected, SNS being a beam trawl survey specifically targeting at evaluating the Common sole population.

The interannual abundance indices found for both adults and juvenile cod came with high uncertainties based on the survey catch data used here (Tables 4.1.7.3 and 4.1.7.4, further depicted in Figure 4.1.7.4). Hence, the outcomes presented are only very preliminary, and the TMB checkConsistency() routine remains to be run to generate simulations for estimating biases out of the estimated coefficients. In addition to this, the model has been run here on 10 years of data

only during the WK. LGNB-SDM is, however, capable of running on longer time-series and on more extended geographical areas as long as dedicated time will allow it.

Besides this, the model outcomes cannot be fully quality assured when the input data might present some issue that would require a cleaning before re-running the model. Hence, it is identified that, in the input dataset:

- There are survey points found lying on land;
- There are hauls with very outstanding haul durations (170min, whereas the average is 30min);
- It may not be appropriate to include all types of surveys when searching for mapping the distribution of a certain species. For example, SNS (sole net survey) likely adds more noise than signal;
- The response variable in the input dataset is extremely overdispersed (87% of zeros). It would be appropriate to remove points on the prediction grid where 0 is a sign of non-sampled areas (i.e. the Norwegian Trench).

The model has internal routines to produce a grid of equally spaced locations and for cleaning the input data that have been disabled for aligning to the input dataset used as a common input to the WK. It would be worth to reactivate them and re-run the model fit in a near future to ensure better outcome. This will for example likely fix the visual artefact apparent on the maps.

As a final exercise within the limited time of the WK, the LGNB-SDM is re-run (see Figure 4.1.7.3) removing the Norwegian Trench area from the model area to obtain estimates that do not interpolate outside the data envelope defined by the spatial extent of the DATRAS data.

Juvenile cod

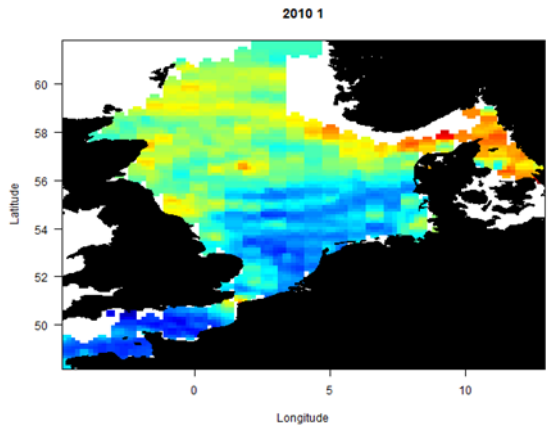

Adult cod

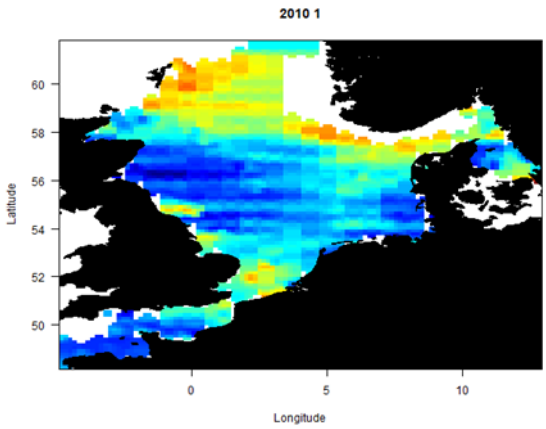

Figure 4.1.7.2. Outcomes of the spatial distribution for juvenile and adult cod over the 2010–2020 period estimated by running the LGN-SDM on the DATRAS data provided during the WK and restricted to the greater North Sea area. The Norwegian Trench closed to the Norway coast is removed prior to run the model to avoid interpolating abundance estimates where they were not DATRAS data. Grid resolution is 0.16 degree in lat and 0.33 in long. (link to repository)

Table 4.1.7.1. Estimated coefficients of the random effects of the LGNB-SDM model applied to the survey data with a catch of adult cod.

	Estimate	Std. Error
Logdelta	-4.150532473	0.278383
Logscale	-0.029980937	0.056542
time_corr	7.859019616	0.700199
beta_r_logsd	-0.390951241	0.098828
Logphi	-0.337882607	0.048497
eta_density	Etc.	Etc.

Table 4.1.7.2. Estimated coefficients of the random effects of the LGNB-SDM model applied to the survey data with a catch of juvenile cod.

	Estimate	Std. Error
Logdelta	-3.59855	0.213954
Logscale	0.114146	0.039835
time_corr	6.842335	0.441259
beta_r_logsd	-0.28397	0.062998
Logphi	-0.35742	0.025353
eta_density	Etc.	Etc.

Table 4.1.7.3. Estimated coefficients of the fixed effects for adult cod of the LGNB-SDM model applied to survey catch data.

ADULT COD	Estimate	Std. Error	z value	Pr(>|z^2|)
YearQuarter2010 1	-0.32123	16.31109	-0.02	0.98
YearQuarter2010 3	-0.52082	16.31082	-0.03	0.97
YearQuarter2010 4	-1.90091	16.32028	-0.12	0.91
YearQuarter2011 1	-0.5982	16.31102	-0.04	0.97
YearQuarter2011 3	-0.56355	16.311	-0.03	0.97
YearQuarter2011 4	-2.10345	16.31977	-0.13	0.90
YearQuarter2012 1	-0.38153	16.31113	-0.02	0.98
YearQuarter2012 3	-0.44246	16.31088	-0.03	0.98
YearQuarter2012 4	-1.24179	16.31811	-0.08	0.94
YearQuarter2013 1	-0.26518	16.3111	-0.02	0.99
YearQuarter2013 3	-0.56443	16.31084	-0.03	0.97
YearQuarter2013 4	-1.85897	16.31965	-0.11	0.91
YearQuarter2014 1	-0.55791	16.3112	-0.03	0.97
YearQuarter2014 3	-0.49921	16.31088	-0.03	0.98
YearQuarter2014 4	-0.65046	16.31754	-0.04	0.97
YearQuarter2015 1	-0.57307	16.31121	-0.04	0.97
YearQuarter2015 3	-0.5413	16.31092	-0.03	0.97
YearQuarter2015 4	0.196695	16.31652	0.01	0.99
YearQuarter2016 1	0.151795	16.3111	0.01	0.99
YearQuarter2016 3	-0.6162	16.31104	-0.04	0.97
YearQuarter2016 4	-0.26418	16.31709	-0.02	0.99
YearQuarter2017 1	-0.06119	16.31115	0.00	1.00
YearQuarter2017 3	-1.08527	16.31131	-0.07	0.95
YearQuarter2017 4	-0.9099	16.31849	-0.06	0.96
YearQuarter2018 1	-0.61831	16.31124	-0.04	0.97
YearQuarter2018 3	-1.68849	16.31172	-0.10	0.92
YearQuarter2018 4	-2.38132	16.32245	-0.15	0.88
YearQuarter2019 1	-1.56328	16.31187	-0.10	0.92
YearQuarter2019 3	-1.53674	16.31172	-0.09	0.92
YearQuarter2019 4	-2.73837	16.3246	-0.17	0.87

YearQuarter2020 1	-1.46291	16.31172	-0.09	0.93
YearQuarter2020 3	-2.08372	16.31186	-0.13	0.90
YearQuarter2020 4	-3.42322	16.33152	-0.21	0.83
GearGOV_CL	-2.59949	58.75002	-0.04	0.96
GearTV	-4.41476	16.31092	-0.27	0.79
SurveyBTS	-6.368	16.31044	-0.39	0.70
SurveyDYFS	-6.55168	16.31185	-0.40	0.69
SurveyFR-CGFS	-1.24646	57.99107	-0.02	0.98
SurveyNS-IBTS	-1.35304	57.9907	-0.02	0.98
SurveySNS	-13.7352	30.16336	-0.46	0.65

Table 4.1.7.4. Estimated coefficients of the fixed effects for juvenile cod of the LGNB-SDM model applied to survey catch data.

	Estimate	Std. Error	z value	Pr(>|z^2|)
YearQuarter2010 1	-0.65748	16.2964	-0.04	0.97
YearQuarter2010 3	-0.18955	16.29554	-0.01	0.99
YearQuarter2010 4	-0.01912	16.29992	0.00	1.00
YearQuarter2011 1	-0.54993	16.2963	-0.03	0.97
YearQuarter2011 3	-0.46505	16.2957	-0.03	0.98
YearQuarter2011 4	0.217174	16.29879	0.01	0.99
YearQuarter2012 1	-0.51524	16.2965	-0.03	0.97
YearQuarter2012 3	-0.56169	16.29558	-0.03	0.97
YearQuarter2012 4	-0.03895	16.29795	0.00	1.00
YearQuarter2013 1	-0.72077	16.29654	-0.04	0.96
YearQuarter2013 3	0.11323	16.29537	0.01	0.99
YearQuarter2013 4	0.385512	16.29964	0.02	0.98
YearQuarter2014 1	-0.46094	16.29653	-0.03	0.98
YearQuarter2014 3	-0.56684	16.29552	-0.03	0.97
YearQuarter2014 4	0.253927	16.29986	0.02	0.99
YearQuarter2015 1	-0.12076	16.29661	-0.01	0.99
YearQuarter2015 3	-1.2838	16.29572	-0.08	0.94
YearQuarter2015 4	-0.64145	16.29977	-0.04	0.97
YearQuarter2016 1	-1.07879	16.29668	-0.07	0.95
YearQuarter2016 3	-0.96268	16.29571	-0.06	0.95
YearQuarter2016 4	0.451306	16.29924	0.03	0.98
YearQuarter2017 1	-0.2421	16.29663	-0.01	0.99
YearQuarter2017 3	-0.69738	16.29561	-0.04	0.97
YearQuarter2017 4	0.078509	16.30112	0.00	1.00
YearQuarter2018 1	-0.94208	16.2966	-0.06	0.95
YearQuarter2018 3	-1.29475	16.2958	-0.08	0.94
YearQuarter2018 4	-0.89433	16.30018	-0.05	0.96
YearQuarter2019 1	-1.33307	16.2971	-0.08	0.93
YearQuarter2019 3	-0.86853	16.29587	-0.05	0.96
YearQuarter2019 4	0.014779	16.30142	0.00	1.00
YearQuarter2020 1	-0.91546	16.29671	-0.06	0.96
YearQuarter2020 3	-0.73201	16.29569	-0.04	0.96
YearQuarter2020 4	-0.23527	16.30136	-0.01	0.99
GearGOV_CL	-1.94263	58.74816	-0.03	0.97
GearTV	-1.65857	16.29559	-0.10	0.92
SurveyBTS	-4.05628	16.29488	-0.25	0.80
SurveyDYFS	-3.9536	16.29516	-0.24	0.81
SurveyFR-CGFS	-1.73828	57.99039	-0.03	0.98
SurveyNS-IBTS	-0.20435	57.99012	0.00	1.00
SurveySNS	-3.8625	16.29627	-0.24	0.81

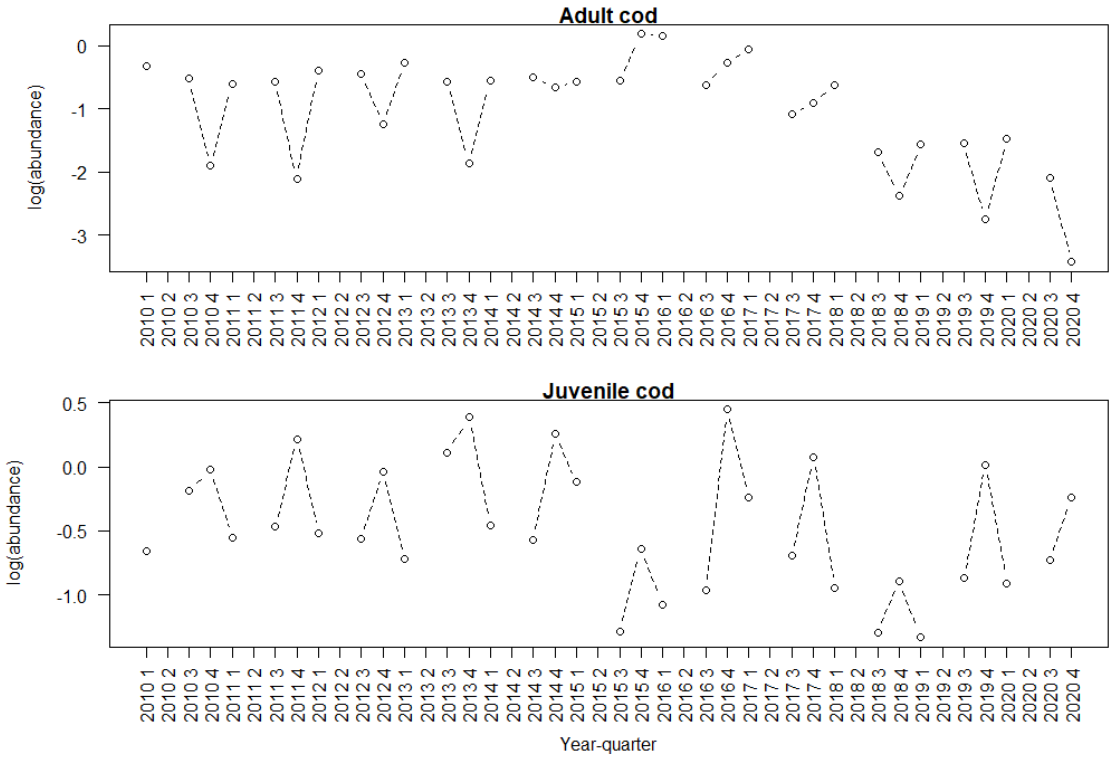

Figure 4.1.7.4. Interannual abundance indices for Adult and Juvenile cod in the greater North Sea over the period 2010–2020 based on the LGNB-SDM outcome run on the catch survey North Sea data (no survey data collected during quarter 2). Note that no standard deviation are shown in this graph because they are found too large which re-emphasizes the fact that this model fitting is very preliminary and should be updated in future re-run of the model after a careful data input grooming.

4.2.6 Model 9: sdmTMB

SdmTMB was fitted to five sets of data, red mullet in GSAs 17–18–19, Atlantic cod, Conger eel, European hake in the East Atlantic and turbot.

4.2.6.1 Red mullet

The spatio-temporal distribution of red mullet over the period 1996–2020 in GSAs 17–18–19 was analysed using the sdmTMB R package (version 0.1.0) in R (version 4.0.3). Biomass density (kg km-2) was modelled with a Tweedie distribution and a log link function to accommodate both zeros and positive continuous values. The spatial components in sdmTMB are included as random fields using a triangulated mesh with knots used to approximate the spatial variability of observations. Bilinear interpolation is used to approximate a continuous spatial field from the estimated values of the spatial surface at these knot locations to other locations including those of actual observations. These spatial random effects are assumed to be drawn from Gaussian Markov random fields with covariance matrices that are constrained by Matérn covariance functions. For the workshop, a mesh with 400 knots with correlation barriers to account for land masses was chosen, which is presented in Figure 4.1.8.1.

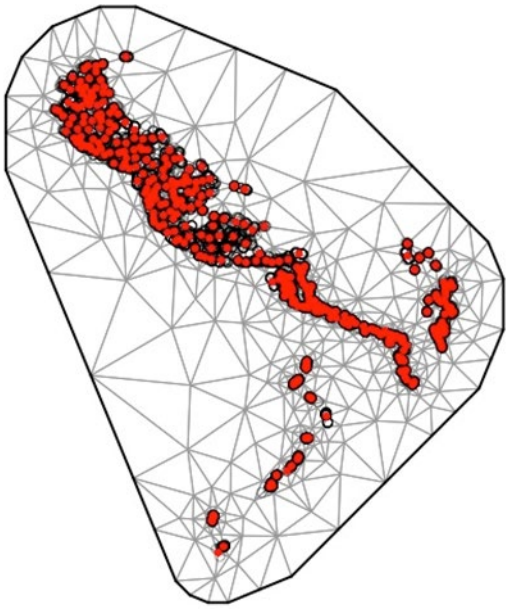

Figure 4.1.8.1. SPDE mesh used with sdmTMB. Red dots indicate knot locations.

For simplicity, spatio-temporal random fields were modelled as independent and identically distributed (IID). Fixed effects included year specific intercepts and a second order polynomial of log transformed depth.

4.2.6.2 Results

Table 4.1.8.1. Estimated fixed effect parameters for the red mullet model.

term	estimate	std.error	conf.low	conf.high
year_f1996	1.37	0.52	0.36	2.37
year_f1997	1.21	0.52	0.19	2.23
year_f1998	1.36	0.52	0.34	2.38
year_f1999	2.41	0.51	1.4	3.41
year_f2000	1.88	0.52	0.86	2.89
year_f2001	2.33	0.51	1.32	3.33
year_f2002	2.05	0.51	1.04	3.05
year_f2003	1.81	0.52	0.8	2.82
year_f2004	2.02	0.51	1.02	3.02
year_f2005	2.41	0.51	1.4	3.41
year_f2006	2.37	0.52	1.36	3.38
year_f2007	2.5	0.52	1.48	3.51
year_f2008	2.89	0.57	1.78	4
year_f2009	2.28	0.51	1.27	3.28
year_f2010	1.82	0.51	0.82	2.82
year_f2011	2.32	0.51	1.32	3.31

year_f2012	3.17	0.5	2.19	4.15
year_f2013	3.49	0.5	2.51	4.46
year_f2014	4.27	0.5	3.3	5.24
year_f2015	3.22	0.5	2.24	4.2
year_f2016	3.75	0.5	2.77	4.73
year_f2017	4.38	0.5	3.4	5.36
year_f2018	3.05	0.51	2.06	4.04
year_f2019	3.97	0.5	2.99	4.95
year_f2020	3.68	0.51	2.69	4.68
poly(log(depth); 2)1		-77.06	5.74	-88.32 -65.8
poly(log(depth); 2)2		-5.92	3.83	-13.43 1.59

Table 4.1.8.2. Standard deviations, spatial range, and other random effects and dispersion terms for the red mullet model. Where phi represents the observation error scale parameter; sigma_O the SD of the spatial process; sigma_E the SD of the spatio-temporal process; tweedie p the Tweedie power parameter, which ranges between 1 and 2.

term	estimate	conf.low	conf.high
range	0.81	0.72	0.92
phi	3.66	3.52	3.81
sigma_O	0.16	0.13	0.2
sigma_E	0.09	0.07	0.1
tweedie_p	1.54	1.53	1.55

The marginal effects (i.e. effects averaged over the other fixed effects) of year and depth are represented in Fig 4.1.8.2. Recent years presents higher biomass compared to previous years yet coupled with higher uncertainty. Biomass density declines rapidly with depth, reaching values close to 0 at 150 m.

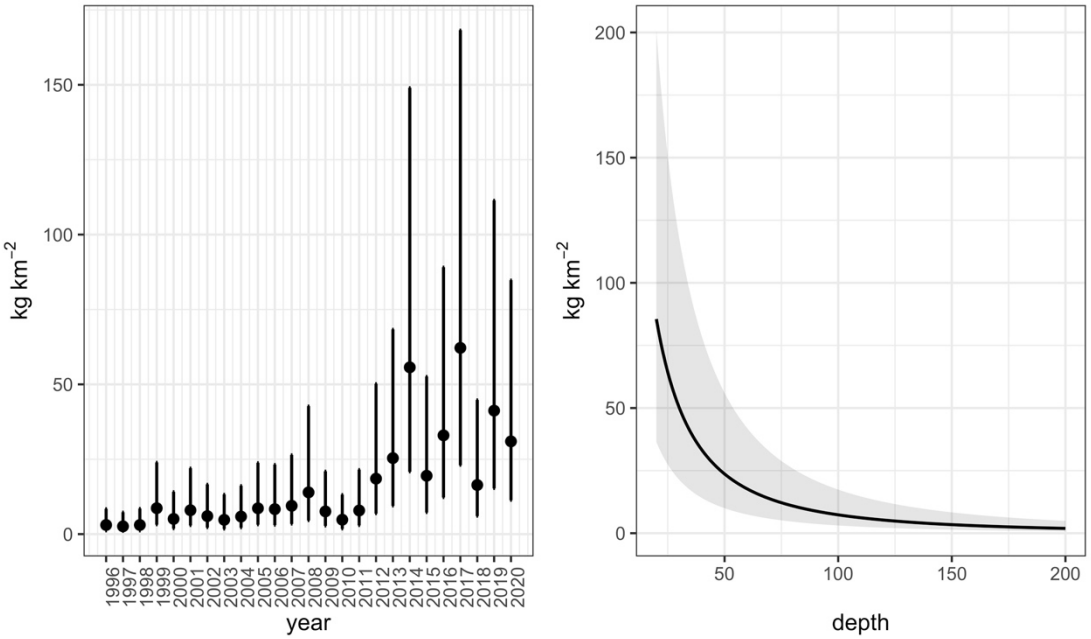

Fig 4.1.8.2. Marginal effect of the year on red mullet biomass density (left panel) and marginal effect of the squared term of log transformed depth (right panel). Dots and the black line indicate means, while intervals and grey bands indicate 95% confidence intervals.

Spatial random effects that represent consistent deviations in space through time that are not accounted for by year and depth fixed effects are shown in Figure 4.1.8.3. Spatio-temporal random effects that represent deviation from the fixed effects predictions and from the spatial random effect deviations are shown in Figure 4.1.8.4. Spatio-temporal predictions (Figure 4.1.8.5) indicated higher biomass density estimates in recent years and persistent hot spot of biomass along the Italian coast, in an offshore area located in the Northern-Central Adriatic, and along the Montenegro and Albania coasts.

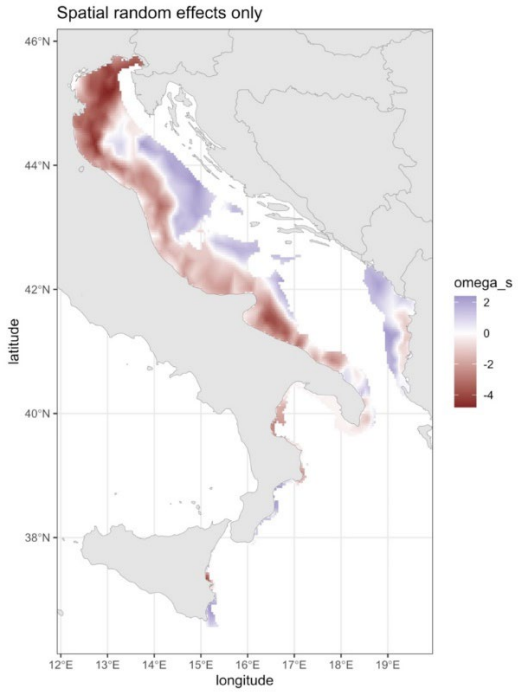

Figure 4.1.8.3. Spatial random effects.

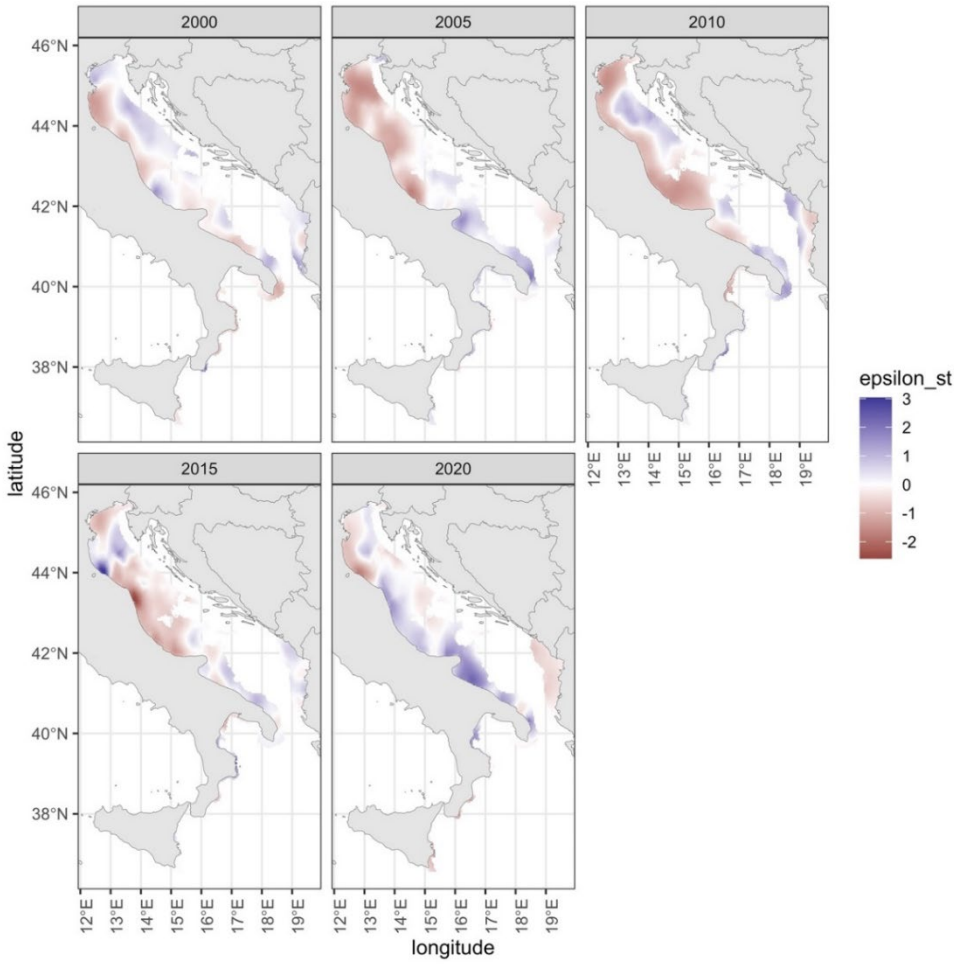

Figure 4.1.8.4. Spatio-temporal random effects.

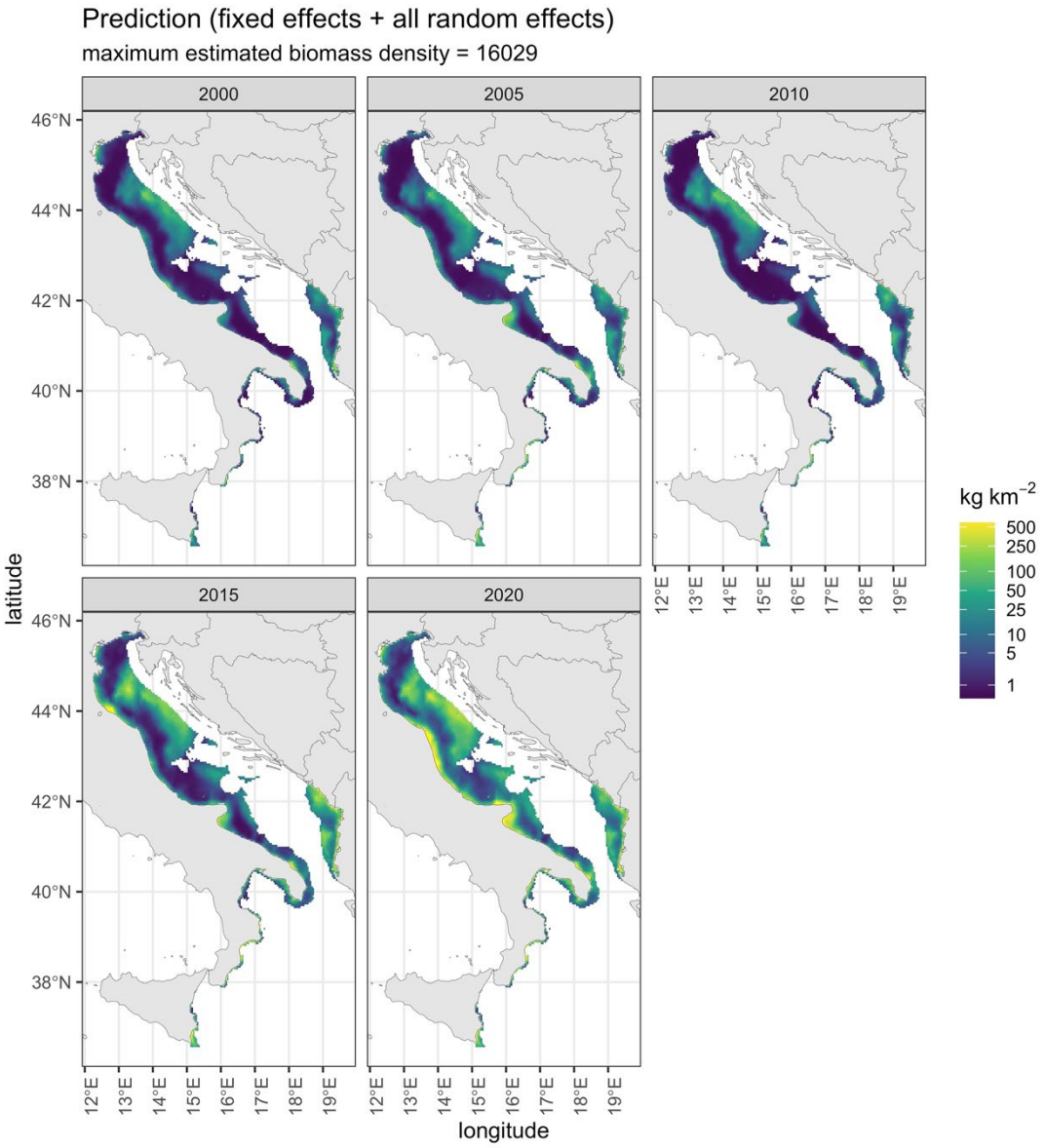

Figure 4.1.8.5. Predicted mean biomass density. Values are truncated to the 99th percentile for clarity.

4.2.6.3 East Atlantic cod, hake, conger and turbot

sdmTMB was used in a different formulation to fit the spatio-temporal density of juveniles and adults of the four species Atlantic cod, Conger eel, European hake, and turbot. This formulation is denoted 'sdmTMB 2' in the comparison results below. The fits were conducted with a Tweedie model for numbers, and a negative binomial model for biomass. Additionally, it took into account quarter (each quarter as a random effect), depth, and used the swept-area as an offset. The spatio-temporal fields were estimated as independent and identically distributed. In order to produce all combinations of species and numbersvs. biomass we used a relatively low amount of knots for the spatial maps (i.e, 300), however we also provide an example with 3000 knots. The models were batch run, and investigated for convergence. 6 out of the 16 combinations did not have final convergence due to either too large standard error or gradients being above a certain threshold (see ?sanity in the sdmTMB package for details). The predicted temporal biomass is shown in figure 4.1.9.1. The center of gravity changes over time (in both directions) is provided for distribution of adult cod provided in figure 4.1.9.2, and distribution maps of adult cod numbers (with 300 and 3000 knots) are shown in figure 4.1.9.3–4. The syntax used in the sdmTMB model is provided here.

```
fit.N <- sdmTMB(
  n.adult ~ Gear+(1 | Quarter)+log(Depth)+offset(log(SweptArea)),
  data = df,
  family = nbinom2(link = "log"),
  mesh = mesh,
  spatial = "on",
  time = 'Year',
  spatio-temporal = 'iid'
)
```

Table 4.1.9.1. sdmTMB models that have full or only partial convergence.

Species	Biomass converged	Numbers converged	Hessian converged
Adult Conger	Yes	Yes	Yes
Juvenile conger	Yes	Yes	Yes
Adult cod	No	Yes	Yes
Juvenile cod	Yes	No	Yes
Adult hake	No	No	Yes
Juvenile hake	Yes	Yes	Yes
Adult turbot	No	No	Yes
Juvenile turbot	Yes	Yes	Yes

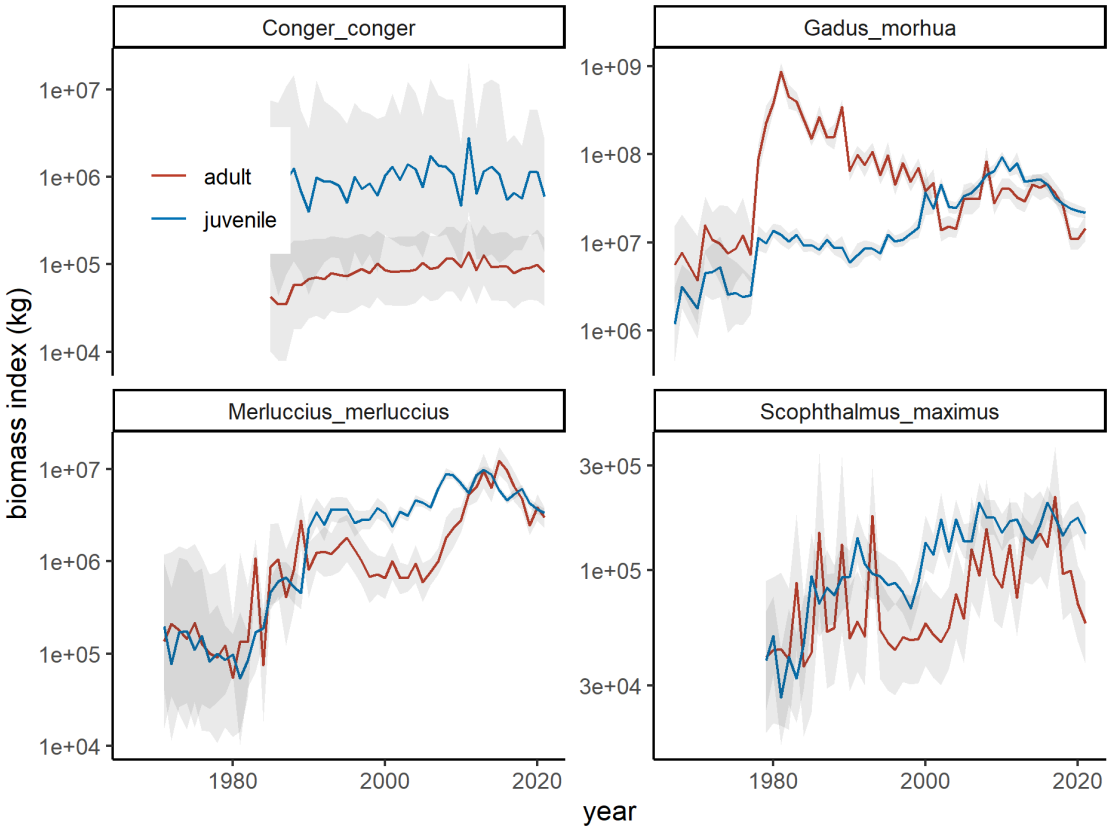

Figure 4.1.9.1. Predicted mean biomass density for juvenile and adults of the four species. Shading represents the 95th confidence interval. The index is calculated without bias adjustment.

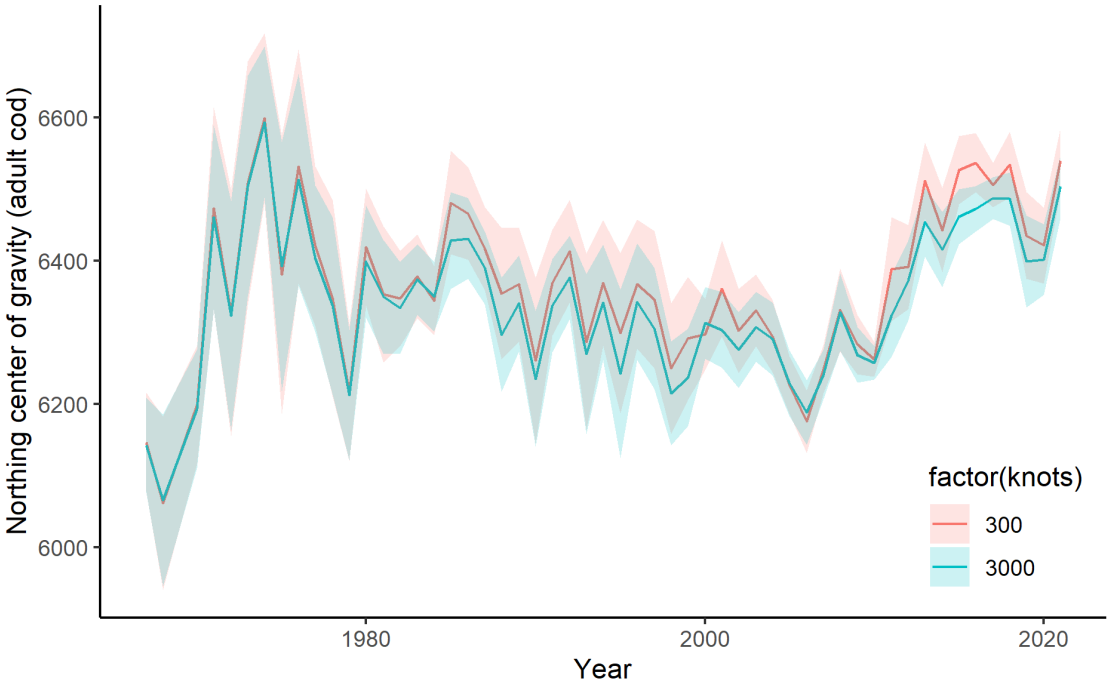

Figure 4.1.9.2. Center of gravity (Northing) for adult cod numbers using 300 and 3000 knots for the spatio-temporal estimation. The red lines indicates 300 knots and the blue line indicates 3000 knots.

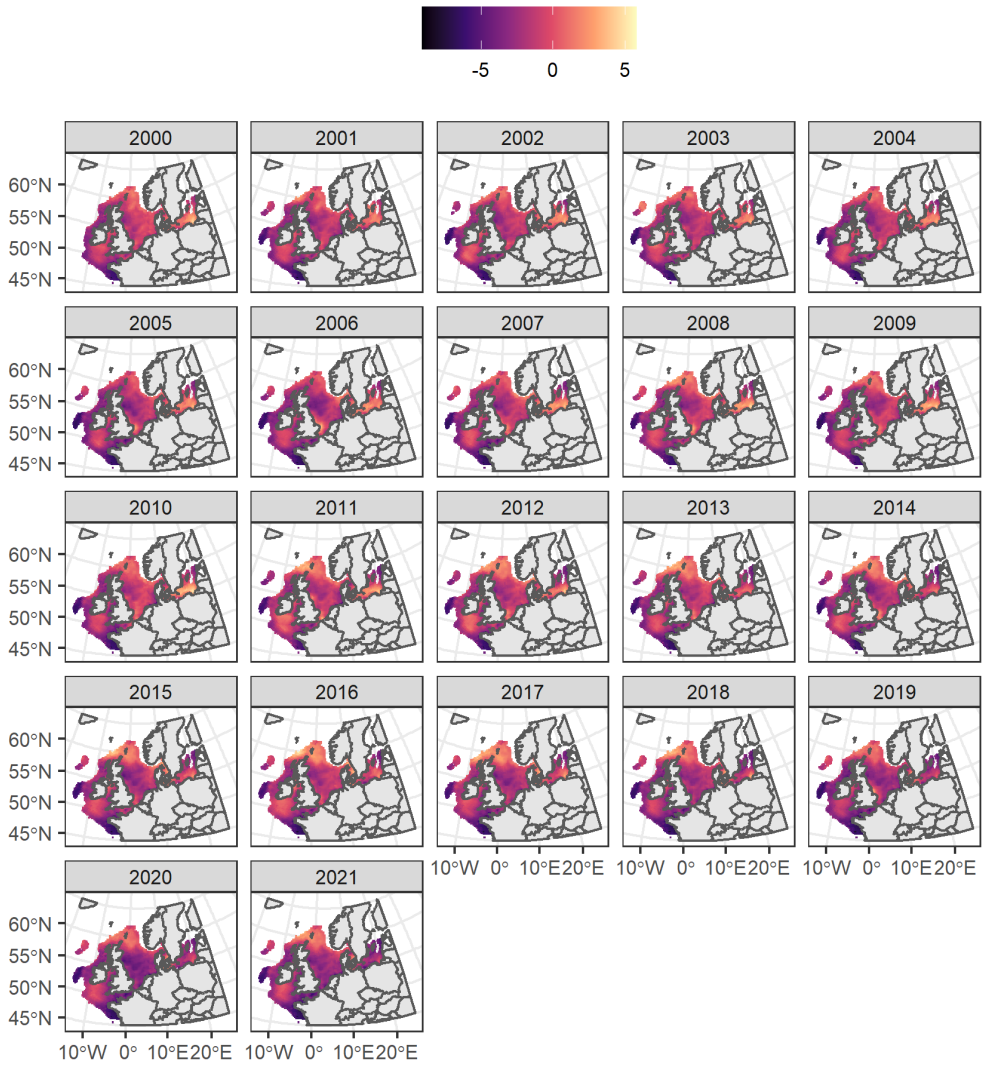

Figure 4.1.9.3. Predicted distribution of numbers of adult Atlantic cod (on log scale) from 2000 to 2021. Estimation was done with 300 knots.

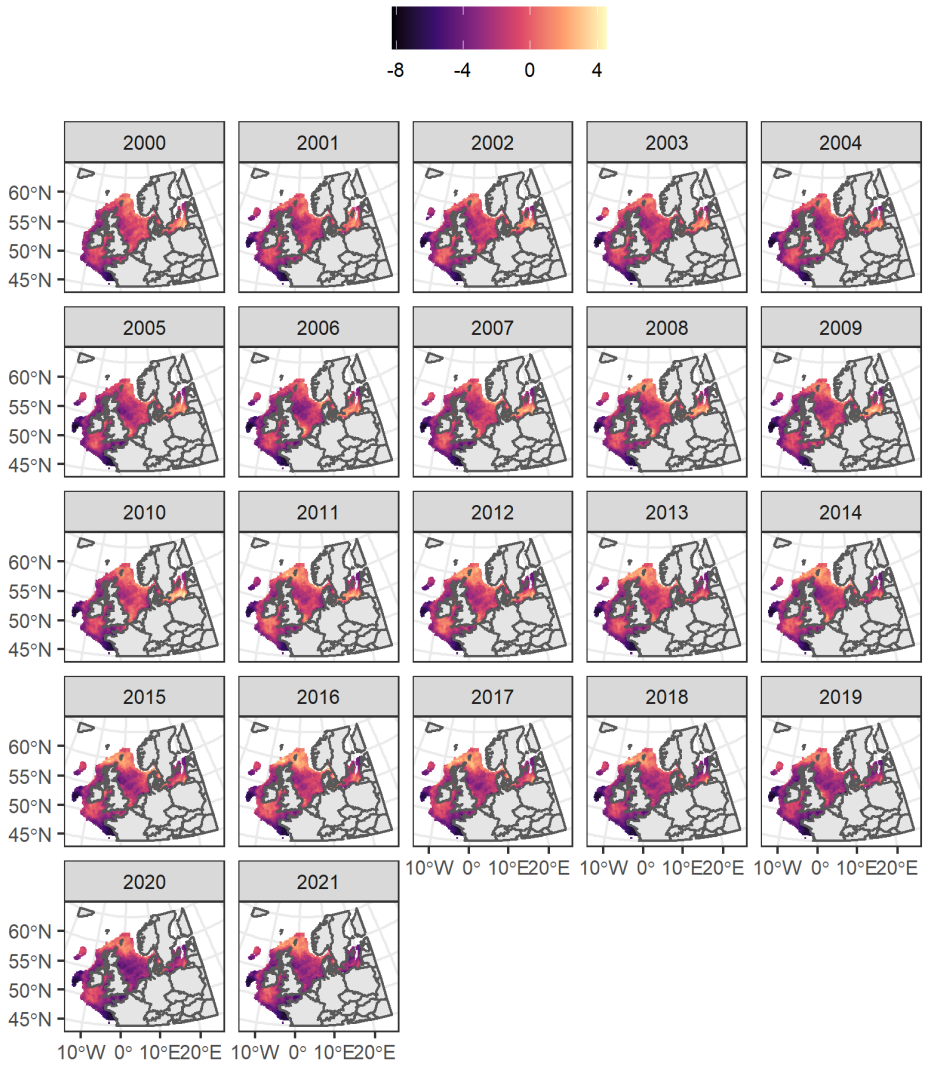

Figure 4.1.9.4. Predicted distribution of numbers of adult Atlantic cod (on log scale) from 2000 to 2021. Estimation was done with 3000 knots.

4.3 Comparison of model predictions

All models except two were fitted for at least one of these species (Table 4.2.1). This resulted in model predictions for Mediterranean red mullet from three models, Mediterranean hake from two models. Atlantic adult cod biomass from five models, Atlantic adult cod numbers from three models, Atlantic juvenile hake biomass from two models and Atlantic juvenile and adult conger eel numbers from two models.

Table 4.2.1. Models, species and areas used for model comparisons

Model	Modelled species/areas
Approximate Bayesian inference using integrated nested Laplace approximation (INLA)	Atlantic adult cod numbers and biomass
GAM model with random effects and train/test approach	Mediterranean red mullet and hake biomass; red mullet adults.

Model	Modelled species/areas
GAM model with random effects	Mediterranean hake biomass
GAM Spatio-temporal generalized additive model	Atlantic cod, hake, conger eel and turbot in biomass and numbers for adults and juveniles
VAST	Atlantic adult cod and juvenile hake biomass; Mediterranean red mullet adults
LGNB-SDM	Atlantic adult cod biomass
sdmTMB	Mediterranean red mullet biomass, Atlantic cod, turbot, East Atlantic hake and conger eel

Applying the indicators of difference in distribution described in section 3.3, the average SPAEF over all maps for a given species are summarized below.

4.3.1 Comparison between GAM 3 and 4 (European hake GSAs 18–19–20)

Predictions on the spatial distribution of European hake biomass (kg/km2) in the Mediterranean Sea (GSAs 18, 19 and 20) were performed and compared with predictions of the models GAM-3 and GAM-4. The models were compared based on annual maps based on MEDITS data for the period 1996–2021. The aim of this comparison is to explore the potential difference in spatio-temporal outcomes between: (i) a model set using GAM3 incorporating a spatial soap film smoother, depth and year used as explanatory variables (hereafter called "simpler case", corresponding to limited change in distribution over time as depth distribution does not change) and (ii) a model set using GAM4 incorporating a space-time soap film smoother, depth and an interaction term of depth and year (hereafter called "complex case").

Comparison was based on metrics SPAEF, center of gravity and hot spots analysis (biomass higher than 90th percentile) by year. Results on average SPAEF for the study period, showed an acceptable level of agreement between the spatial distributions predicted by the two configurations (average = 0.43, 0 is perfect match). However, annual SPAEF indicated more pronounced similarities in spatial outcomes after 2010 rather than the previous years (Fig 4.2.1.1). This is also revealed by analysing the Centre of gravity which showed similarities between the two configurations, although the "complex case" resulting in higher annual variability rather than the "simpler case" (Fig 4.2.1.2). This is due to the spatial-temporal interactions that is included only in the "complex case". Additionally, hot spots varied by year and indicated a good level of overlap between the two configurations in the areas where the peaks of hake biomass are located (Figure 4.2.1.3).

Despite the overall agreement between the two configurations, some differences were revealed in the spatial outcomes by year. Although the year effect allowed the fish densities to be varied by year in both cases, the "complex case" revealed more pronounced annual spatial changes rather than the "simpler case". Such result is attributed to the time varying interaction terms used in the "complex case" instead of the single term year used in the "simple case".

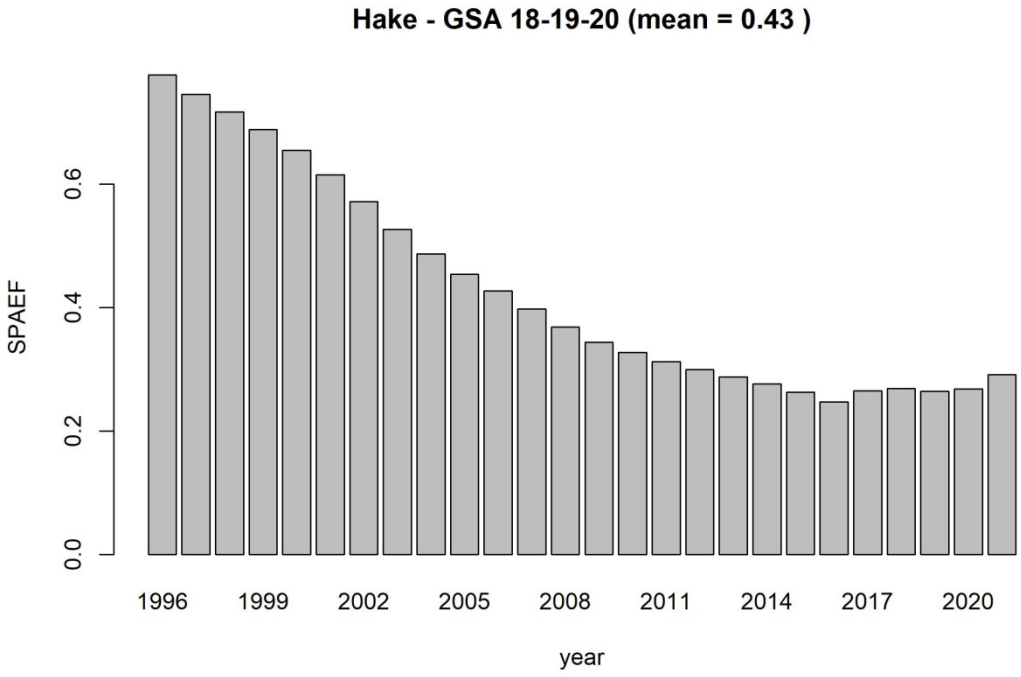

Figure 4.2.1.1. SPAtial EFficiency metric (SPAEF) by year. Values of 0 indicate perfect agreement between the predicted spatial distributions, while values approaching ∞ indicating disagreement.

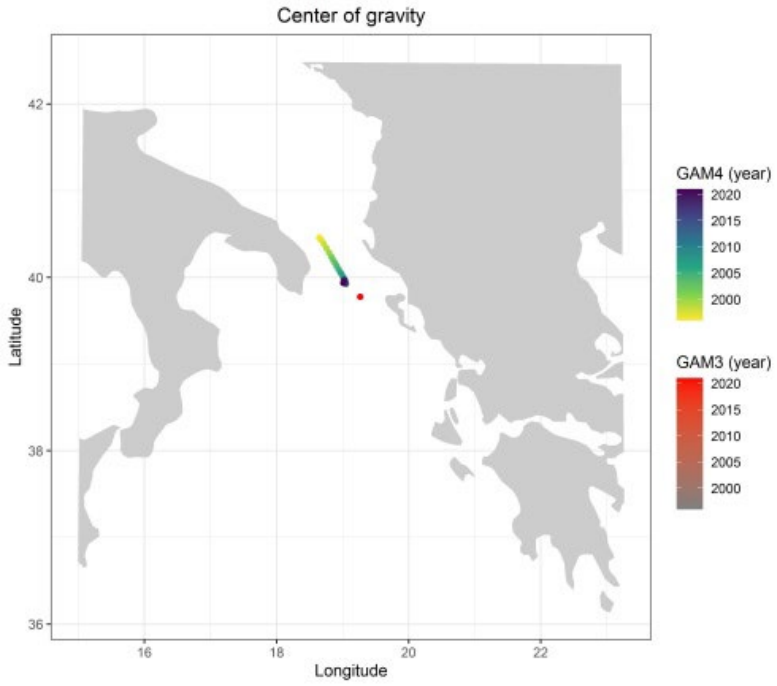

Figure 4.2.1.2. Spatial distribution of the Centre of gravity for the two GAM configurations.

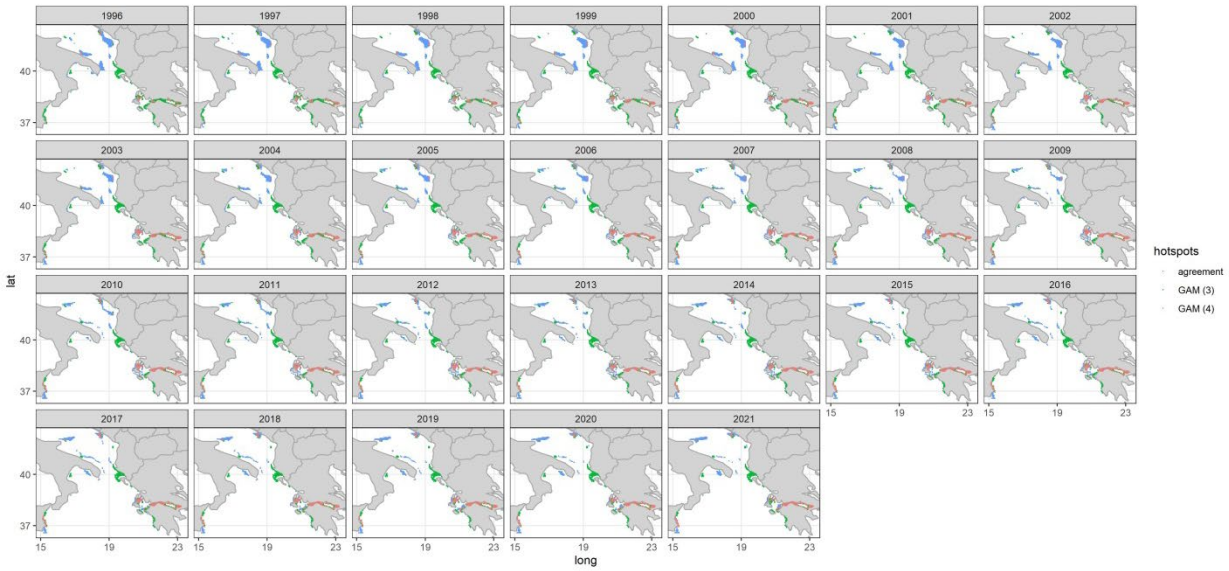

Figure 4.2.1.3. Annual hot spots for the predicted spatial distribution of hake biomass (90th percentiles). In green the predicted values by the simpler case (GAM3), in blue the predicted values by the complex case (GAM4) and in pink the agreement between the two configurations.

Table 4.2.1.1 Pairwise comparison of Mediterranean hake biomass distribution from GAM models 3 and 4 (GSAs 18–19–20).

Model	GAM (3)
GAM (4)	0.43

4.3.2 Comparison between GAM 3 and sdmTMB (red mullet GSAs 17–18–19)

GAM3 and sdmTMB models were applied on MEDITS data and predictions were performed by year for the period 1996–2020. The spatial predictions of the red mullet biomass (kg/km^2) in GSAs 17, 18, 19, as derived through the two models were compared through SPAEF, center of gravity, CV and hot spots analysis (biomass higher than 90th percentile) by year.

Results on average SPAEF across the available years, showed an acceptable level of agreement between the spatial distributions predicted by the two models (average = 0.44, Table 4.2.2.1). However, annual SPAEF indicated oscillating level of overlap with the highest dissimilarity in 2018 (Fig 4.2.2.1). Analysing the coordinates of the Centre of gravity, both models reveal an oscillating trend on the two directions (Lat-Lon) along the years; in the case of the GAM3 it is more smoothed due to the use of the splines, while for sdmTMB is more jagged due to the use of spatial random effects (Fig 4.2.2.2). Although the Centers of Gravity estimated by the two models are quite in line along the years, the latitude predicted by GAM3 is slightly lower than the one of sdmTMB.

Additionally, hot spots varied by year and indicated a good level of overlap between the two models, especially on the coastal areas and offshore Croatian coast where the peaks of red mullet biomass are located (Figure 4.2.2.3).

In terms of CV the two models return a similar picture, although the sdmTMB has generally CV values higher than GAM3, especially in the areas of Ionian Apulian coast (Figure 4.2.2.4).

Table 4.2.2.1. Pairwise comparison of Mediterranean red mullet biomass distribution from different models (GSAs 17–18–19).

Model	GAM (3)
sdmTMB (9)	0.44

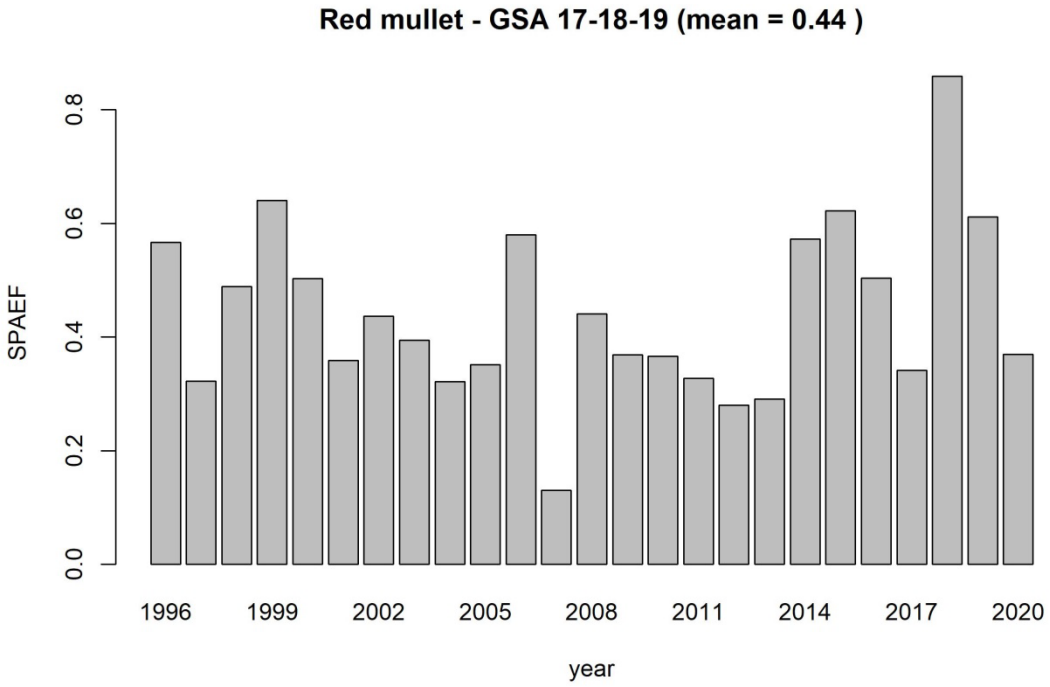

Figure 4.2.2.1 SPAtial EFficiency metric (SPAEF) by year. Values approaching 0 are indicating an agreement between the predicted spatial distributions, while values approaching ∞ indicating a disagreement.

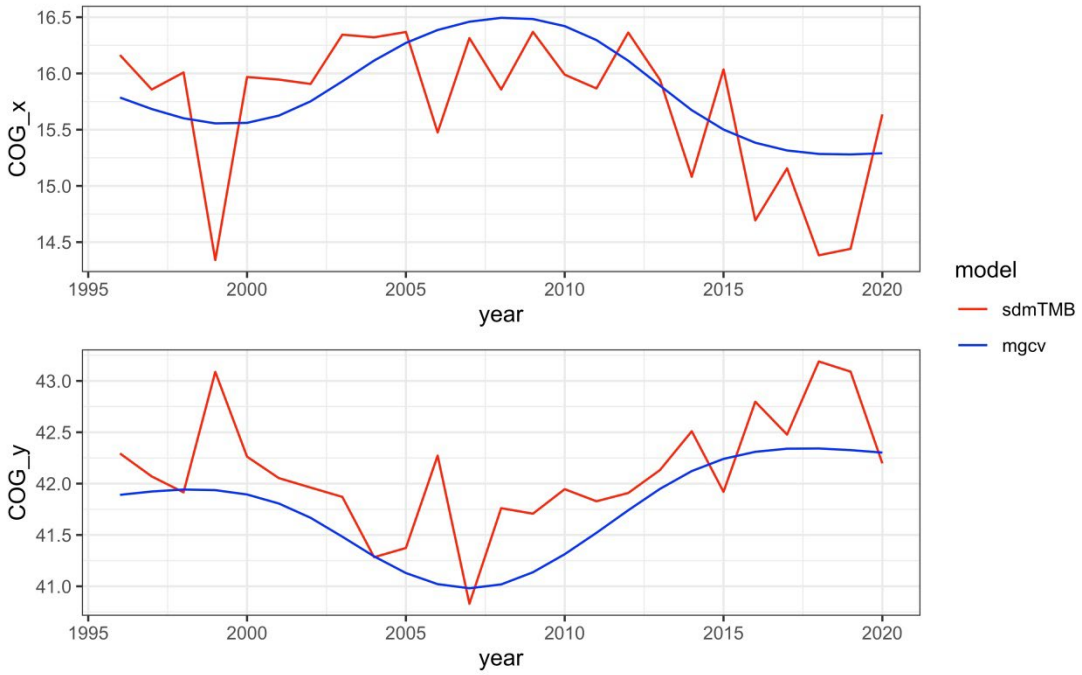

Figure 4.2.2.2. Centre of gravity for the GAM and sdmTMB by year.

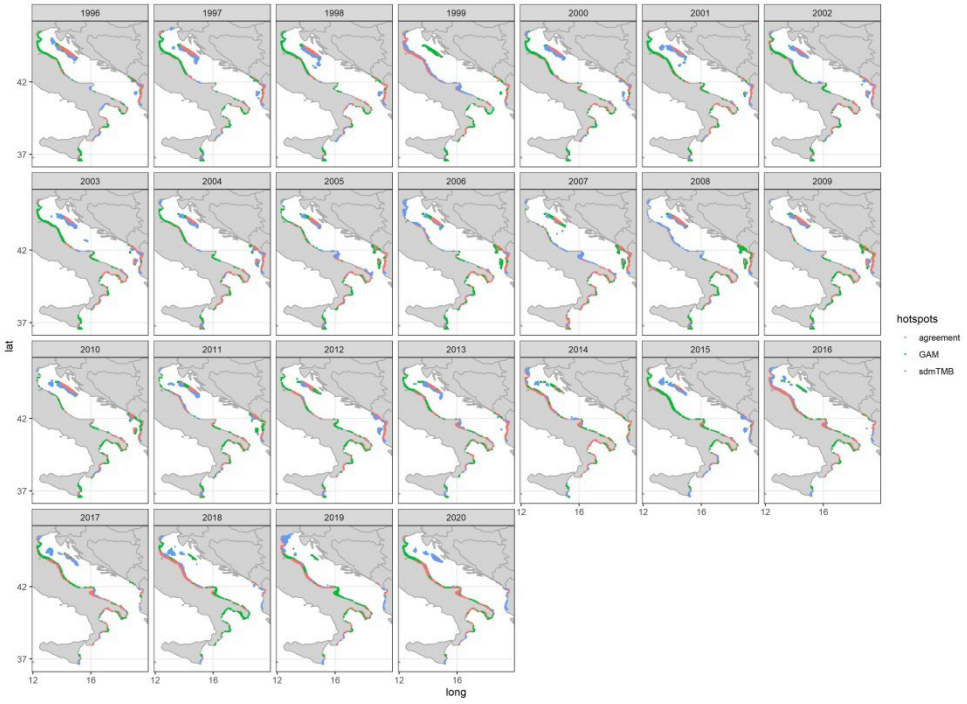

Figure 4.2.2.3. Annual hot spots for the predicted spatial distribution of hake biomass (90th percentiles). In green the predicted values by the GAM, in blue the predicted values by the sdmTMB and in pink the agreement between the two models.

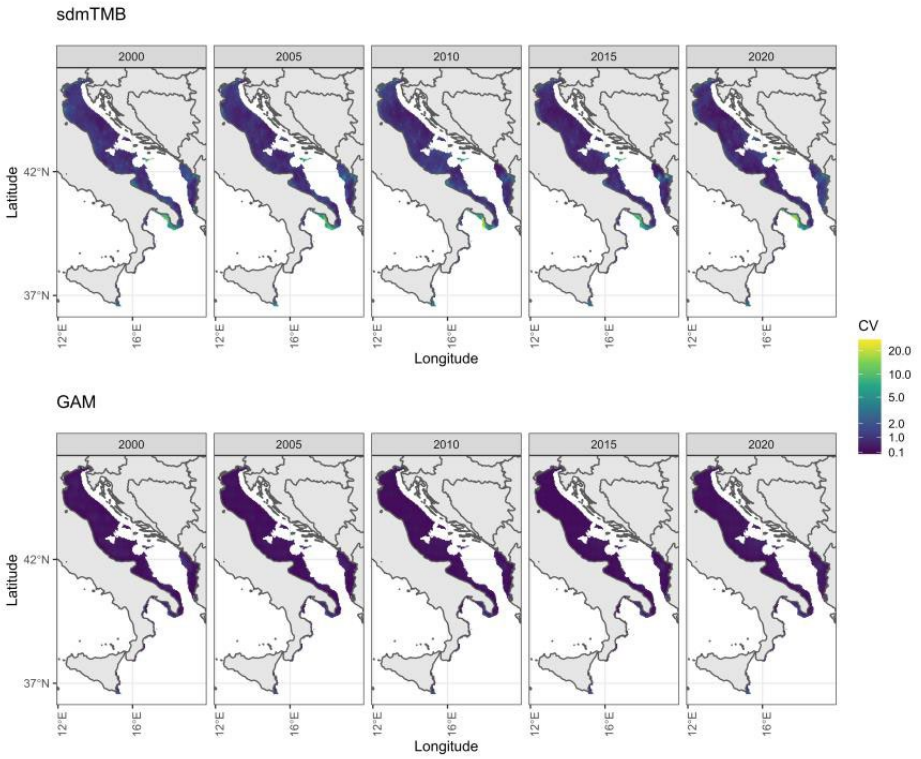

Figure 4.2.2.4. Spatial comparison of the CV estimated by the GAM (model 3) (bottom panel) and sdmTMB (upper panel).

4.3.3 Comparison between GAM 3 and VAST (red mullet GSA 18)

GAM3 and VAST models were applied on MEDITS data and predictions were performed by year for the period 1996–2020. The spatial predictions of the red mullet abundance of adults (N/km2, individuals with total length >= 11 cm) in GSA 18, as derived through the two models were compared through SPAEF, center of gravity, CV and hot spots analysis (biomass higher than 90th percentile) by year.

Results on average SPAEF across the available years were greater than 1 between the spatial distributions predicted by the two models (average = 1.25). The annual SPAEF indicated oscillating levels of overlap with the highest dissimilarity in 2017 and slightly smaller values in the last years (Fig 4.2.3.1). From comparative perspective with others areas (e.g. GSA 6, below) that present lower values of SPAEF, these high values above 1 can also be due to the spatial complexity, which in the case of red mullet in the GSA18 encompasses two sides of the Adriatic Sea representing a more complex spatial scenario.

Analysing the Centre of gravity, both models reveal a widely moving trend in the middle of the area: VAST showed mainly a longitudinal oscillation, while GAM3 indicates both longitudinal and latitudinal oscillations (Fig 4.2.3.2). This suggest that GAM3 was able to better identify (and capture) the changes in the dynamics over the latitudinal gradient. VAST model, in general, points northern distributions (higher CG) than GAM; this pattern contrast to the observed comparison for this species in GSA6. However an expansion of the area occupied by the stock in GSA18 is expected on the basis of increasing biomass trend in the area in the last decade.

Additionally, hot spots varied by year and indicated overlaps along the East coast and on the North of Gargano promontory (Figure 4.2.3.3). In general, this temporal heterogeneity in the hot spots identified was clustered by periods, with the early of the time-series showing a similar pattern and hot spot agreements identified mainly offshore Albania, while a in the second part of the time-series an agreement was identified for the hot spot of Gargano Promontory and along the Montenegrin coasts.

Finally, VAST does not seem to identify the hot spot in the Southwest of the area, identified by GAM3; probably it is due to the default setting of 2 modes in VAST and to the fact that this hot spot is more evident in recent years. Further exploration could be, thus, carried out in future, exploring the 3 modes setting.

Table 4.2.3.1. Pairwise comparison of Mediterranean red mullet adult abundance distribution from different models (GSA 18).

Model	GAM (3)
VAST	1.25

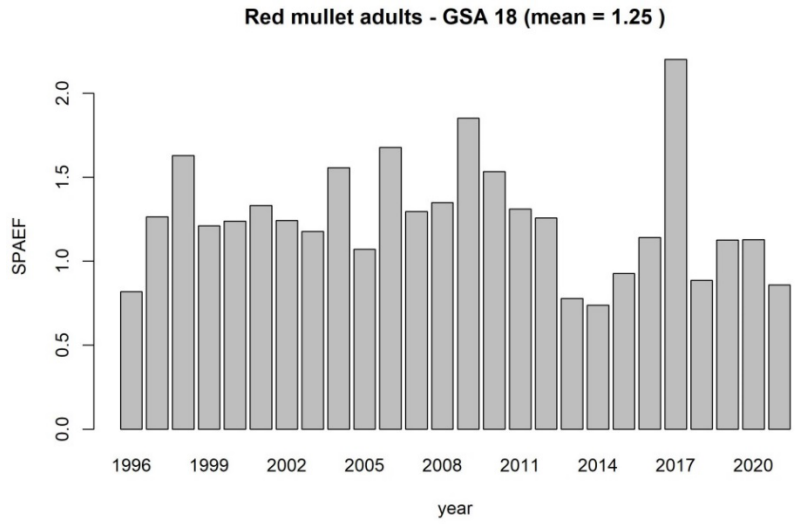

Figure 4.2.3.1. SPAtial EFficiency metric (SPAEF) by year. Values approaching 0 are indicating an agreement between the predicted spatial distributions, while values approaching ∞ indicating a disagreement.

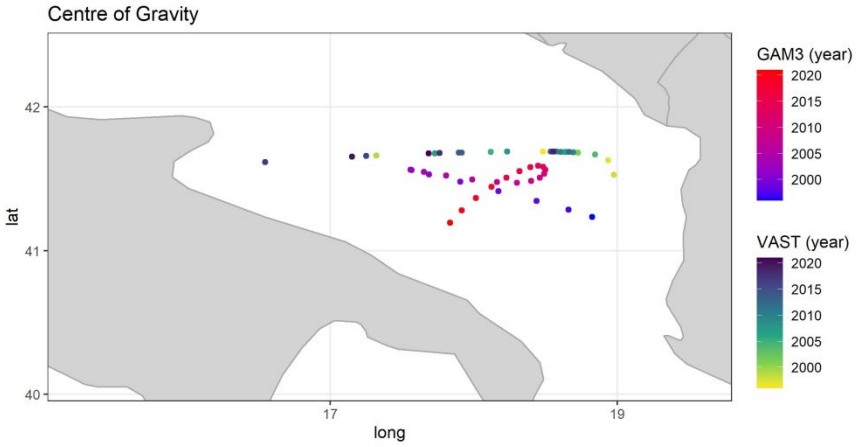

Figure 4.2.3.2. Centre of gravity for the GAM and VAST by year.

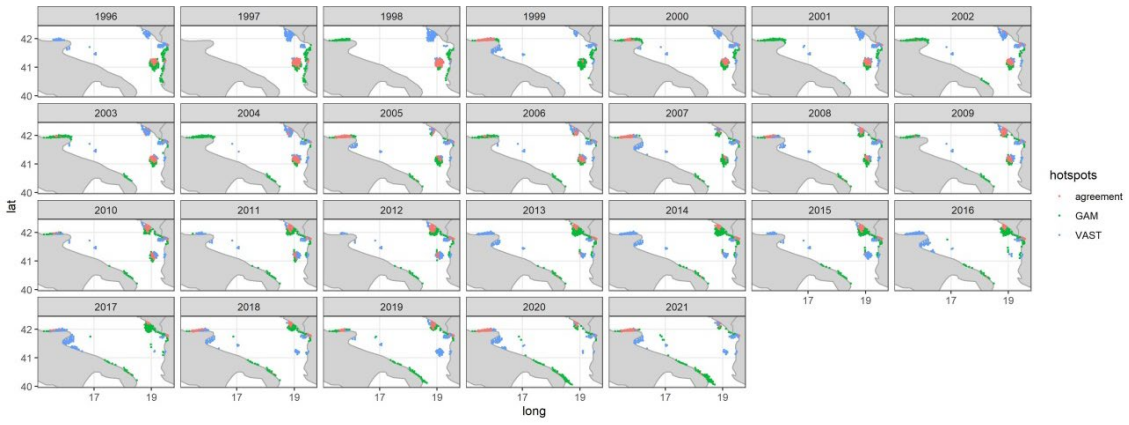

Figure 4.2.3.2. Annual hot spots for the predicted spatial distribution of hake biomass (90th percentiles). In green the predicted values by the GAM3, in blue the predicted values by the VAST and in pink the agreement between the two models.

4.3.4 Comparison between GAM 3 and VAST (red mullet GSA 6)

GAM3 and VAST models were applied on MEDITS data and predictions were performed by year for the period 1996–2019. The spatial predictions of the red mullet abundance of adults (N/km2) in GSA 6, as derived through the two models were compared through SPAEF, center of gravity and hot spots analysis (biomass higher than 90th percentile) by year.

Results on SPAEF comparing the spatial distributions predicted by the two models showed level of agreement varying along the years between 0.5 and 1, with an average = 0.74. However, the highest values of SPAEF are more concentrated in the first years, then the values decrease at about 0.6 (Fig 4.2.4.1). This trend could be associated with the directional drift observed consistently by both methods in the CG (see below) and a likely temporal changes of the temporal contribution of the three main hot spots known for the species (Paradinas *et al.*, 2020). Lower mean value of SPAEF compared with GSA18 could be associate to less complex spatial structure and/or smaller number of hot spots.

Analysing the trend of the Centre of gravity, interestingly both models reveal a northeast shift along the years (Fig 4.2.4.2). Within this general pattern GAM3 displays, on average, higher mean values than VAST. This could, among other potential reasons, due to how different models capture and model the hot spots (see below).

Additionally, the distribution of the hot spots identified by the two models highlights that until 2003 there is agreement in the area offshore Alicante; from 2004 the agreement of the models is present also in the Northern part of the area (Figure 4.2.4.3). In general, the two methods provide contrasting identification of the hot spot but generally consistent over years. While GAM3 reveal consistent hot spot over the coastal areas at shallow waters, VAST identify recurrently the two more persistent hot spot: one offshore the Ebro delta, and one south Palos Cape (both already reported, Paradinas *et al.*, 2020).

Table 4.2.4.1. Pairwise comparison of Mediterranean red mullet adult abundance distribution from different models (GSA 6).

Model	GAM (3)
VAST	0.74

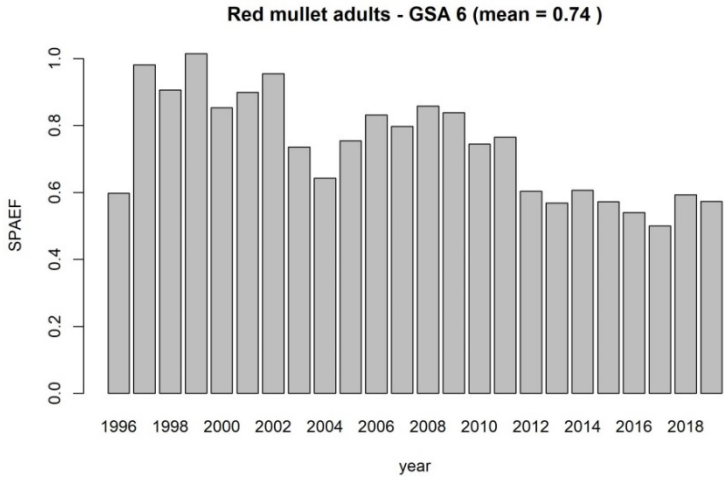

Figure 4.2.4.1. SPAtial EFficiency metric (SPAEF) by year. Values approaching 0 are indicating an agreement between the predicted spatial distributions, while values approaching ∞ indicating a disagreement.

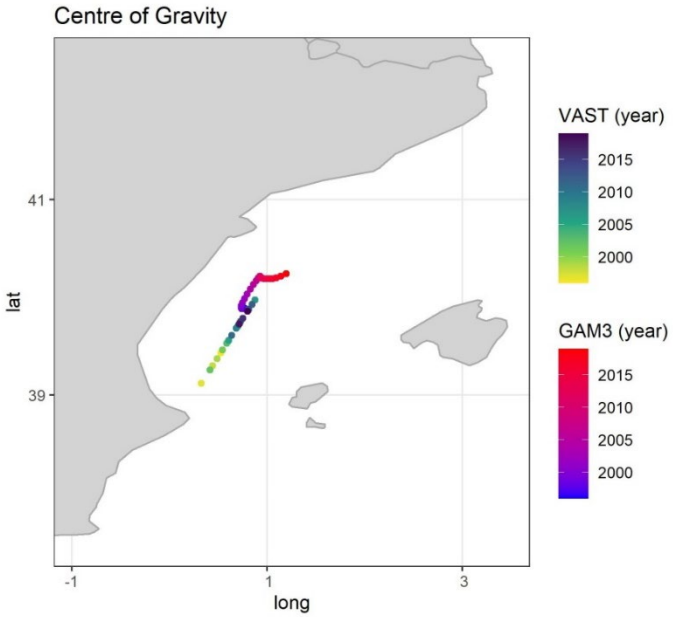

Figure 4.2.4.2. Centre of gravity for the GAM3 and VAST by year.

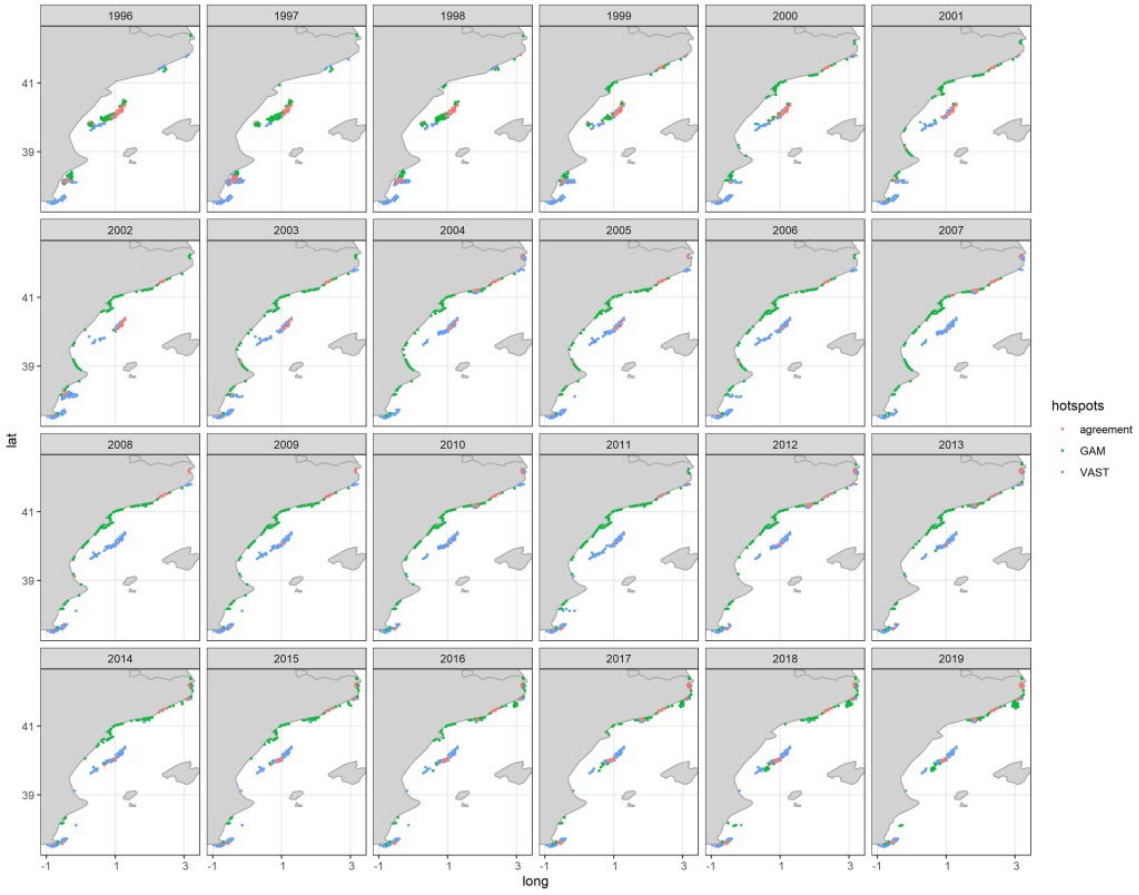

Figure 4.2.4.3. Annual hot spots for the predicted spatial distribution of hake biomass (90th percentiles). In green the predicted values by the GAM3, in blue the predicted values by the VAST and in pink the agreement between the two models.

4.3.5 Comparison between model predictions for adult cod biomass

A comparison of the distribution of cod (adult biomass) as estimated by the different models was done based on different criteria, the SPAEF metric, the Centre of Gravity, the Effective Occupied Area and maps of the regional density and hot spots (CPUE > 90% quantile). The objective of this comparison is to identify how the different spatio-temporal model configuration differ. As a reference, the raw CPUE values are also plotted.

The general patterns regarding the development of the COG over time are very similar between the models (Figure 4.2.5.1). However, between 2000 and 2010, there is a remarkable difference. VAST (and INLA up to 2004) follow more the COG development of the raw CPUE data in the longitudinal direction, whereas the other models predict that the COG is located more westwards during that period. In the North–South direction, the main discrepancy is found between INLA and the other models in the last 2 decades, where INLA predicts that the COG is more southwards. In general, the patterns of the sdmTMB model are more erratic, while the patterns of the INLA model tends to be the smoothest which is consequence of the temporal structure in the model (sdmTMB IID effects over time while INLA has an AR1 process over time with knots every 3 years).

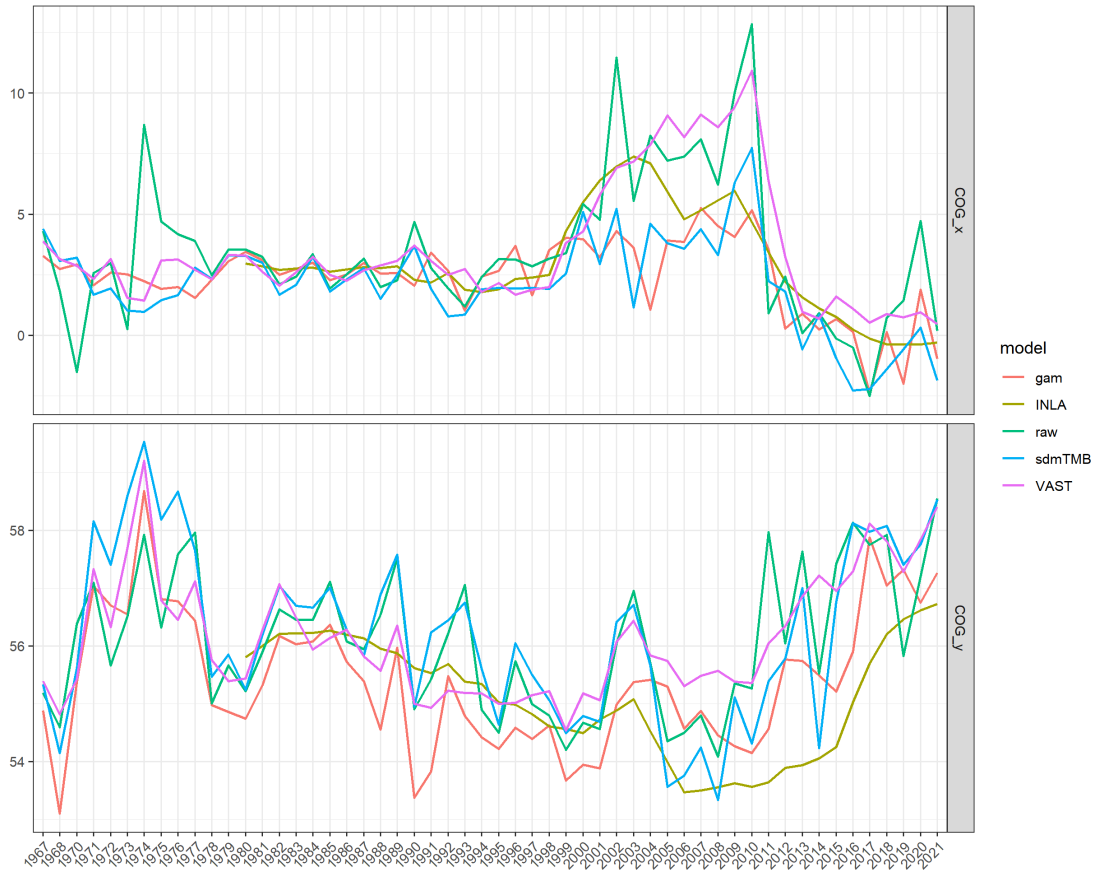

Figure 4.2.5.1. Centre-of-Gravity in the longitude (x) and latitude (y) direction by year. Remark that this figure is based on different extrapolation grids over time, and therefore, does not reflect changes in the distribution of the stock. Data for the LGNB model is not shown as it only covers the North Sea.

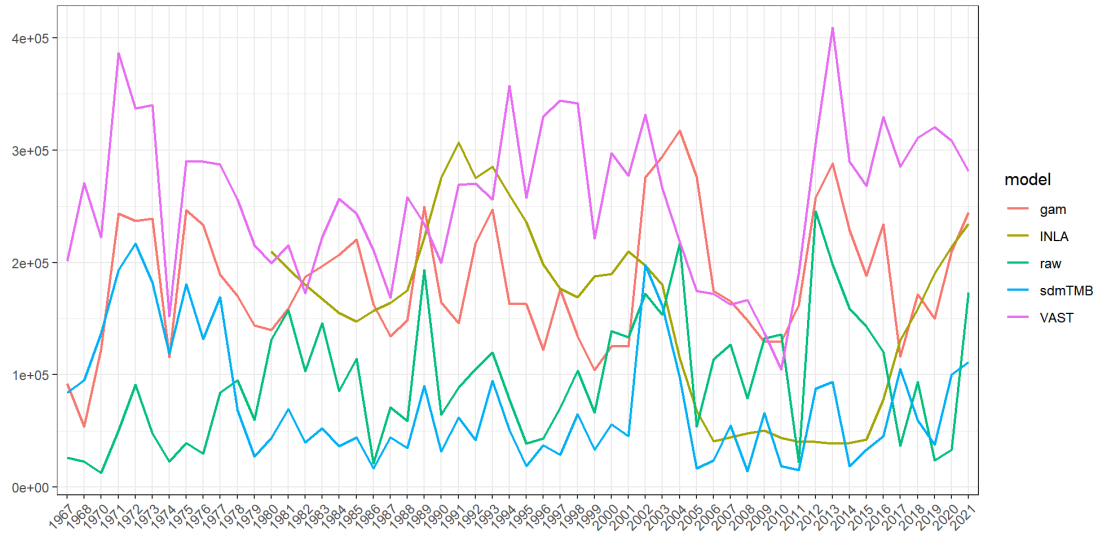

Figure 4.2.5.2. Effective Area Occupied metric by year. Note that the metric is not shown for the LGNB model.

The agreement on the temporal development of the effective area occupied metric is much less than was the case for COG. VAST, gam and INLA (except between 2005 and 2017) are generaly in better agreement, while the sdmTMB follows the raw data metric. This indicates that the distribution of the first 3 models is less patchy compared to the sdmTMB model. This pattern is also visible in the maps that show the hot spots (cells where the biomass is greater than the 90% quantile of the biomass, Figure 4.2.5.4).

In terms of the spatial distribution, the models differ from year-to-year, but some general trends are clear. The gam, VAST and INLA tend to be more similar then the other models. However, the gam and VAST model predict lower densities in the Baltic Sea and Celtic Sea, respectively, compared to the other models. In contrast, INLA has the highest densities of adult cod biomass in the southern North Sea. The gam, VAST and INLA model show more similar patterns over time compared to the sdmTMB model which is a consequence of the temporal process (smoother/AR1) that those models have.

The agreement between the model predictions (SPAEF) varied both over time and between models (Figure 4.2.5.3 and Table 4.2.5.1). LGNB-SDM differed most from the other models with SPAEF estimates of 1.35 to 2.33 on average whereas SdmTMB(1), INLA, sdmTMB(2) and GAM were more similar to values ranging from 0.65 to 0.97.

Table 4.2.5.1. Pairwise comparison of cod adult biomass distribution from different models.

Model				
GAM (5)	0.8059			
LGNB-SDM	2.3094	1.5710		
SdmTMB (1)	0.6483	0.9742	1.3534	
sdmTMB (2)	1.0540	1.2458	2.3263	0.6911
	INLA	GAM (5)	LGNB-SDM	sdmTMB (1)

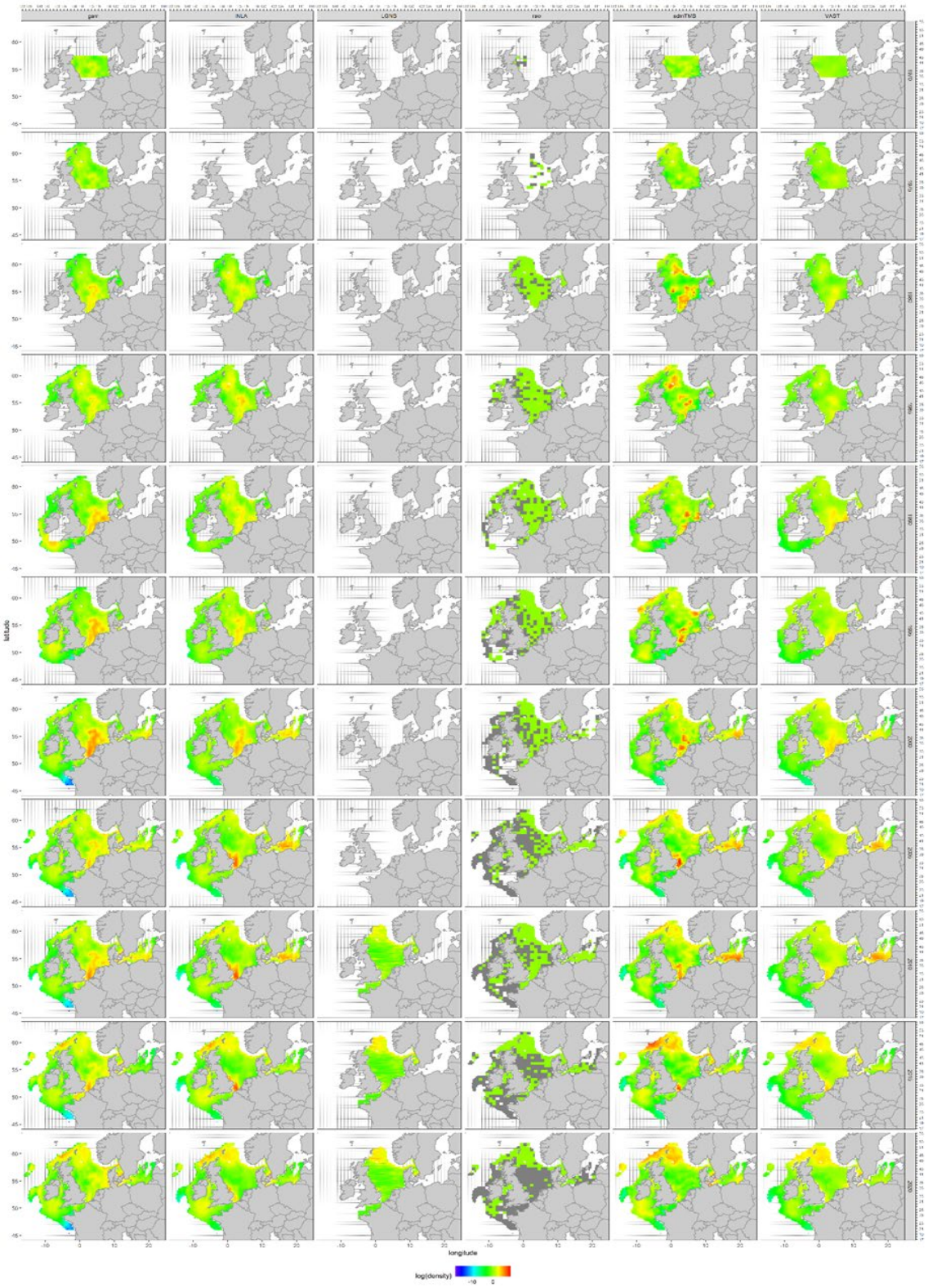

Figure 4.2.5.3: Spatial distribution of the log density of cod adult biomass as predicted by the different models and the raw data.

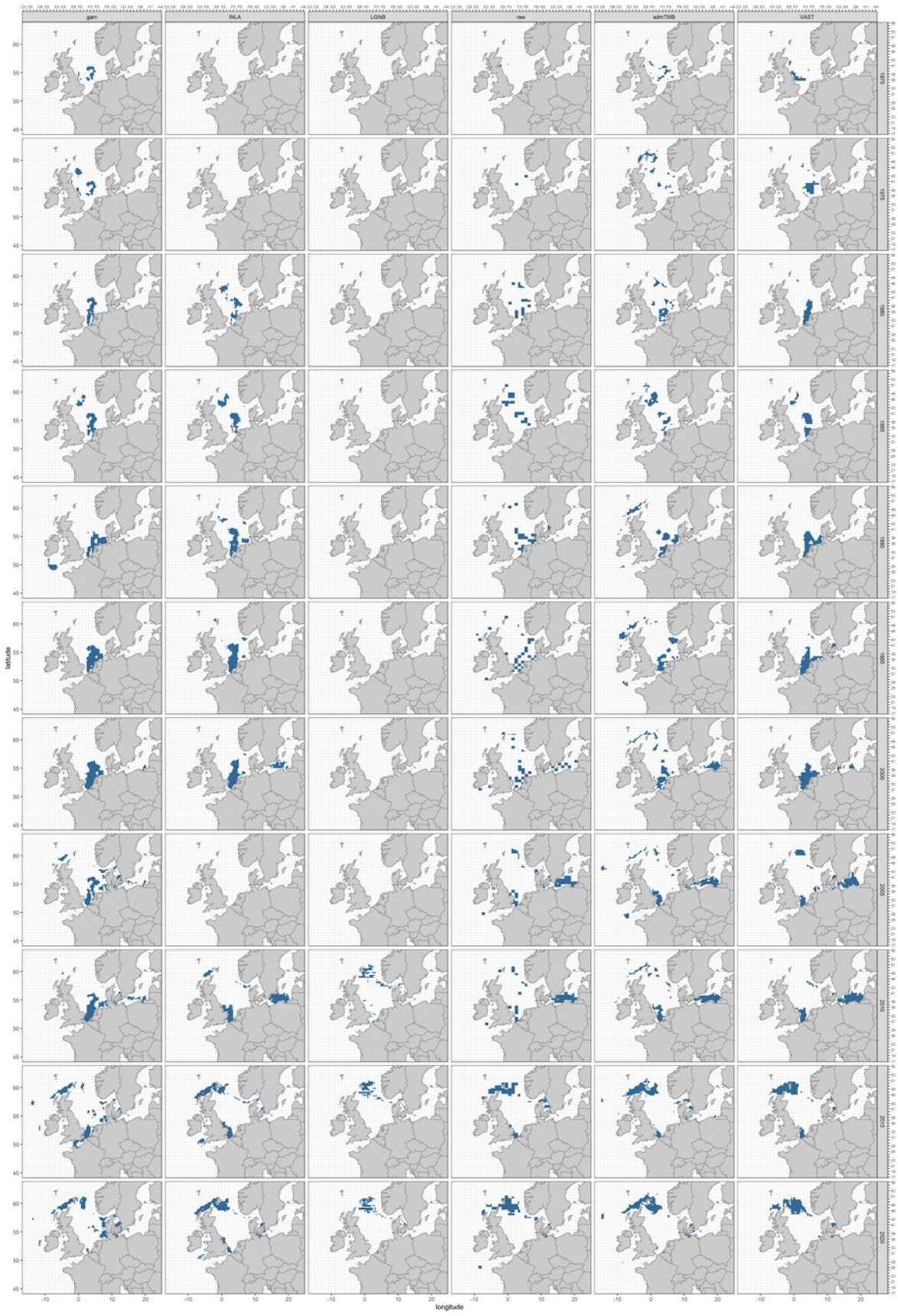

Figure 4.2.5.4. Hot spot areas where the predicted biomass is greater than the 90% quantile of the predicted biomass by gridcell.

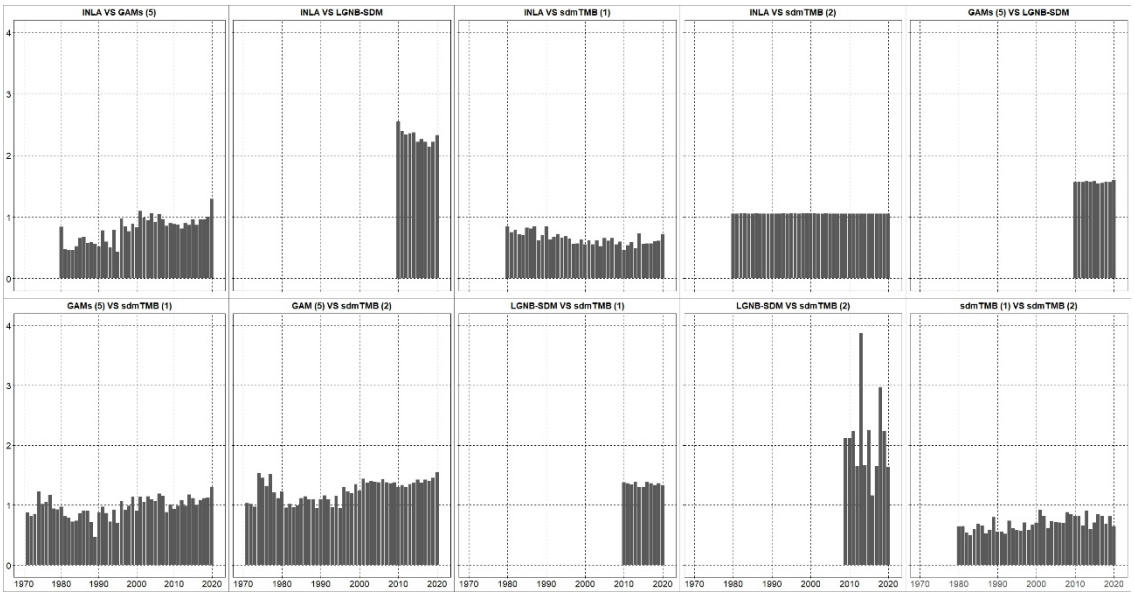

Figure 4.2.5.5. Agreement (SPAEF) between model predicted distribution of adult cod biomass. 0 is perfect agreement.

4.4 Summary

All seven models used to predict distribution were able to produce satisfactory distribution maps for at least one species within the workshop time constraints, both with DATRAS data in the Atlantic and the MEDITS data in the Mediterranean. The fact that all models used the same data for a set of species, prepared according to the best practice guidelines described in section 3.1, provided a unique opportunity to objectively compare the predictions from these models using the best practice guidelines described in section 3.4.

In the Mediterranean, no one-on-one comparison between models was done due to the many GSA used. Instead, all models were compared to the GAM-3 model which was fitted to the most species/GSA combinations. Models were compared based on the SPAEF metric, centre of gravity, and identification of biomass hot spots (90th percentile). GAM-4 estimated distributions similar to GAM-3 (mean SPAEF 0.43) although with more variability owing to its higher complexity (spatio-temporal interactions). GAM-4 also predicted more pronounced changes in distribution due to time-varying interaction term. Distributions estimated with sdmTMB showed good overlap with GAM-3 (mean SPAEF 0.44). However, despite good consistency between both models, the trends in centre of gravity were more jagged with sdmTMB due to random effects when compared to the smoother trends from GAM-3 which uses a spline, and GAM-3 tends to estimate a centre of gravity with lower latitude than that of sdmTMB. Distributions from the VAST model for red mullet in GSA 18 were not a great match with GAM-3 (mean SPAEF 1.25), which could be due to spatial complexity. The centre of gravity estimated also differed between models: VAST estimated longitudinal movement while GAM-3 estimated both latitudinal and longitudinal movements, indicating that GAM-3 may be better able to capture changes in centre of gravity. As with sdmTMB, GAM-3 estimated lower latitudes of centre of gravity compared to VAST. The models also differed in identifying hot spots, with VAST failing to identify some hot spots indicated by GAM-3. For red mullet in GSA 6, distributions from VAST showed medium overlap with GAM-3 (mean SPAEF 0.74) which is lower than in GSA 18 and could be due to less spatial complexity. However, both models showed similar trends in centre of gravity and identified similar shifts. As for the identification of hot spots, despite some discrepancies both models are generally consistent.

In the Atlantic, model comparison was restricted to adult cod and one-on-one comparisons were done between all models: GAM-5, INLA, sdmTMB 1 and 2 (two configurations used), LGNB-SDM (North Sea only) and VAST. Comparison criteria were also slightly different as on top of the SPAEF metric, centre of gravity, and identification of biomass hot spots (90th percentile), models were also compared based on estimation of effective occupied area. Centre of gravity trends were consistent across all models, but some differences for part of the period (2000–2010) were identified where VAST and INLA followed the longitude of the raw CPUE more closely while for the latitude the main difference was that INLA predicted a more southern centre of gravity compared to the other models. For the effective occupied area, there was less consistency across models. sdmTMB more closely matched the raw CPUE, while VAST, GAM-5 and INLA tend to predict a more similar and less patchy distribution. As for the identification of hot spots, GAM-5, INLA and VAST were more similar between them than the other models and showed similar patterns over time, albeit with some discrepancies, which is due to these models all using similar temporal process (smoother/AR1). SPAEF values showed that LGNB-SDM differed the most from the other models (SPAEF between 1.35 and 2.33) while the models sdmTMB 1 and 2, GAM and INLA were similar to values < 1 (0.65 to 0.97).

The best practice guidelines described in section 3 can be implemented to produce distribution maps and compare outputs between models, as exemplified here. The model configurations, diagnostics and validations described here for the chosen candidate models can easily be replicated in order to produce updates of these maps. While all candidate models showcase here produced satisfactory distribution maps, the choice of which model to use will depend on the users' preferences and needs. The content of the sections 2–4 should assist in making that choice.

5 ToR d: Repository for scripts and distribution maps

Populate an ICES hosted repository with scripts (models) and resulting distribution maps for several species (Science Plan codes: 4.2).

The predicted distribution of the focal species is available at ICES SharePoint. However, due to the large difference between predictions from different models and the limited time available in the workshop, the output of several models is given. The group agreed that an approach to combining results in a single map should be developed, ideally in a subsequent workshop.

6 Possible directions for future work on fish distribution mapping

WKFISHDISH2 participants discussed the ideas for further analysis or research that had emerged during the workshop together with the potential for following up on these ideas in an additional workshop. There was broad interest among the participants for continuing the work and a follow up workshop featuring at least some participant overlap was considered a good way to organize this. The possibility to include the suggested terms of reference in existing working groups was also discussed but it was a general perception that these working groups would have many additional obligations and hence would not be as focused as a dedicated workshop. As a suggestion, WKFISHDISH2 came up with the following potential terms of reference for a follow up workshop:

Workshop 3 on Fish Distribution (WKFISHDISH3), chaired by xx, will be established and meet at ICES HQ, Copenhagen, Denmark (with online option) xx-xx June 2023 to:

a) Evaluate best approaches to estimating vessel/gear effects using data from additional sources (surveys not in DATRAS, observer data, citizen science data).
b) Determine if vessel/gear effects are consistent across species, indicating that a bias in swept-area may be present in some cases
c) Consider how to include information on length of fish in models
d) Investigate the use of environmental covariates and their use for predictions
e) Investigate model ability to reproduce distributions used to simulate data in other models (model consistency in situations where distribution is known)
f) Investigate approaches to derive quantitative model credibility measures.
g) Update maps based on results of tors a-e.

.

WKFISHDISH3 will report by 15 August 2023 for the attention of ACOM.

Supporting information

Priority	Scientific surveys are costly for the contributing nations, but limited effort is made to use the results for products beyond annual abundance indices of commercial species available for the wider public. WKFISHDISH2 is established to facilitate that survey data are routinely used to produce distribution maps, as an advisory product, following the ICES advice framework and principles. Currently, ICES does not routinely present distribution maps of marine species as part of their advisory services, although such maps are often requested by clients and the public along with the opportunity to download distribution data. Distribution maps could further contribute to answering specific requests from clients. WKFISHDISH2 is therefore given a high priority. Data from the Mediterranean trawl surveys from selected case studies can also serve the purpose of mapping species distribution. Experiences gained in precedent European projects proved the usefulness of such maps for end-users. Area closure on the basis of the identification of essential fish habitats is currently one of the measures emerging in multiannual management plans for the Mediterranean subregions.
Scientific justification	
Resource requirements	None specified.
Participants	Around 20 experts and participants from the ICES Secretariat.

Secretariat facilities	None specified.
Financial	No financial implications.
Linkages to advisory and science committees	None specified.
Linkages to other groups	None specified.
Linkages to other organizations	None specified.

7 References

AA. VV. 2017. MEDITS Handbook, Version n. 9. MEDITS Working Group, 106 pp. http://www.sibm.it/MEDITS%202011/principaledownload.html

Akaike, H. (1974). A new look at the statistical model identification. IEEE transactions on automatic control, 19(6), 716–723.

Anderson, S. C., Ward, E. J., English, P. A., and Barnett, L. A. (2022). sdmTMB: an R package for fast, flexible, and user-friendly generalized linear mixed effects models with spatial and spatio-temporal random fields. bioRxiv.

Augustin, N. H., Trenkel, V. M., Wood, S. N., and Lorance, P. 2013. Space–time modelling of blue ling for fisheries stock management. Environmetrics, 24: 109–119.

Bakka, H., Vanhatalo, J., Illian, J.B., Simpson, D. and Rue, H., 2019. Non-stationary Gaussian models with physical barriers. Spatial statistics, 29, pp.268–288.

Bastardie, F., Rufener, M-C., Bossier, S., Håkansson, K. B., Christensen, A., Kristensen, K., and Nielsen, J. R. 2022. North Sea resource distribution and fishery opportunities (NORDFO). DTU Aqua. DTU Aqua-rapport No. 402-2022 https://www.aqua.dtu.dk/-/media/institutter/aqua/publikationer/rapporter-401-450/402-2022_north-sea-resource-distribution-and-fishery-opportunities-nordfo.pdf

Baudron, A. R., Brunel, T., Blanchet, M. A., Hidalgo, M., Chust, G., Brown, E. J., ... and Fernandes, P. G. (2020). Changing fish distributions challenge the effective management of European fisheries. Ecography, 43(4), 494–505.

Beguin, J., Martino, S., Rue, H., and Cumming, S. G. 2012. Hierarchical analysis of spatially autocorrelated ecological data using integrated nested Laplace approximation. Methods in Ecology and Evolution, 3: 921–929. doi: https://doi.org/10.1111/j.2041-210X.2012.00211.x

Berg, C. W., Nielsen, A., Kristensen, K. 2014. Evaluation of alternative age-based methods for estimating relative abundance from survey data in relation to assessment models. Fisheries Research, 151, 91–99, https://doi.org/10.1016/j.fishres.2013.10.005

Berg, F., Shirajee, S., Folkvord, A., Godiksen, J. A., Skaret, G., and Slotte, A. 2021. Early life growth is affecting timing of spawning in the semelparous Barents Sea capelin (*Mallotus villosus*). Progress in Oceanography, 196: 102614. doi: https://doi.org/10.1016/j.pocean.2021.102614

Bertrand J.A., De Sola L.G., Papaconstantinou C., *et al.* 2002. The general specifications of the MEDITS surveys. Sci. Mar.66 (Suppl. 2): 9–17.https://doi.org/10.3989/scimar.2002.66s2

Breivik, O. N., Aanes, F., Søvik, G., Aglen, A., Mehl, S., and Johnsen, E. 2021. Predicting abundance indices in areas without coverage with a latent spatio-temporal Gaussian model. ICES Journal of Marine Science, 78: 2031–2042. doi: 10.1093/icesjms/fsab073

Brodie S. J., Thorson J. T., Carroll G., Hazen E. L., Bograd S., Haltuch M. A., Holsman K. K. *et al.* 2020. Trade-Offs in covariate selection for species distribution models: a methodological comparison. Ecography, 43: 11–24.

Carbonara, P., Zupa, W., Follesa, M. C., Cau, A., Capezzuto, F., Chimienti, G., ... and Maiorano, P. (2020). Exploring a deep-sea vulnerable marine ecosystem: Isidella elongata (Esper, 1788) species assemblages in the Western and Central Mediterranean. Deep Sea Research Part I: Oceanographic Research Papers, 166, 103406.

Chen, Y., Shan, X., Jin, X., Yang, T., Dai, F., and Yang, D. 2016. A comparative study of spatial interpolation methods for determining fishery resources density in the Yellow Sea. Acta Oceanologica Sinica, 35: 65–72.

Chen, Y., Shan, X., Ovando, D., Yang, T., Dai, F., and Jin, X. (2021). Predicting current and future global distribution of black rockfish (Sebastes schlegelii) under changing climate. Ecological Indicators, 128, 107799.

Chipman, H.A., George, E.I. and McCulloch, R.E., 2010. BART: Bayesian additive regression trees. The Annals of Applied Statistics, 4(1), pp.266–298.

Engel, M., Mette, T. and Falk, W., 2022. Spatial species distribution models: Using Bayes inference with INLA and SPDE to improve the tree species choice for important European tree species. Forest Ecology and Management, 507, p.119983.

Fernandes PG, Fallon NG. Fish distributions reveal discrepancies between zonal attachment and quota allocations. Conservation Letters. 2020;e12702. https://doi.org/10.1111/conl.12702

Gonzalez, G. M., Wiff, R., Marshall, C. T., and Cornulier, T. (2021). Estimating spatio-temporal distribution of fish and gear selectivity functions from pooled scientific survey and commercial fishing data. Fisheries Research, 243, 106054.

Grüss, A. *et al.* 2019. Evaluation of the impacts of different treat-ments of spatio-temporal variation in catch-per-unit-effort standardization models. – Fish. Res. 213: 75–93.

Hartig, Florian (2022). DHARMa: Residual Diagnostics for Hierarchical (Multi-Level / Mixed) Regression Models. R package version 0.4.5. http://florianhartig.github.io/DHARMa/

ICES. 2020. ICES Workshop on evaluating survey information Celtic Sea gadoids (WKESIG). ICES Scientific Reports. 2:107. 26 pp. http://doi.org/10.17895/ices.pub.7574

ICES. 2021. Scallop Assessment Working Group (WGScallop). ICES Scientific Reports. 3:114. 106 pp. https://doi.org/10.17895/ices.pub.9561

Koch J., Demirel M. C., Stisen S. 2018. The SPAtial EFficiency metric (SPAEF): multiple-component evaluation of spatial patterns for optimization of hydrological models. Geoscientific Model Development, 11: 1873–1886.

Leach, K., Montgomery, W. I., and Reid, N. 2016. Modelling the influence of biotic factors on species distribution patterns. Ecological Modelling, 337: 96–106. doi: https://doi.org/10.1016/j.ecolmodel.2016.06.008

Maina, I., Kavadas, S., Damalas, D., Pantazi, M., Katsanevakis, S., 2018. Dynamics of trawling effort in the Aegean Sea: investigating the potential of vessel monitoring system (VMS) data. ICES J. Mar. Sci. 75 (6), 2265–2275. https://doi.org/10.1093/icesjms/fsy083

Maina, I., Kavadas, S., Katsanevakis, S., Somarakis, S., Tserpes, G., Georgakarakos, S., 2016. A methodological approach to identify fishing grounds: a case study on Greek trawlers. Fish. Res. 183, 326–339. https://doi.org/10.1016/j.fishres.2016.06.021

Maina, I., Kavadas, S., Vassilopoulou, V., Bastardie F., 2021. Fishery spatial plans and effort displacement in the eastern Ionian Sea: A bioeconomic modelling. Ocean and Coastal Management. 203, 105456, https://doi.org/10.1016/j.ocecoaman.2020.105456

Martins T.G., Simpson D., Lindgren F., Rue H. Avard Bayesian computing with INLA: New features. Comput. Stat. Data Anal. 2013;67:68–83. doi: 10.1016/j.csda.2013.04.014

Martins T.G., Simpson D., Lindgren F., Rue H. Avard. 2013. Bayesian computing with INLA: New features. Comput. Stat. Data Anal. 67:68–83. doi: 10.1016/j.csda.2013.04.014

Nielsen, J.R., Kristensen, K., Lewy, P. and Bastardie, F., 2014. A statistical model for estimation of fish density including correlation in size, space, time and between species from research survey data. PLoS One, 9(6), p.e99151

Pante, E., Simon-Bouhet, B. 2013. marmap: A Package for Importing, Plotting and Analyzing Bathymetric and Topographic Data in R. PLoS ONE 8(9): e73051. doi:10.1371/journal.pone.0073051

Panzeri, D., Libralato, S., Carlucci, R., Cipriano, G., Bitetto, I., Spedicato, M. T., ... and Solidoro, C. (2021a). Defining a procedure for integrating multiple oceanographic variables in ensemble models of marine species distribution. In 2021 International Workshop on Metrology for the Sea; Learning to Measure Sea Health Parameters (MetroSea) (pp. 360–365). IEEE.

Panzeri D., Bitetto I., Carlucci R., Cipriano G., Cossarini G., D'Andrea L., Masnadi F., Querin S., Reale M., Russo T., Scarcella G., Spedicato M.T., Teruzzi A., Vrgoč N., Zupa W., Libralato S. (2021b). Developing spatial distribution models for demersal species by the integration of trawl surveys data and relevant

ocean variables. In Copernicus Marine Service Ocean State Report, Issue 5, Journal of Operational Oceanography, 14:sup1, s114–s123; https://doi.org/10.1080/1755876X.2021.1946240

Paradinas, I., Conesa, D., López-Quílez, A., Esteban, A., López, L. M. M., Bellido, J. M., and Pennino, M. G. (2020). Assessing the spatio-temporal persistence of fish distributions: a case study on two red mullet species (*Mullus surmuletus* and *M. barbatus*) in the western Mediterranean. Marine Ecology Progress Series, 644, 173–185.

Petitgas, P., Woillez, M., Renard, D., Bez, N., and Rivoirard, J. 2017. Handbook of Geostatistics in R for Fisheries and Marine Ecology. ICES Co-operative Research Report, 338. ICES. https://ices-library.figshare.com/articles/_/18624080 (Accessed 28 June 2022).

Rivoirard, J., Simmonds, J., Foote, K. F., Fernandes, P., and Bez, N. 2000. Geostatistics for estimating fish abundance. Blackwell Science., Oxford. 206 pp.

Rue H., Martino S., Chopin N. 2009. Approximate Bayesian inference for latent Gaussian models by using integrated nested Laplace approximations. J. R. Stat. Soc. Ser. B Stat. Methodol. 71:319–392. doi: 10.1111/j.1467-9868.2008.00700.x

Rue H., Martino S., Chopin N. Approximate Bayesian inference for latent Gaussian models by using integrated nested Laplace approximations. J. R. Stat. Soc. Ser. B Stat. Methodol. 2009;71:319–392. doi: 10.1111/j.1467-9868.2008.00700.x

Rue, H. and Held, L. 2005. Gaussian Markov Random Fields. Theory and Applications. Chapman and Hall, New York, https://doi.org/10.1201/9780203492024

Rufener, M-C., Kristensen, K., Nielsen, J. R., & Bastardie, F. 2021. Bridging the gap between commercial fisheries and survey data to model the spatio-temporal dynamics of marine species. Ecological Applications, 31(8), [e02453]. https://doi.org/10.1002/eap.2453

Spedicato M.T., Massutí E., Mérigot B., Tserpes G., Jadaud A., Relini G. 2019. The MEDITS trawl survey specifications in an ecosystem approach to fishery management. Sci. Mar. 83S1: 9–20. https://doi.org/10.3989/scimar.04915.11X

Thorson, 2019. Forecast skill for predicting distribution shifts: A retrospective experiment for marine fishes in the Eastern Bering Sea. Fish Fish. 20(1): 159–173. https://doi.org/10.1111/faf.12330

Thorson, J.T., Barnett, L.A.K., 2017. Comparing estimates of abundance trends and distribution shifts using single- and multispecies models of fishes and biogenic habitat. ICES J. Mar. Sci. 74, 1311–1321. https://doi.org/10.1093/icesjms/fsw193

Thorson, J.T., Scheuerell, M.D., Shelton, A.O., See, K.E., Skaug, H.J., and Kristensen, K. 2015. Spatial factor analysis: a new tool for estimating joint species distributions and correlations in species range. Methods Ecol. Evol. 6(6): 627–637. doi:10.1111/2041-210X.12359

Walker N. D., Maxwell D. L., Le Quesne W. J. F., Jennings S. 2017. Estimating efficiency of survey and commercial trawl gears from comparisons of catch-ratios. ICES Journal of Marine Science, 74: 1448–1457.

Weber, D., and Englund, E. 1992. Evaluation and comparison of spatial interpolators. Mathematical Geology, 24: 381–391.

Willmott, C. J., and Matsuura, K. (2005). Advantages of the mean absolute error (MAE) over the root mean square error (RMSE) in assessing average model performance. Climate research, 30(1), 79–82.

Wood, S. N. 2017. Generalized Additive Models. An Introduction with R. 2nd edition, Chapman and Hall, New York.

Wood, S.N. (2011) Fast stable restricted maximum likelihood and marginal likelihood estimation of semi-parametric generalized linear models. Journal of the Royal Statistical Society (B) 73(1):3–36

Wood, S. N., Bravington, M. V., and Hedley, S. L. (2008). Soap film smoothing. Journal of the Royal Statistical Society: Series B (Statistical Methodology), 70(5), 931–955.

Zhou, S., Campbell, R. A., and Hoyle, S. D. 2019. Catch per unit effort standardization using spatio-temporal models for Australia's Eastern Tuna and Billfish Fishery. ICES Journal of Marine Science, 76: 1489–1504. doi: 10.1093/icesjms/fsz034

Zuur, A. F., Ieno, E. N., and Elphick, C. S. (2010). A protocol for data exploration to avoid common statistical problems. Methods in ecology and evolution, 1(1), 3–14.

Annex 1: List of participants

Name	Institute	Country (of institute)	E-mail
Alan Baudron	MSS	UK	alan.baudron@gov.scot
Anna Rindorf	DTU Aqua	Denmark	ar@aqua.dtu.dk
Maria Teresa Spedicato	COISPA	Italy	spedicato@coispa.it
François Bastardie	DTU Aqua	Denmark	fba@aqua.dtu.dk
Klaas Sys	ILVO	Belgium	klaas.sys@ilvo.vlaanderen.be
Manuel Hidalgo	IEO-CSIC	Spain	jm.hidalgo@ieo.csic.es
Nis Sand Jacobsen	DTU Aqua	Denmark	nsja@aqua.dtu.dk
Romaric Jac	IMR	Norway	romaric.jac@hi.no
Tobias Mildenberger	DTU Aqua	Denmark	tobm@aqua.dtu.dk
Natacha Carvalho	EEA	Other	natacha.carvalho@eea.europa.eu
Alessandro Ligas	CIBM	Italy	ligas@cibm.it
Alexander Kempf	Thünen Institute	Germany	alexander.kempf@thuenen.de
Bernhard Kuehn	Thünen Institute	Germany	bernhard.kuehn@thuenen.de
Chun Chen	WUR	NL	chun.chen@wur.nl
Claudia Junge	IMR	Norway	claudia.junge@hi.no
Claudia Musumeci	CIBM	Italy	musumeci@cibm.it
Clyde Blanco	ILVO	Belgium	clyde.blanco@ilvo.vlaanderen.be
Derek Bolser	Oregon State University	USA	bolserd@oregonstate.edu
Elena Couce	Cefas	UK	elena.couce@cefas.co.uk
Eros Quesada	SLU Aqua	Sweden	eros.quesada@slu.se
Federico Maioli	University of Bologna	Italy	f.maioli@unibo.it
Georgina Hunt	University of Aberdeen	UK	georgina.hunt@abdn.ac.uk
Irida Maina	HCMR	Greece	imaina@hcmr.gr
Isabella Bitetto	COISPA	Italy	bitetto@coispa.it

Name	Institute	Country (of institute)	E-mail
Joanna Bluemel	Cefas	UK	joanna.blue-mel@cefas.co.uk
Jochen Depestele	ILVO	Belgium	jochen.depestele@ilvo.vlaanderen.be
Joseph Ribeiro	Cefas	UK	joseph.ribeiro@cefas.co.uk
Louise Vaughan	MI	Ireland	louise.vaughan@marine.ie
Marc Taylor	Thünen Institute	Germany	marc.taylor@thuenen.de
Morten Vinther	DTU Aqua	Denmark	mv@aqua.dtu.dk
Niall Fallon	MSS	UK	niall.fallon@gov.scot
Nikolaus Probst	Thünen Institute	Germany	niko-laus.probst@thuenen.de
Osman Neto	University of the Azores	Portugal	osman.c.neto@uac.pt
Paul Fernandes	Heriot-Watt University	UK	p.fernandes@hw.ac.uk
Porzia Maiorano	University of Bari Aldo Moro	Italy	porzia.maiorano@uniba.it
Stefanos Kavadas	HCMR	Greece	stefanos@hcmr.gr
Walter Zupa	COISPA	Italy	zupa@coispa.it
Jan De Haes	ICES	Other	jan.dehaes@ices.dk
Lara Salvany	ICES	Other	lara.salvany@ices.dk
Fabian Zimmermann	IMR	Norway	fabian.zimmermann@hi.no
Guldborg Søvik	IMR	Norway	guldborg.soevik@hi.no
Mathieu Wolliez	Ifremer	France	mathieu.woillez@ifremer.fr
Max Lindmark	SLU Aqua	Sweden	max.lindmark@slu.se
Youen Vermard	Ifremer	France	youen.vermard@ifremer.fr
Aaron Berger	NOAA	USA	aaron.berger@noaa.gov
Anna Nora Tassetti	CNR	Italy	annanora.tassetti@cnr.it
Berthe Maria Johanna Vastenhoud	DTU Aqua	Denmark	bmjv@aqua.dtu.dk
Bríd O'Connor	MI	Ireland	brid.o'connor@marine.ie
Casper Berg	DTU Aqua	Denmark	cbe@aqua.dtu.dk
Ching Villanueva	Ifremer	France	ching.villanueva@ifremer.fr
Damian Villagra Villanueva	ILVO	Belgium	damian.villagra@ilvo.vlaan-deren.be

Name	Institute	Country (of institute)	E-mail
David Reid	MI	Ireland	david.reid@marine.ie
Dimitrios Damalas	HCMR	Greece	shark@hcmr.gr
Dorota Szalaj	University of Lisbon	Portugal	dszalaj@fc.ul.pt
Guillem Chust	AZTI	Spain	gchust@azti.es
Iosu Paradinas	AZTI	Spain	jparadinas@azti.es
Jan Jaap Poos	WUR	NL	janjaap.poos@wur.nl
Julia Calderwood	MI	Ireland	julia.calderwood@marine.ie
Leire Ibaibarriaga	AZTI	Spain	libaibarriaga@azti.es
Liesa Celie	ILVO	Belgium	liesa.celie@ilvo.vlaanderen.be
Logan Binch	WUR	NL	logan.binch@wur.nl
Paco Melià	Polytechnic University of Milan	Italy	paco.melia@polimi.it
Sebastian Uhlmann	MI	Ireland	sebastian.uhlmann@marine.ie